Examine and quantifying the potential of artificial upwelling for its capacity for additional CO_2 uptake and long-term storage in the ocean.

Dissertation

ZUR ERLANGUNG DES DOKTORGRADES

DER MATHEMATISCH – NATURWISSENSCHAFTLICHEN FAKULTÄT

DER CHRISTIAN-ALBRECHTS-UNIVERSITÄT ZU KIEL

VORGELEGT VON

MALTE JÜRCHOTT

KIEL, AUGUST 2024

Tag der mündlichen Prüfung: 29.10.2024

……...

Prof. Dr. Christian Berndt, Vorsitz der Prüfungskommission

……...

Prof. Dr. Andreas Oschlies, Erster Gutachter

……...

Prof. Dr. Klaus Wallmann, Zweiter Gutachter

……...

Prof. Dr. Arne Körtzinger, Mitglied Prüfungskommission

“Das, wobei unsere Berechnungen versagen, nennen wir Zufall.”
Albert Einstein

Zusammenfassung

In den letzten Jahren wurden verschiedene Methoden zur Kohlendioxidentfernung (CDR) aus der Atmosphäre als potenzielle Instrumente für negative CO_2 Emissionen diskutiert, um zukünftige, schwer vermeidbare CO_2 Emissionen zu kompensieren und so die globale mittlere Oberflächenlufttemperatur zu stabilisieren. Künstlicher Auftrieb (AU) wurde als eine marine CDR-Methode vorgeschlagen und beschreibt die Idee, vertikale Pumpen im offenen Ozean zu installieren, um nährstoffreiches Tiefenwasser an die Oberfläche zu transportieren und somit das marine Ökosystem zu düngen und den Kohlenstofffluss aus der Atmosphäre in das Ozeaninnere über die biologische Kohlenstoffpumpe anzuregen. Es mangelt zurzeit jedoch an einem detaillierten und quantitativen Verständnis über die durch AU stimulierten Prozesse und deren Beitrag zum Potenzial von AU als marine CDR-Methode.

Im zweiten Kapitel dieser Arbeit verwenden meine Co-Autoren und ich das UVic 2.9 Fe_Mask Erdsystemmodell mittlerer Komplexität in einer ohne-Land Modellkonfiguration, um einen nahezu globalen AU-Einsatz unter verschiedenen zukünftigen CO_2-Emissionspfaden (RCP) zu simulieren (ohne Eisenlimitierung für das Ökosystem dabei zu berücksichtigen), um die biologisch-fokussierte Darstellung von AU zu überprüfen. Wir stellen in allen AU-Experimenten eine allgemeine Zunahme des marinen Kohlenstoffinventars fest, aber das Ausmaß dieser Zunahme hängt stark vom zukünftigen CO_2-Emissionspfad ab (bis zu +1 Pg C pro Jahr unter dem höchsten CO_2-Emissionspfad, RCP 8.5). Während der marine Kohlenstoffanteil, welcher der biologischen Kohlenstoffpumpe zuzuschreiben ist, in allen AU-Experimenten zunimmt und nur eine moderate Abhängigkeit im Verhältnis zum CO_2-Emissionspfad zeigt, reagiert der marine Kohlenstoffanteil, welcher der Löslichkeitspumpe zuzuschreiben ist (d. h. Änderungen im physikalisch-chemischen Kohlenstoffaufnahmeprozess des Oberflächenozeans), unter RCP 2.6 mit CO_2-Ausgasung und unter RCP 8.5 mit CO_2-Aufnahme in derselben Größenordnung wie die biologische Kohlenstoffpumpe. Wir fassen zusammen, dass die biologisch-fokussierte Darstellung von AU zu eng gefasst ist und quantitativ wichtige Prozesse im Zusammenhang mit der Löslichkeitspumpe nicht berücksichtig.

Im dritten Kapitel untersuchen wir die Reaktion der biologischen Kohlenstoffpumpe auf AU detaillierter und konzentrieren uns dabei insbesondere auf mögliche Eisenlimitierung für das marine Ökosystem. In dieser Studie simulieren wir globales und regionales AU und die ozeanische Eisendüngung (OIF) jeweils einzeln und in Kombination im UVic 2.9 Fe_Mask Model. Zusätzlich simulieren wir AU einzeln im UVic 2.9 Fe_Dyn Modell, welches Eisen als prognostischen Tracer im Inneren des Ozeans enthält und daher eine detailliertere Untersuchung von Änderungen der eisenspezifischen Prozesse in der Tiefe ermöglicht. Alle Experimente wurden in ohne-Land Modellkonfigurationen und unter dem moderaten RCP 4.5 CO_2-Emissionspfad durchgeführt. Unsere Ergebnisse zeigen, dass globale AU-Experimente weder das gesamte Kohlenstoffinventar des Ozeans, noch den Teil welcher der biologischen Kohlenstoffpumpe zuzuordnen ist, signifikant erhöhen, da es dem Ökosystem an der Meeresoberfläche an Eisen fehlt. Die Kombination aus global angewendetem AU + OIF führt zu einer größeren Kohlenstoffaufnahme des Ozeans (angetrieben über die biologische Kohlenstoffpumpe; insgesamt +1.37 Pg C pro Jahr) als jeweils beide Methoden einzeln. Wir stellen einen Anstieg der Exportproduktion organischen Materials in allen in diesem Kapitel diskutierten marinen CDR-Experimenten fest, können jedoch keine konsistente Beziehung zwischen dem Anstieg der Exportproduktion und der Reaktion des Kohlenstoffinventars der biologischen Kohlenstoffpumpe feststellen. Der Anstieg der Exportproduktion und die damit verbundene Respiration in der Tiefe begünstigt jedoch die Ausdehnung von Sauerstoffminimumzonen und verursachen einen überproportionalen Anstieg der Denitrifikation im Vergleich zur N_2-Fixierung, wodurch das globale marine Nitratinventar reduziert wird. Zusammenfassend ist AU für sich alleine simuliert als marine CDR-Methode in unseren Modellexperimenten unwirksam und erfordert die gleichzeitige Anwendung von OIF, um das Kohlenstoffinventar des Ozeans zu erhöhen.

Im vierten Kapitel stellen wir nicht nur die anfängliche biologisch-fokussierte Darstellung, sondern die allgemeine Klassifizierung von AU als marine CDR-Methode infrage. Das Ziel einer CDR-Methode ist negative CO_2 Emissionen zu erzeugen, um die globale mittlere Oberflächenlufttemperatur zu stabilisieren. Da AU kaltes Wasser aus dem Ozeaninneren an die Oberfläche pumpt, verursacht es gleichzeitig einen Rückfluss wärmeren Wassers in das Ozeaninnere, was direkte Auswirkungen auf die Wärmeverteilung im Ozean und damit der gesamten Erde hat. Um die Auswirkungen von AU auf den globalen Kohlenstoffkreislauf in Relation auf dessen Auswirkungen auf den Wärmehaushalt der Erde zu untersuchen, verwenden wir das UVic 2.9 Fe_Dyn-Modell unter dem moderaten RCP 4.5 CO_2-Emissionspfad in einer ohne-Land und einer mit-Land Konfiguration und simulieren zwei

AU-Implementierungen, welche die Wärmeverteilung im Ozean entweder direkt oder nicht direkt beeinflussen. Wir stellen fest, dass sich der Kohlenstoff- und Wärmehaushalt der Erde nur wesentlich ändern, wenn AU direkt den Wärmehaushalt der Erde beeinflusst. Gleichzeitig ist der festgestellte Rückgang der globalen mittleren Oberflächenlufttemperatur deutlich größer im Verhältnis zum negativen CO_2-Emissionseffekt. Darüber hinaus erhöht sich das terrestrische Kohlenstoffinventar um +14 Pg C als Folge der verringerten globalen mittleren Oberflächenlufttemperatur (Kohlenstoff-Klima-Feedback), während das Kohlenstoffinventar des Ozeans durch eine Rückkopplung des Erdsystems -2 Pg C verliert (Kohlenstoff-Konzentrations-Feedback).

Zusammenfassend, die in dieser Arbeit diskutierten Ergebnisse führen zu den allgemeinen Schlussfolgerungen, dass (i) die biologisch-fokussierte Darstellung von AU quantitativ wichtige Prozesse im Zusammenhang mit der Löslichkeitspumpe nicht berücksichtig und (ii) AU zu keinen signifikanten negativen CO_2 Emissionen ohne zusätzliche Anwendung von OIF führt, (iii) jedoch durch dessen direkte Auswirkungen auf den Wärmehaushalt der Erde zu einer signifikanten Reduzierung der globalen mittleren Oberflächenlufttemperatur führt.

Summary

Over the last few years, several carbon dioxide removal (CDR) methods have received attention as potential tools to introduce negative CO_2 emissions to the Earth system to compensate future remaining CO_2 emissions and thus, to stabilize global mean surface air temperature. Artificial upwelling (AU) has been proposed as a marine CDR method and describes the idea of deploying vertical pipes in the open ocean to upwell nutrient rich deep water to the surface to fertilize the marine ecosystem and stimulate the carbon flux from the atmosphere into the interior ocean via the biological carbon pump. However, its potential as a marine CDR method and a refined and quantitative understanding of the underlying process stimulated via AU is lacking.

In the second chapter of this thesis my co-authors and I use the UVic 2.9 Fe_Mask Earth system model of intermediate complexity in a no-Land model configuration to simulate close to global AU deployment under different future CO_2-emission driven representative concentration pathways (RCP) and without the consideration of iron-limitation for the ecosystem to challenge the biology-focused narrative of AU. We find in all AU-experiments an overall increase in the marine carbon inventory, but the magnitude of this increase depends strongly on the future CO_2-emission pathway (up to +1 Pg C $year^{-1}$ under the high-CO_2-emission pathway, RCP 8.5). While the marine carbon inventory attributable to the biological carbon pump increases in all AU-experiments and only shows a moderate CO_2-emission pathway dependency, the carbon inventory attributable to the solubility pump (i.e., changes in physical-chemical carbon uptake processes) responds with CO_2-outgassing under RCP 2.6, but becomes equally effective in CO_2-uptake under RCP 8.5 compared to the biological carbon pump. We conclude that the initial narrative of additional ocean carbon uptake via artificial upwelling being driven via the biological carbon pump is too simplified and misses quantitatively important ocean carbon response processes associated with the solubility pump.

In the third chapter we investigate the response of the biological carbon pump to AU with a specific focus on iron-limitation for the marine ecosystem. In this study we simulate global and regional AU and ocean iron fertilization (OIF) individually and in combination in the

UVic 2.9 Fe_Mask model. Additionally, we simulate AU individually in the UVic 2.9 Fe_Dyn model, which contains iron as a prognostic tracer in the ocean interior and therefore, allows for an in-depth investigation into iron specific process and concentrations at the pipes source depth. All experiments are carried out in no-Land model configurations and under the moderate RCP 4.5 CO_2-emission pathway. Our results show that global AU-only experiments do neither significantly increase the total ocean carbon inventory, nor the carbon inventory attributable to the biological carbon pump, due to a lack of iron prevalent at the surface ocean. The combination of globally applied AU + OIF yields a greater ocean carbon uptake response (driven via the biological carbon pump; net +1.37 Pg C $year^{-1}$) than both methods individually. We detect an increase in export production of organic matter in all marine CDR experiments discussed in this chapter, but cannot find a consistent relationship between the increase in export production and the response of the ocean carbon inventory attributable to the biological carbon pump. However, the increase in export production and associated respiration at depth promotes the expansion of oxygen minimum zones and causes a disproportionately larger increase in denitrification than N_2-fixation, which reduces the overall ocean nitrate inventory. Overall, artificial upwelling simulated by itself is, according to our model experiments, ineffective as a marine CDR method and requires simultaneously applied ocean iron fertilization to enhance ocean carbon uptake.

In the fourth chapter we challenge not just the initial ecosystem-driven narrative of AU, but its overall classification as a marine CDR method. The ultimate purpose of a CDR method is to stabilize global mean surface air temperature via the introduction of negative CO_2 emissions to the Earth system. However, since AU does upwell cold water from the interior ocean to the surface and causes a backflow of warmer water into the ocean interior in lockstep, it directly impacts the Earth's heat distribution. To investigate the impact of AU on the global carbon cycle in relation to its impact on Earth's heat budget, we use the UVic 2.9 Fe_Dyn model under the moderate RCP 4.5 CO_2-emission pathway in a no-Land and a with-Land configuration and simulate two AU implementations, which either do or do not directly redistribute ocean heat. We find that Earth's carbon inventories and heat budget only significantly changes, if AU directly redistributes ocean heat, and that the detected decrease in global mean surface air temperature is much greater and out of relation in comparison to the negative CO_2-emissions effect of AU. Additionally, the terrestrial carbon inventory increases by +14 Pg C as a consequence of decreased global mean surface air temperature (carbon climate feedback), while the ocean carbon inventory looses -2 Pg C via a carbon concentration feedback.

Overall, the results discussed in this thesis lead to the overall conclusions that (i) the initial biology-focused narrative of AU misses quantitatively important processes associated with the solubility pump and that (ii) AU does not significantly cause negative CO_2 emissions to the Earth system without simultaneously fertilizing the ecosystem with additional iron. However, (iii) AU is effective in reducing global mean surface air temperature via its direct impact on the redistribution of heat in the Earth system.

Acknowledgements

First of all, I want to thank Andreas Oschlies and Wolfgang Koeve for giving me the opportunity to work on this topic and being a part of the BM, for the support and advice in all areas, the stimulating discussions and the supervision.

A special thanks goes to Wolfgang Koeve for being a great and very involved supervisor to me, for providing guidance, advice and support in any area I asked for it, for introducing me with great care to UVic, for giving me a great amount of freedom to explore my own research ideas and thus, for laying the foundation for me to trust in myself in the scientific environment. Thank you!

I also want to thank Andreas Oschlies, Wolfgang Koeve and Jan Taucher for being my ISOS supervisors and the entire Test-ArtUp team for their support, exchange and discussions.

Apart from that I want to thank the entire Biogeochemical Modelling department for warmly welcoming me in this group. A special thanks goes to my old Seeburg office mates Neha and Haichao for the discussions and our joint lunch-breaks in between, to Tronje for many great bicycle tours around Kiel and to Vanessa for relaxing post-lunch walks with Piet.

Finally, I want to thank all my friends and my family for supporting me in many different ways and a special thanks goes to my family dogs Flocke and Juna for sharing their joy with me!

Contents

1. Introduction

1.1. Motivation

Since humankind started in the 19th century to systematically exploit and burn fossil fuels and change the terrestrial landscape primarily via deforestation and agriculture on an industrial scale, large quantities of anthropogenic greenhouse gases have been emitted into Earth's atmosphere (IPCC 2023). It took until the end of the 20th century for scientists to prove with high certainty a causal relationship between anthropogenic greenhouse gas emissions into the atmosphere and an increase in global mean surface air temperature (IPCC 1990, IPCC 1995). Since then, decreasing emissions has been on the political agenda for most countries to limit future surface air temperature increase in an effort to preserve nature and basic human needs such as area to live and food production. In the year 2015 most of Earth's leaders collectively decided in the Paris Agreement (UNFCCC 2015) to limit global mean surface air temperature increase well below 2°C compared to preindustrial times and even reach 'net zero' greenhouse gases by the middle of the 21st century (IPCC 2018).

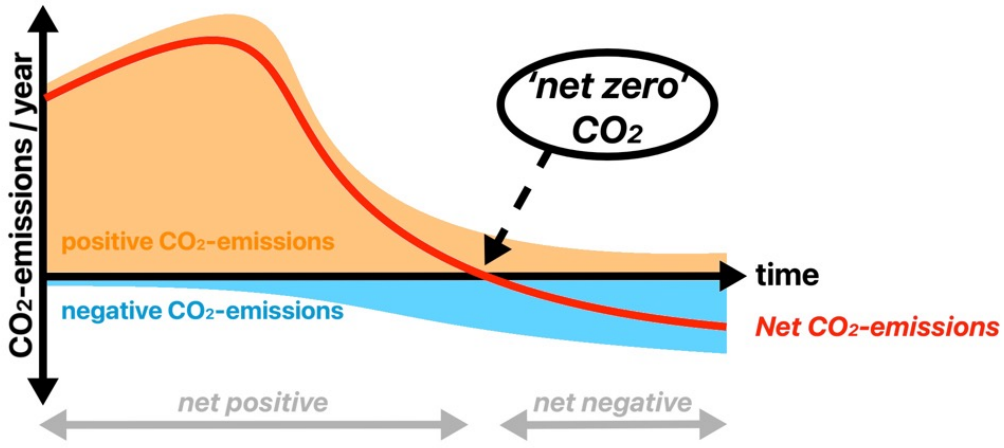

Figure 1-1: Stylised pathway of net CO_2 emissions (red) over time and split into individual contributions via positive (orange) and negative (blue) CO_2 emissions with 'net zero' CO_2 marked. Non-CO_2 greenhouse gases are not shown in this figure.

The stated goal of reaching ‘net zero’ describes a desired state of the Earth in which anthropogenic greenhouse gas emissions and their removal out of the atmosphere are in balance as a means to stabilize global mean surface air temperature (Fig. 1.1) (IPCC 2022). It’s not expected that humankind will be able to achive zero greenhouse gas emissions to be emitted into the atmosphere in this century due to hard-to-abate emissions e.g., from the agriculture sector, which inevitably calls for the need to actively remove greenhouse gas emissions from the atmosphere to be able to reach a ‘net zero’ state (Bahiker et al., 2022).

1.2. Carbon dioxide removal (CDR)

A specific focus of removing greenhouse gas emission from the atmosphere lies on carbon dioxide removal (CDR), since CO_2 is categorized as a long-lived greenhouse gas in the atmosphere (Solomon et al., 2007) and is the most abundantly emitted anthropogenic greenhouse gas, which for example made up about 64% (38 ± 3 Gt CO_2-eq) of the net anthropogenic greenhouse gas emissions for the year 2019 (IPCC 2022). The ocean and the land are currently CO_2 sinks and took up about 25 % of CO_2 emissions each over the past decades, while the remaining 50 % stayed in the atmosphere (Fig. 1.2a) (IPCC 2021). The general idea behind proposed CDR technologies is to either artificially enhance CO_2 uptake of the ocean and land or to capture CO_2 directly from the atmosphere or a point source and store it in for example geological reservoirs or in materials (Keller et al., 2018, Bahiker et al., 2022, NASEM 2022) (Fig. 1.2b-d). The amount of CDR currently assumed between the years 2020 and 2100 in all illustrative mitigation pathways (IMP) that limit warming to 2˚C is 609 (188 to 1520) Gt CO_2 (main value represents the median and bracketed values denote 5-95th percentile range) and requires several CDR methods to be deployed simultaneously (Bahiker et al., 2022). In the following sections the concepts of the different CDR approaches will be generally introduced with examples and discussed in the context of advantages, risks and the perturbation of the global carbon cycle.

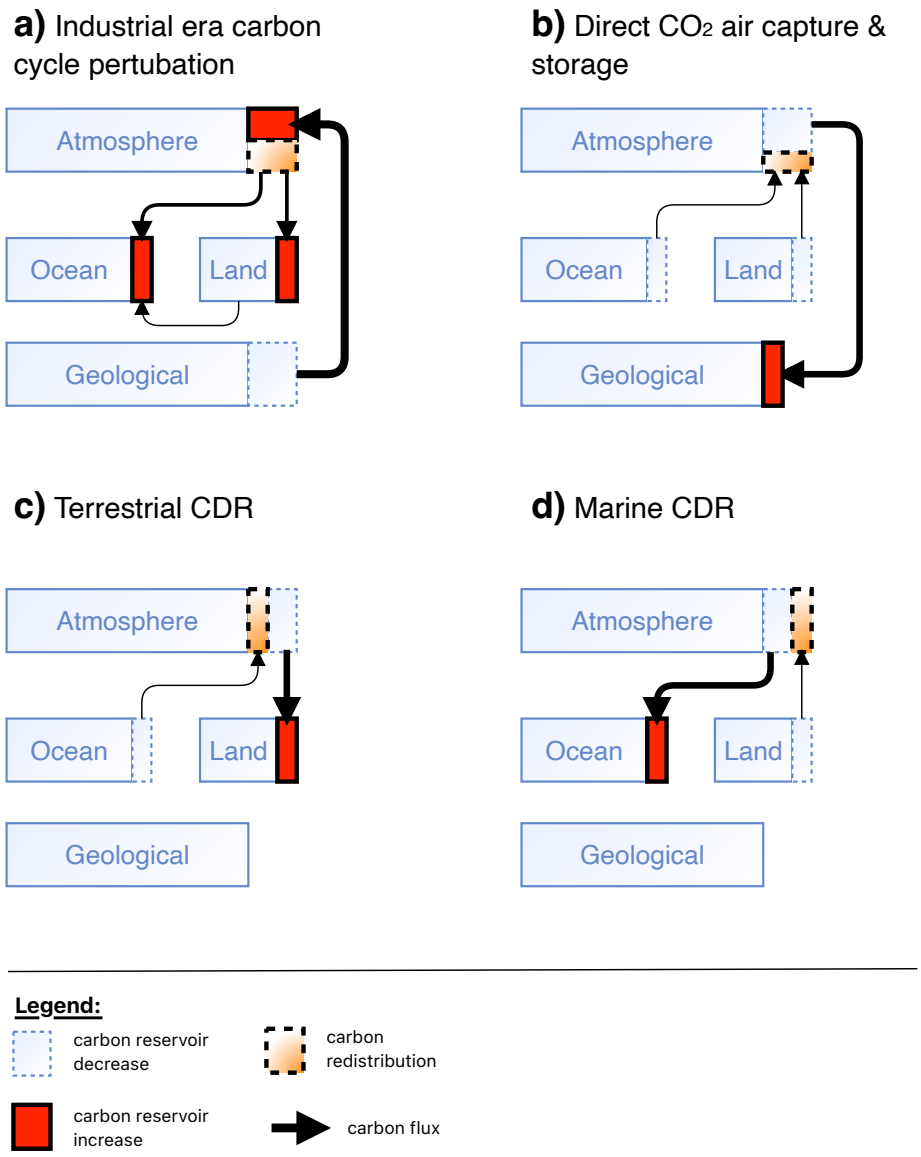

Figure 1-2: Schematic representation of Earth's carbon cycle response to a) industrial era carbon emissions into the atmosphere and relative changes due to b) direct CO_2 air capture and storage c) terrestrial and d) marine carbon dioxide removal (CDR). Figure is modified after Keller et al., 2018.

1.2.1. Direct CO_2 air capture and storage

The idea behind direct CO_2 air capture and storage is to use in part already existing technology to extract CO_2 from the atmosphere, liquify or dissolve it in water and pump it via pipelines into a geological reservoir for long term storage (Pires et al., 2011, Boot-Handford et al., 2014, Bui et al., 2018). Advantages of this idea are the potential for long term CO_2 storage up to millennia, a high technology readiness level for small-scale application and easy monitoring, reporting and verification (MRV) of stored CO_2 (Bui et al., 2018). Challenges

and risks include limitations associated with suitable storage sites (Fuhrmann et al., 2024) and the needed infrastructure, as well as the potential for leakage (Dixon and Romanak 2015), if the CO_2 remains in the geological reservoir in a liquid form and escapes through naturally occurring geological fault structures (Bui et al., 2018). If the CO_2 is directly taken out of the atmosphere in a significant amount, the reduced atmospheric CO_2 concentration will trigger carbon concentration Earth system feedbacks, which lead to a CO_2 release into the atmosphere from the terrestrial and ocean reservoir and partly offsets the direct CO_2 air capture effort to reduce atmospheric CO_2 concentrations (Fig. 1.2b) (Keller et al., 2018).

1.2.2. Terrestrial CDR

Terrestrial CDR is the general term for CDR methods, which try to enhance the CO_2 uptake capacity of the terrestrial carbon sink (Boysen et al., 2017, Bahiker et al., 2022). Ideas range from enhancing the CO_2 storage capacity of the soil, the restoration of peat lands, afforestation, enhanced weathering of silicate minerals as well as using plant growth to capture CO_2 from the atmosphere, burn the biomass to produce energy and in the end capture the released CO_2 after the burning process at the point source and store it in a geological reservoir (BECCS) (Fuss et al., 2014, Keller et al., 2014, Boysen et al., 2017, Bahiker et al., 2022). Advantages are potential land ecosystem benefits or energy production, while challenges and risks are mostly related to limited land area, competing interests in land-use, CO_2 storage durability and a potential decrease in soil health and negative implications for food production (Boysen et al., 2017). Especially CO_2 storage durability might become an issue, if CO_2 is stored in living biomass and subject to e.g., extreme weather events, droughts and wild fires (Brack and King 2021). If the natural CO_2 uptake capacity of the terrestrial reservoir gets significantly enhanced via CDR methods, the corresponding reduced atmospheric CO_2 concentration will trigger carbon concentration Earth system feedbacks in which the ocean reservoir will respond with CO_2 outgassing and partly offset the terrestrial CDR impact on the atmospheric CO_2 concentration (Fig. 1.2c) (Keller et al., 2018).

1.2.3. Marine CDR

As opposed to terrestrial CDR, marine CDR is the general term for CDR methods, which try to enhance the uptake capacity of the global oceans (NASEM 2022, Amann et al., 2024). The

main foci lie on alkalinity enhancement to chemically improve the surface ocean's capacity to take up CO_2 (Renforth and Henderson 2017) and so-called blue carbon approaches, which aim to enhance either costal vegetative ecosystems to store more CO_2 in the sediments (Macreadie et al., 2021) or open ocean ecosystems via the addition of nutrients to enhance organic particle export production and thus, CO_2 storage in the ocean interior (Aumont & Bopp 2006, Boyd et al., 2007, Keller et al., 2014). Advantages mainly cover ecosystem benefits and potentially improved fish production (Kirke 2003, Macreadie et al., 2021), while challenges and risks are discussed in the context of ocean CO_2 uptake efficiencies, restricted coastal areas, changes in ecosystem structure, accelerated ocean oxygen loss due to enhanced respiration of sinking organic matter in the ocean interior and possible short CO_2 sequestration time scales (Keller et al., 2014, Siegel et al., 2021, NASEM 2022). If the natural CO_2 uptake capacity of the global oceans gets significantly enhanced via marine CDR methods, the corresponding reduction in the atmospheric CO_2 concentration will trigger carbon concentration Earth system feedbacks, in which the terrestrial reservoir will respond with CO_2 outgassing and partly offset the marine CDR impact on the atmospheric CO_2 concentration (Fig. 1.2d) (Keller et al., 2018).

1.3. Natural ocean upwelling

The upwelling of water masses from the ocean interior to the surface ocean is a naturally occurring regional process and one aspect of the global ocean circulation (Cessi 2019). The major upwelling regions are located at the eastern boundaries of ocean basins, at the equator and around Antarctica and are generally classified as wind-driven upwelling systems (Kämpf and Chapman 2016). The Earth's rotation and associated effects, such as the Coriolis force, play a dominant role in wind-driven upwelling systems mainly by promoting regional wind patterns, which result in an upward flow of seawater (Kämpf and Chapman 2016).

Natural upwelling systems can be further classified in terms of their source water depth, the ecosystem response and their impact on the carbon cycle. While the natural upwelling in the Southern Ocean extends into the deep ocean and reaches older waters, other natural upwelling systems such as the Equatorial Pacific and eastern boundary upwelling systems (EBUS) upwell much younger waters from around 200 meters depth (Cessi 2019, Koeve et al., 2015).

In terms of the ecosystem response to natural upwelling, we can separate the Southern Ocean and the Equatorial Pacific upwelling system from EBUS. The Southern Ocean and the Equatorial Pacific have been classified as high-nutrient-low-chlorophyl (HNLC) regions (Pollard et al., 2006, de Baar et al., 2005, Martin et al., 1990, Fay et at., 2024). Those regions accumulate high concentrations of macro-nutrients at the surface ocean, but are limited by iron, which limits primary production to an extend of overall low ecosystem productivity. In contrast, EBUS show very high biological productivity driven by the upwelling of nutrient-rich water from below the photic zone (Chavez and Messié 2009). The four main eastern boundary upwelling systems (EBUS) are the California (CCS), Humboldt (HCS), Canary (CnCS) and the Benguela (BCS) current system (Fig. 1.3) (Abrahams et al., 2021).

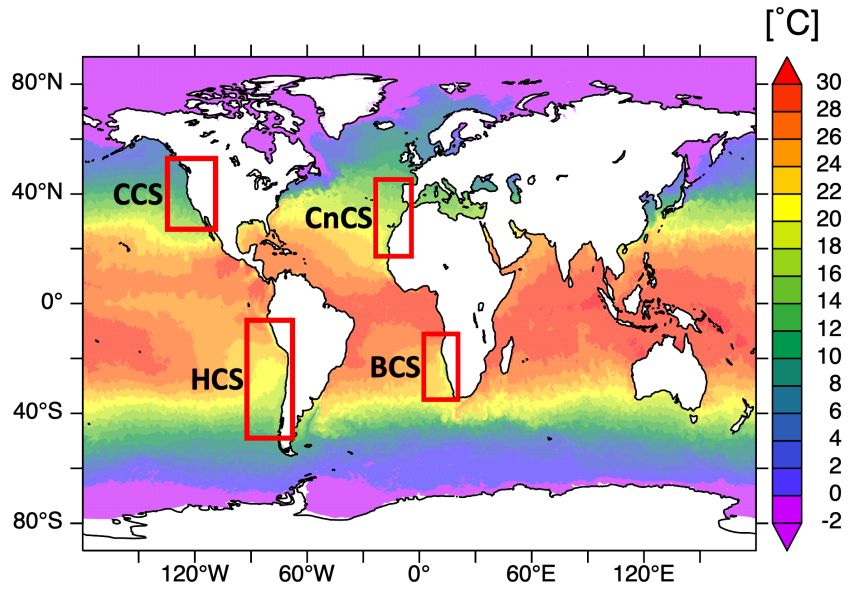

Figure 1-3: Sea surface temperature in ˚C for 1st of March, 2022 from data product ESA CCI/C3S SST Climate Data Record v3.0 (Copernicus Climate Change Service (C3S) 2019) with red rectangles indicating area of four main eastern boundary upwelling systems: California (CCS), Humboldt (HCS), Canary (CnCS) and Benguela (BCS) current system (Abrahams et al., 2021).

The upwelling of nutrient-rich water results generally in a bottom-up controlled food web in which fast growing diatoms are the most common phytoplankton species (Chavez and Messié 2009, Kämpf and Chapman 2016). However, despite high biological productivity in EBUS, iron has been identified as well as a limiting nutrient for primary producers in the California and the Humboldt current system (Hutchins et al., 1998, Chase et al., 2007, Hutchins et al.,

2002). The high primary production rates in EBUS feed over into secondary production of zooplankton and fish, but the trophic transfer efficiency varies considerably with season and region (Kämpf and Chapman 2016). One common characteristic of ecosystems in EBUS seems to be the wasp-waist species richness pattern in which one or at most a few small, plankton-feeding pelagic fish occupy an intermediate trophic level (Bakun 1997). Those few species such as sardines and anchovies are highly relevant for fisheries and human food production and next to dead phytoplankton, zooplankton and faecal pellets can contribute to organic carbon export into the ocean interior and sediments (Dale et al., 2014, Jiao et al., 2004). The high production of organic particles at the ocean surface, export into the ocean interior and respiration at depth especially in EBUS also contributes together with regional circulation patterns ('shadow zones') to extended oxygen minimum zones below the surface ocean (Paulmier et al., 2008). Oxygen minimum zones promote the production of non-CO_2 greenhouse gases such as N_2O via denitrification, which, if emitted into the atmosphere, could offset ocean CO_2 uptake of the ocean in terms of its impact on global mean surface air temperature (Paulmier et al., 2008, Paulmier and Ruiz-Pino 2009, Chavez and Messié 2009). Another effect of enhanced denitrification is the loss of bioavailable nitrate, which can further limit primary production next to iron limitation (Chavez and Messié 2009).

Whether EBUS are net sources or sinks for atmospheric CO_2 is currently unclear, despite high biological productivity, and seems to varie with region, season, wind strength and direction (Kämpf and Chapman 2016, Jiao et al., 2004). In contrast, the upwelling in the Equatorial Pacific region has been clearly identified as a current net source of CO_2 (+0.35 Pg C $year^{-1}$) into the atmosphere (Fey et al., 2024). The two main contradicting processes, which influence the surface ocean CO_2-flux in natural upwelling regions, are (i) the upwelling of cold and DIC-rich water and subsequent heating, which reduces CO_2 solubility and promotes outgassing, and (ii) the export of organic particles and respiration at depth primarily in the water column (Jiao et al., 2004), i.e., the biological carbon pump (Frenger et al., 2024). However, a net sink of CO_2 via the biological carbon pump requires from a theoretical viewpoint either an elevated carbon-to-nutrient stoichiometry in organic particles beyond Redfield or the upwelling and utilization of preformed nutrients (Duteil et al., 2012). Due to the excess of macro-nutrients at the surface ocean in natural upwelling regions, elevated carbon-to-nutrient stoichiometry in organic matter beyond Redfield has not been observed in these ocean regions (Moreno and Martiny 2018) and high concentrations of preformed nutrients below the surface ocean are generally associated with greater depth well below 200 meters and require downwelling in other HNLC-regions (Duteil et al., 2012). High biological

productivity as observed in EBUS can therefore, not directly be translated into net ocean carbon sink.

1.3.1. Artificial upwelling

The idea behind artificial upwelling as a marine CDR technology is to use vertical ocean pipes to pump waters rich in preformed nutrients from the ocean interior to the surface ocean primarily in oligotrophic ocean regions as a means to stimulate ocean ecosystem productivity and export production and thus, enhance the ocean carbon storage associated with the biological carbon pump (Fig. 1.4) (Lovelock and Rapley 2007, GESAMP 2019, NASEM 2022). In contrast to the overall shallow upwelling in natural upwelling systems with an unclear or even negative net CO_2-flux (Kämpf and Chapman 2016, Fey et al., 2024), the source depth of the vertical ocean pipes would reach much deeper into the interior ocean and upwell higher concentrations of preformed nutrients, which in theory could result in enhanced ocean carbon uptake via the biological carbon pump. However, this simplified and biology-driven concept of artificial upwelling is not quantitatively confirmed and does not account for e.g., physical ocean surface temperature changes, which have already been identified as an important process for the surface ocean CO_2-flux in natural upwelling systems (Jiao et al., 2004, Fey et al., 2024).

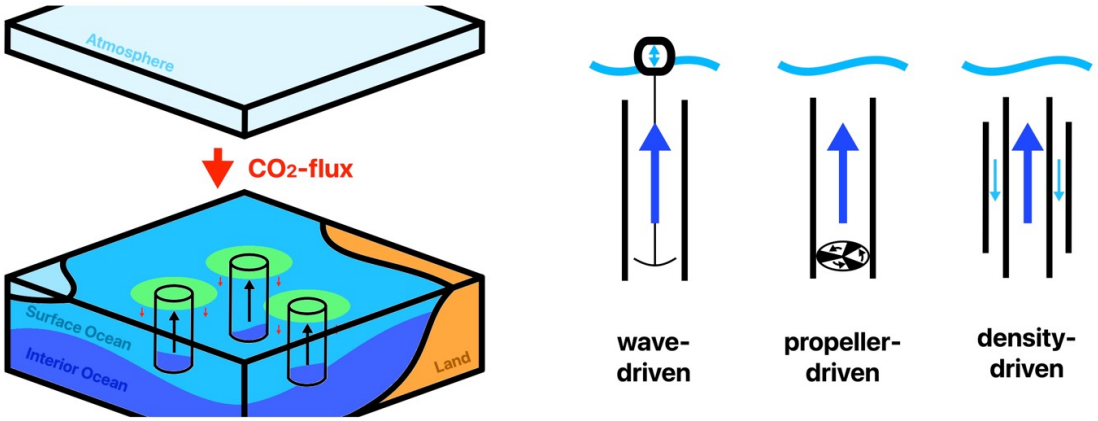

Figure 1-4: Simplified illustration of conceptual artificial upwelling pipes (right) deployed in the ocean to pump up interior ocean waters to the surface to stimulate the biological carbon pump and cause a CO_2-flux from the atmosphere into the ocean (left).

Current pipe technologies, which are under investigation, are wave-driven, propeller-driven and density-driven pipes (Fig. 1.4), but none has jet exceeded the prototype and testing stage (Kithil 2006, Kemper et al., 2022, Kemper et al., 2023). Since the artificial upwelling pipe technology is not jet refined and the current international law on the open ocean beyond any countries national economic zone can be interpreted in a way that it prohibits most marine CDR deployments (Proelss 2022), a successful artificial upwelling field trial in the near future might be a challenge to achieve.

Lacking the near-time opportunity of an open ocean field trial, the effectiveness of artificial upwelling as a marine CDR technology can be investigated in three different ways: First, we can investigate natural occurring upwelling. Second, we can simulate artificial upwelling in controlled laboratory and mesocosm experiments and third, we can simulate artificial upwelling in advanced computer models.

First and as mentioned in the previous chapter, the overall shallow upwelling in natural upwelling systems causes an unclear or even negative net CO_2-flux into the atmosphere (Kämpf and Chapman 2016, Fey et al., 2024). High biological productivity and enhanced export production as a consequence of upwelling, as observed in EBUS, is therefore, very likely not sufficient by itself to promote the argument of additional ocean carbon uptake (Jiao et al., 2004, Kämpf and Chapman 2016). However, the transfer of knowledge from shallow natural upwelling to deeper artificial upwelling might be inappropriate, due to the different source depths of the upwelled water and related differences in e.g., preformed nutrient concentrations (Duteil et al., 2012).

Second, artificial upwelling has been intensely investigated in mesocosm experiments at the coast of Gran Canaria. Mesocosms are several meters long, at the bottom closed, transparent plastic containers, which are filled with seawater and float in the ocean (Riebesell et al., 2013). The advantage of such mesocosms is that they can capture the complexity of an ecosystem via encapsulating natural and usually local sea water, which generally contains all prevalent ecosystem species up to very small fish. Disadvantages of mesocosms are (i) the changed water column behavior inside the tube due to their encapsulation-effect and blocking e.g., horizontal wave activity and (ii) limitations concerning the measurement of e.g., export production, remineralization depths and related carbon sequestration time scales due to the limited length of the mesocosms (Riebesell et al., 2013).

For the purpose of studying artificial upwelling, mesocosms were filled with local, oligotrophic ocean water and afterwards nutrient-rich water with various individual nutrient concentrations has been added in different modes (e.g., pulsed or continuous) to simulate the effect of artificial upwelling. Observed changes indicate that the addition of nutrient-rich water did significantly increase overall biological production primarily driven by diatoms (Ortiz et al., 2022) and the nutrient ratio between nitrate and silicate influenced the carbon to nitrate ratio in biomass with higher Si:N ratios promoting higher C:N ratios (Goldenberg et al., 2022). Although a higher carbon-to-nutrients stoichiometry in organic matter is desired for enhanced carbon uptake via the biological carbon pump, organic particle properties have changed in lockstep towards reduced sinking speeds with negative implications for export production, respiration depth and sequestration time scales (Baumann et al., 2021, Baumann et al., 2023). Enhanced carbon content in organic matter did as well alter the ecosystem food web, since higher C:N biomass has less nutritional value for higher trophic levels (Goldenberg et al., 2024). The finding of enhanced C:N ratios in biomass via artificial upwelling is unexpected and in contradiction to observed C:N ratios in natural upwelling systems and might be an artefact of the mesocosm's experimental setup, since higher nutrient availability is generally associated with lower carbon-to-nutrient ratios in biomass (Moreno and Martiny 2018). Other expected changes via artificial upwelling, such as the cooling of sea surface temperature via the upwelling of cold deep water or the carbon sequestration time scale, cannot be investigated due to the nature of performed mesocosm experiments. We can conclude from these mesocosm experiments that the response of the marine ecosystem to artificial upwelling is quite complex and depends on several variables such as added nutrient ratios and concentrations, but primary production and the production of sinking organic particles overall increased. However, we cannot make reliable assumptions based on these experiments on e.g., changes in organic matter respiration depths below the mesocosm's depth and thus, quantitative assessments on the long-term carbon uptake potential of artificial upwelling.

As a third option, we can investigate upscaled artificial upwelling in Earth system models and diagnose its impact on the main Earth system components such as the global carbon cycle and individual carbon reservoirs. The great advantage of Earth system models, in contrast to e.g., mesocosm experiments, is the capability of quantitatively diagnosing carbon-cycle relevant processes such as changes in export production, carbon sequestration depths and time scales, as well as making predictions via running the model in a transient into an imagined future (O'Neill et al., 2016). Additionally, idealized model tracers can be implemented in Earth

system models, which can provide further information on e.g., the age of the water in the deep ocean since it was last in contact with the atmosphere (Koeve et al., 2015), concentrations of preformed and remineralized nutrients in the ocean interior, as well as the fraction of the ocean carbon inventory attributable to the biological carbon pump (Frenger et al., 2024). The main disadvantages of Earth system models are their reduced complexity via simplifications and coarse horizontal and vertical resolution in an effort to reduce computational costs.

Several independent simulations have already been performed in different Earth system models with different implementations of artificial upwelling. While some studies found little to none atmospheric CO_2 reduction via globally applied artificial upwelling (Dutreuil et al., 2009, Yool et al., 2009), others found higher and up to 138 Gt carbon removed from the atmosphere over 80 years until the end of this century following a maximum CDR potential approach (Oschlies et al., 2010, Keller et al., 2014), but an in-depth and quantitative analysis on the processes, which caused the additional ocean carbon uptake, is missing. At the same time, severe side effects occurred as a consequence of large scale artificial upwelling deployment such as the increase in N_2O production (Dutreuil et al., 2009) and storage of additional heat in the ocean interior, which radiates back into the atmosphere, if artificial upwelling is abruptly stopped (Oschlies et al., 2010). The upwelling of cold water to the ocean surface also cooled down the atmosphere, decreased global mean surface air temperature and indirectly influenced the terrestrial carbon cycle towards an increased land carbon sink (Oschlies et al., 2010, Keller et al., 2014). Overall, the current body of literature on the CDR-potential of artificial upwelling simulated in Earth system models lacks a refined understanding of the underlying process stimulated via artificial upwelling.

1.3.2. Open scientific questions

Since artificial upwelling has been initially proposed as a biology-driven marine CDR method, fundamental questions such as a possible CO_2-path dependency of additional ocean carbon uptake via artificial upwelling and the underlying mechanisms have not been quantitatively investigated. We already know from natural upwelling systems that physical-chemical changes in the surface ocean induced via upwelling (e.g., surface temperature changes) can as well influence the response of the carbon cycle (Jiao et al., 2004, Fey et al., 2024). In addition, Earth system model studies indicated a direct impact of artificial upwelling on Earth's heat budget (Oschlies et al., 2010, Keller et al., 2014), which is triggered via the

upwelling of cold water to the surface ocean, but a quantitative analysis of changes in global mean surface air temperature as a consequence of changes in the carbon cycle versus changes in Earths heat budget has so far not been done. Furthermore, the response of the ecosystem and potential carbon uptake via the biological carbon pump in natural upwelling systems is shaped by the amount of upwelled preformed nutrients and the availability of iron (Martin et al., 1990, Hutchins et al., 1998, Hutchins et al., 2002, de Baar et al., 2005, Pollard et al., 2006, Chase et al., 2007, Duteil et al., 2012), but both variables have so far not been considered and quantitatively investigated in terms of their impact on the CDR-potential of artificial upwelling. As a consequence, we currently lack a fundamental understanding under which conditions artificial upwelling might work as a marine CDR method and which are the driving processes. The aim of this thesis is to use the UVic 2.9 Earth system model of intermediate complexity to simulate large-scale artificial upwelling to expand our knowledge on the CDR potential of artificial upwelling and to develop a refined and quantitative understanding of the stimulated processes to close these fundamental knowledge gaps.

1.4. Outline and authors contribution

This thesis is a contribution to the scientific understanding of a possible, future, large scale artificial upwelling deployment and its impact on Earth's ecosystem, heat budget and main carbon reservoirs via the simulation of artificial upwelling in the UVic 2.9 Earth system model of intermediate complexity. A specific focus lies on the development of a refined and quantitative understanding of the underlying processes and co-dependencies stimulated via artificial upwelling.

Chapter 2 examines the impact of the future CO_2-emission pathway on the maximum additional ocean carbon uptake potential of artificial upwelling and quantifies the individual contributions via the biological carbon pump and the solubility pump. This chapter is based on a paper that is already published in Geophysical Research Letters. Wolfgang Koeve and Malte Jürchott designed the study, Wolfgang Koeve carried out the model experiments and Malte Jürchott performed the data analysis. Malte Jürchott wrote the paper with contributions from Andreas Oschlies and Wolfgang Koeve.

Chapter 3 discusses the effects of iron-limitation and ocean iron fertilization on additional ocean carbon uptake via globally and regionally simulated artificial upwelling. This chapter is

based on a paper, which has been submitted to Environmental Research Letters and is under review. Malte Jürchott, Wolfgang Koeve and Andreas Oschlies designed the study. Malte Jürchott carried out the model experiments and performed the data analysis. Malte Jürchott wrote the paper with contributions from Wolfgang Koeve and Andreas Oschlies.

Chapter 4 explores the impact of artificial upwelling on Earth's main carbon reservoirs in relation to its impact on global mean surface air temperature and underlying co-dependencies. This chapter is based on a manuscript in preparation. Malte Jürchott designed the study, carried out the model experiments and performed the data analysis. Malte Jürchott wrote the manuscript with contributions from Andreas Oschlies, Nadine Mengis, Iyy Frenger and Wolfgang Koeve.

2. Artificial Upwelling – A Refined Narrative

This chapter contains an already published article (see citation below). I adjusted the text and figure, table and page numbering of the article to fit with the format of the overall thesis document. Please refer to the original paper published by Geophysical Research Letters.

Citation: Jürchott, M., Oschlies, A., & Koeve, W. (2023). Artificial upwelling—A refined narrative. Geophysical Research Letters, 50(4), e2022GL101870. doi: 10.1029/2022GL101870

Abstract

The current narrative of artificial upwelling (AU) is to translocate nutrient rich deep water to the ocean surface, thereby stimulating the biological carbon pump (BCP). Our refined narrative takes the response of the solubility pump and the CO_2 emission scenario into account. Using global ocean-atmosphere model experiments we show that the effectiveness of a hypothetical maximum AU deployment in all ocean areas where AU is predicted to lower surface pCO_2, the draw down of CO_2 from the atmosphere during years 2020-2100 depends strongly on the CO_2 emission scenario and ranges from 1.01 Pg C / year (3.70 Pg CO_2 / year) under RCP 8.5 to 0.32 Pg C / year (1.17 Pg CO_2 / year) under RCP 2.6. The solubility pump becomes equally effective compared to the BCP under the highest emission scenario (RCP 8.5), but responds with CO_2 outgassing under low CO_2 emission scenarios.

2.1. Introduction

Earths' atmospheric CO_2 concentration (pCO_2^{atm}) has strongly increased since preindustrial times and continues to rise despite considerable CO_2 emission reduction efforts (IPCC, 2022). Assuming that humanity ambitiously intensifies emission reduction efforts, we still have to deal with hard-to-abate CO_2 emissions (Thoni et al., 2020). To compensate these residual emissions and reach a net zero carbon emission world around mid century, we likely need to actively remove CO_2 from the atmosphere (IPCC, 2022), which has led to an increased interest in marine carbon dioxide removal (CDR) technologies (GESAMP, 2019).

One proposed marine CDR idea is to use artificial upwelling (AU) to pump up nutrients from the interior ocean to the sea surface via ocean pipes to stimulate the biological carbon pump (BCP) (Lovelock & Rapley, 2007). This process is supposed to enhance primary production at the sea surface, thereby increase export production and finally lead to a net CO_2 flux from the atmosphere into the interior ocean. Several studies have already shown that this simplistic view of stimulating the BCP (Volk & Hoffert, 1985) via AU is not sufficient for a comprehensive evaluation of this technology in terms of its carbon drawdown potential and its climate effects (Dutreuil et al., 2009; Yool et al., 2009; Oschlies et al., 2010; Keller et al., 2014). Especially pumping up water with a high concentration of dissolved inorganic carbon (DIC) may even lead to a net CO_2 outgassing despite an increase in export production (Dutreuil et al., 2009). Nevertheless, the prevailing narrative of viewing AU and it's CDR potential as being primary driven by the BCP, and therefore independent of the underlying CO_2-emission scenario, still remains (GESAMP, 2019; Baumann et al., 2021; Koweek, 2022).

One may be tempted to argue that AU in a fixed C-N-P stoichiometry ("Redfield") world model should result in a net zero carbon uptake through the BCP. However, pumping up preformed nutrients (Duteil et al., 2012) to the sea surface may contribute to an additional carbon uptake. AU will also affect properties such as alkalinity, sea surface temperature and preformed DIC, which collectively may cause a response of the solubility pump (Volk & Hoffert, 1985) with the potential to influence the atmosphere to ocean carbon flux, too. Also the dependence of the CO_2-uptake due to AU on the atmospheric pCO_2 path (the assumption of the underlying CO_2 emission scenario) under which it takes place is not well understood.

To get a better understanding of the effects of AU and the processes involved, we simulate AU in an Earth System model of intermediate complexity combined with an idealized tracer approach and under a range of CO_2 emission scenarios to (i) evaluate the general impact of

AU on the ocean's carbon uptake under different CO_2 emission scenarios, (ii) to explicitly quantify the respective importance of the BCP and the solubility pump in the model simulations, and (iii) to identify the important carbon uptake, release and storage regions in the ocean.

2.2. Methods

2.2.1. Model

We use the UVic 2.9 Earth System model of intermediate complexity (Weaver et al., 2001; Keller et al., 2012) in a noLand configuration with a dynamically coupled atmosphere, sea-ice and ocean component (Gent & McWilliams, 1990; Orr et al. 1999; Koeve et al., 2020). A detailed description of this model version is given in the supplementary methods section. The three-dimensional ocean component has a spatial resolution of 3.6° longitude and 1.8° latitude and consists of 19 vertical levels with 50 m thickness close to the surface and up to 500 m in the deep ocean. The used model version contains a fully simulated carbon cycle including dissolved inorganic carbon (DIC) and alkalinity as prognostic tracers, a marine ecosystem model representation of the BCP in which we assume a fixed C-N-P organic matter stoichiometry (Keller et al., 2012), as well as a simple $CaCO_3$ counter pump approximation (Schmittner et al., 2008). In the model primary production is not sensitive to CO_2 and the nutrients nitrate and phosphate are simulated as prognostic tracers, while iron-limitation is prescribed via an iron concentration mask at the oceans surface layer (Galbraith et al., 2010).

In our UVic 2.9 noLand model version all interactions with the land-component are disabled in order to isolate the effects of AU exclusively on the ocean. The use of a noLand model allows us to better understand and distinguish the involved processes and effects of AU especially on the marine carbon cycle.

2.2.2. Simulating AU

The simulation of AU is adopted from previous studies conducted with an earlier version of the UVic model (Oschlies et al., 2010; Keller et al., 2014). Model tracers like nutrients, temperature, DIC and alike are transferred via AU adiabatically from the lowest grid box at

the end of the pipes to the surface grid box at a rate of 1 cm/day averaged over the area of the grid box, while a compensating down-welling flux through all intermediate levels ensures volume conservation. AU-induced changes in e.g. the temperature depth profile change water column physics, circulation and impact the simulated ecosystem. To replace 1 cm/day of surface water it would be necessary to deploy a dense network of pipes, e.g. with one pipe per square kilometer, each with a volumetric flow rate of about 0.12 m^3/s (Koweek, 2022). A deployment algorithm is used at model runtime to automatically deploy the ocean pipes only where (a) the phosphate concentration is lower than a threshold concentration at the sea surface (0.4 $mmol/m^3$ in this study) and (b) complete uptake of upwelled macronutrients would lead to a reduction in local surface-water pCO_2 (Fig. 2.1c, S 2.1 and S 2.2a). This procedure ensures that pipes are only deployed in regions where CO_2 outgassing is unlikely. It turns out that almost all regions where pipes meet these conditions for deployment at any time during the simulation, subsequently maintain these conditions throughout the simulations. Additionally, the length of the pipes is limited to 1000 m and optimized by the algorithm to maximize for additional local CO_2-uptake (Fig. S 2.2b). Besides upwelling nutrients, AU has an impact on all other tracers including DIC, alkalinity, salinity and temperature. Since our model does not include a dynamic iron cycle, we follow the approach of Keller et al. (2014) and assume that AU relaxes any iron limitation at the sea surface in regions where pipes are deployed. Hence, our experiments considered a best-case scenario for the impact of a close to global application of AU on a Redfield-like BCP.

2.2.3. Separation of marine carbon pumps

The separation of the marine carbon pumps is achieved by introducing two idealized tracers to the model, which measure the individual impact on the carbon cycle via the BCP (DIC^{rem}) and the solubility pump (DIC^{pre}) (Bernardello et al., 2014; Koeve et al., 2020). The idealized tracer DIC^{rem} is set to zero upon any contact with the atmosphere and increases in the interior ocean by the amount of DIC released into the water column via organic matter degradation, thus exclusively counting the amount of DIC tracing back to the BCP. The idealized tracer DIC^{pre} adopts the value of total DIC at the surface layer and preserves it while being transported to greater depth through ocean circulation. Therefore, DIC^{pre} exclusively counts the amount of DIC added to the interior ocean via physical-chemical processes at the ocean's surface that are associated with the solubility pump. There is no explicit idealized tracer of

DIC stored in the interior ocean by means of the $CaCO_3$ counter pump. DIC^{ca}, however, may be diagnosed from $DIC^{ca} = DIC - DIC^{pre} - DIC^{rem}$. As discussed below, any change in DIC^{ca} should not be confused with the impact of a changing $CaCO_3$ counter pump on atmospheric pCO_2. The idealized tracer Ideal-Age (calculated similar compared to DIC^{rem}) counts the time of a water mass since it was last in contact with the atmosphere and therefore, provides additional information about the age of a water mass in the interior ocean (England, 1995; Koeve & Kähler, 2016). All three idealized tracers are influenced by ocean circulation and mixing, but do not interact with other model tracers.

2.2.4. Experimental Design

Table 2-1: Model experiments conducted with the UVic 2.9 ESM noLand model version.

Name	Emission Forcing	Pipe Simulation
REF_0.0	no-emission	No Pipes
REF_2.6	RCP 2.6	No Pipes
REF_4.5	RCP 4.5	No Pipes
REF_6.0	RCP 6.0	No Pipes
REF_8.5	RCP 8.5	No Pipes
ArtUp_0.0	no-emission	Pipes
ArtUp_2.6	RCP 2.6	Pipes
ArtUp_4.5	RCP 4.5	Pipes
ArtUp_6.0	RCP 6.0	Pipes
ArtUp_8.5	RCP 8.5	Pipes

Following model spin-up under preindustrial conditions we simulate the historical period from the year 1765 to 2006 with CO_2-emissions to the atmosphere, which are consistent with historical fossil fuel and land-use carbon emissions and apply from 2006 to 2100 different CO_2-emission forcings consistent with RCP 2.6, 4.5, 6.0 and 8.5 (Meinshausen et al., 2011), which are corrected for the noLand model configuration (Tab. 2.1, Fig. S 2.3 and Supplementary Methods) (Koeve et al., 2020). This makes sure that the noLand reference model experiments (REF) experience the same climate change as do fully coupled (with Land) counterparts. An idealized no-emission model simulation applies AU in a hypothetical world without any historical or future CO_2 emissions. We simulated the effects of AU in the

ArtUp-simulations for the time period 2020 to 2100 and performed respective reference simulations without AU for comparisons. By comparing the ArtUp- to the Reference-simulation (i.e. ArtUp – REF) conducted under the same CO_2 emission scenario we can explicitly study the effects of applied AU. We compared these results with respect to the different CO_2 emission scenarios to study the effectiveness of AU under different CO_2 emission scenarios.

2.3. Results

2.3.1. Impact of AU on the Ocean's Carbon Budget

AU leads to a carbon drawdown from the atmosphere into the ocean in comparison to the respective reference simulation (REF), while the additional ocean's carbon uptake is strongly dependent on the RCP CO_2 emission scenario over the course of the experiments (Fig. 2.1b, d). Under the RCP 8.5 and RCP 6.0 CO_2 emission scenarios, AU leads to an almost linear and continuous carbon drawdown from the atmosphere into the ocean (on average 1.01 Pg C / year for RCP 8.5; multiply by 3.664 for conversion to Pg CO_2), while the carbon drawdown under the RCP 4.5 CO_2 emission scenario starts to slow down after 50 years of pipe deployment. Under the RCP 4.5 CO_2 emission scenario the cumulative carbon drawdown after 80 years is already ~50% less compared to the RCP 8.5 CO_2 emission scenario simulation. The RCP 2.6 CO_2 emission scenario and the no-emission simulation show an even earlier and stronger decline in the ocean's AU-induced carbon uptake, until they reach a plateau after a few decades (on average 0.32 Pg C / year for RCP 2.6). The model simulations show that the potential of AU to draw down carbon from the atmosphere increases with higher CO_2 emission scenarios, while the carbon drawdown potential decreases and even stagnates under lower CO_2 emission scenarios.

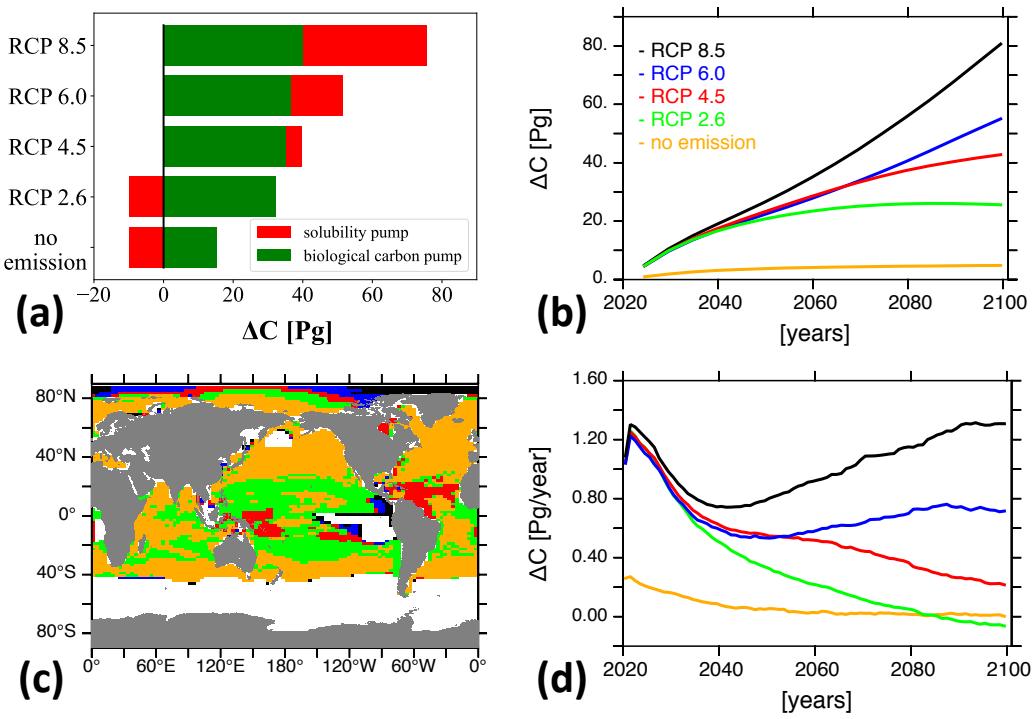

Figure 2-1: Pipe covered area and global carbon uptake from AU. (a) Cumulative net increase in the ocean's carbon budget in the year 2100 (Pg C) due to AU, divided into the individual carbon uptake of the BCP (green) and the solubility pump (red). Time history of (b) cumulative and (d) annual average net increase in the ocean's carbon budget via AU compared to respective reference simulation for different CO_2 emission scenarios (ArtUp – REF; Pg C, see Fig S 2.4 as well). (c) Pipe covered area in year 2100 (plotted pipe covered area of each emission scenarios includes the area of lower CO_2 emission scenarios); color code as indicated in (b); see Fig S 2.1 and S 2.2a for details).

2.3.2. Biological Carbon Pump vs. Solubility Pump

In the global deployment scenario, the BCP responds to AU under every CO_2 emission scenario by an additional carbon uptake and only shows a moderate emission scenario dependency, while the solubility pump shows a strong emission scenario dependency and can even release carbon into the atmosphere and thereby counter the BCP uptake under low emission scenarios (Fig. 2.1a). Since we apply a fixed C-N-P stoichiometry for primary production and degradation in our model, the additional carbon uptake via the BCP cannot be explained by pumping up re-mineralized nutrients, but by introducing preformed nutrients from the interior ocean to the sea surface (Fig. 2.2a). Preformed nutrients are nutrients, which leave the surface ocean by circulation, particularly in temperate and high latitude regions, without being taken up by primary producers e.g. due to iron or light limitation and do not come with a Redfield-equivalent CO_2 counterpart (Fig. S 2.5). Thus, preformed nutrients can lead to an additional carbon uptake via the BCP. The fixed stoichiometry also implies that pumping up DIC^{rem} to the sea surface will not lead to an outgassing of CO_2 into the

atmosphere as long as its re-mineralized nutrient counterpart gets taken up close to the pipes by primary producers again.

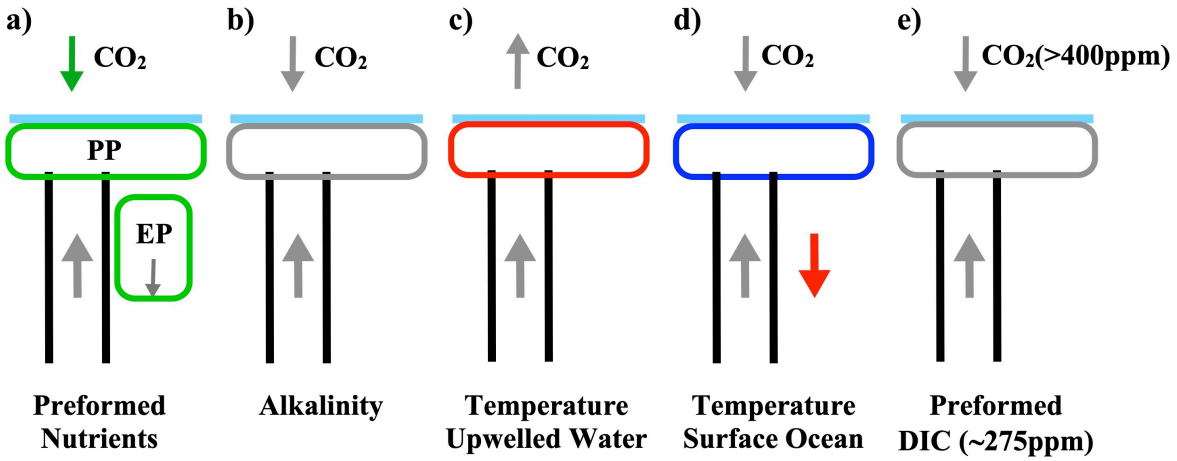

Figure 2-2: Theoretical concept of the processes stimulated by AU (black lines) and their impact on the air-sea CO_2 flux and the surface ocean (box below air-sea boundary). Arrows in the atmosphere indicate air-sea CO_2 flux direction, arrows in the ocean indicate tracer movement and colors red / blue indicate respective water temperature increase / decrease. (a) Covers the increase in primary production (PP) and export production (EP) associated with the BCP (green), (b) to (e) cover the impacts of the individual processes associated with the solubility pump.

The response of the solubility pump can be explained by a combination of several processes including pumping up alkalinity, preformed DIC and changes in water temperature. In the global average, the alkalinity concentration in our model increases with depth due to $CaCO_3$ production at the sea surface and dissolution in the interior ocean (Fig. S 2.6a). By simulating AU we pump up alkalinity, on average, which translates into alkalinity enhancement at the sea surface similar to what is intended by artificial ocean alkalinity enhancement by adding minerals like olivine to the ocean surface (Köhler et al., 2010; Hartmann et al., 2013). Ocean alkalinity enhancement is associated with a CO_2 flux from the atmosphere into the ocean (Fig. 2.2b) (Keller et al., 2014), but since the amount of alkalinity added to the sea surface is about the same under every emission scenario in our experiments (Fig. S 2.6b), we do expect a similar CO_2-uptake effect and therefore, this process can most likely not explain the dependency of the solubility pump to the emission scenario. AU also results in a change in water temperatures, since the water pumped up from the deep ocean is significantly colder compared to the surface water. At the surface, the pumped up water increases in temperature (decrease in max. CO_2-solubility; Fig. 2.2c), while it is cooling down the surface ocean at the same time (increase in max. CO_2-solubility; Fig. 2.2d). Both carbon fluxes related to

temperature effects will partly counteract each other, but since, over the area where pipes are deployed, the relative temperature increase of the pumped up water is much greater than the relative temperature decrease of the surface water (Fig. S 2.7), the net effect on the carbon flux is expected to result in CO_2 outgassing into the atmosphere. Furthermore, AU pumps up DIC^{pre} from the interior ocean to the sea surface and in contact with the atmosphere (Fig. 2.2e). DIC^{pre} is the amount of carbon taken up by the ocean via physical-chemical processes and its concentration in the interior ocean strongly depends on the pCO_2^{atm} concentration and water temperature at the time and location of the water mass formation region. The water pumped up is mostly old enough to be equilibrated under preindustrial pCO_2^{atm} levels (~275 ppm; Fig. 2.3c) and bringing it in contact with an elevated pCO_2^{atm} level (>400 ppm, except for the no-emission scenario) results in a carbon flux from the atmosphere into the ocean, which also increases under higher emission scenarios (Fig. S 2.8). While a quantitative separation of the individual processes influencing the response of the solubility pump is challenging (and beyond the scope of this paper), we propose from the discussion above that the outgassing under the RCP 2.6 emission scenario is most likely dominated by the temperature increase of the pumped-up water. Under higher emission scenarios the positive impact of pumping up water to the sea surface, which had been equilibrated under preindustrial atmospheric CO_2 levels exceeds the negative impact of the temperature increase of the pumped up water mass.

2.3.3. Carbon Storage Depths and Location

For the RCP 8.5 emission scenario 56.1 Pg C (69.5 %) of the AU-induced air-sea carbon flux gets added below the maximum pipes source depths of 1200m and can be referred to as stored over the next centuries (Tab. S 2.1) (Lampitt et al., 2008; Siegel et al., 2021). Using pump-specific tracers, we diagnose individual shares of 11.6 Pg C (20.7 %) for the BCP and 22.6 Pg C (40.2%) for the solubility pump. The remaining 21.9 Pg C (39.1%), computed as residual (see Methods), is assumed to be associated with the carbon export via the $CaCO_3$ counter pump (but see discussion below). Therefore, 63.5% of the total carbon taken up via the solubility pump and only 29% of the total carbon taken up via the BCP gets stored below 1200m. The inefficiency of the BCP to add carbon below 1200m gets amplified through AU by a reduction in the global transfer efficiency (T_{eff}) of -7.2% (Tab. S2.2). The transfer efficiency, here calculated as the integral of remineralized $detritus^{\geq 1200m}$ / remineralized

detritus$^{\geq 130m}$, gives an estimate of how strong the organic matter degradation is between the carbon export depth and the carbon storage depth. A reduction in T_{eff} triggered by AU indicates a higher organic matter degradation rate between 130m and 1200m (reasons discussed below). Overall, the budget changes of DIC, DIC^{pre} and DIC^{rem} show that a substantial amount of the carbon added to the ocean via AU gets stored below the maximum source depths of the pipes, with the solubility pump showing a high efficiency in transporting the additional carbon to the deep ocean.

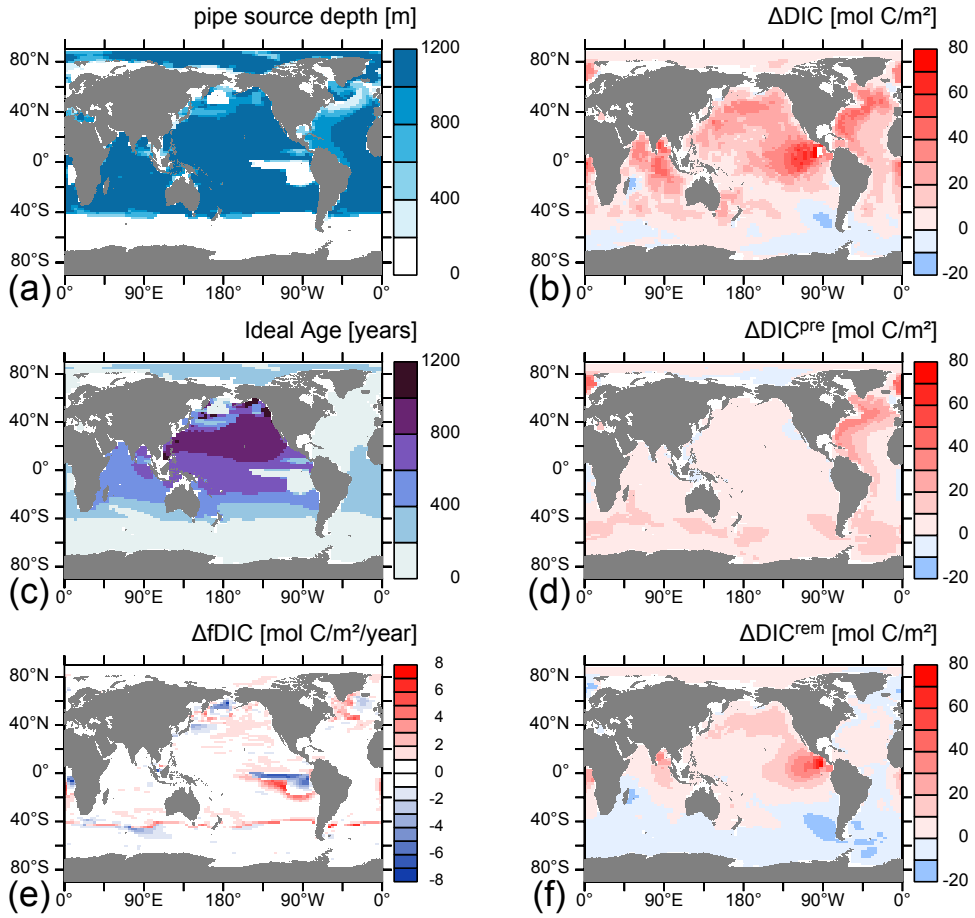

Figure 2-3: Regional effects of AU for experiments under the RCP 8.5 emission scenarios for the year 2100. (a) Pipe distribution and pipe source depth (m). (c) Average age (since last contact with the atmosphere) of water at pipes source depth (years). (e) CO_2 flux at ocean-atmosphere boundary (positive downward; mol C m^{-2} $year^{-1}$). (b, d, f) Cumulative net change in DIC (b), DIC^{pre} (d) and DIC^{rem} (f) below 1200m depths from 2020-2100 compared to the respective reference simulation (ArtUp – REF; mol C/m^2).

The increased carbon uptake of the ocean via AU below 1200m is unevenly distributed in the ocean with hotspots in the North Atlantic, North Pacific and around the equator (Fig. 2.3b). The solubility pump is the main driver for the additional carbon storage in the North Atlantic

(Fig. 2.3d). The additional carbon uptake of the solubility pump has its origin at the atmosphere to ocean boundary (Fig. 2.3e) and the shallow pipes in the north Atlantic (Fig. 2.3a) cannot explain the carbon transport below the pipes source depth. Thus, we propose that one contributing factor to the high efficiency of the solubility pump in this region is the large-scale ocean circulation. The CO_2-uptake via the BCP below 1200m related to AU is dominated by the central-east Pacific region (Fig. 2.3f). This region has a strong naturally occurring stratification, which gets first undermined by the pipe's pumping action and second weakened by the temperature exchange between the surface water and the deep ocean. Thus, the temperature gradient between the surface water and the deep ocean decreases and allows preformed nutrients to enter the surface ocean more efficiently. This results in an additional carbon uptake via an enhanced BCP and leads to a greater export of DIC^{rem} below 1200m.

2.4. Discussion

The residual portion of 21.9 Pg C below 1200 m that is attributed neither to the BCP nor to the solubility pump, is associated with the $CaCO_3$ counter pump. This additional deep carbon flux leaves the impression of the $CaCO_3$ counter pump being important in terms of additional ocean CO_2-uptake, but, as is well known, the $CaCO_3$ counter pump cannot constitute a CO_2 flux into the ocean due to its flux of alkalinity being twice as high as the DIC flux (Riebesell et al., 2009). In our model, the production of $CaCO_3$ is linked to the detritus production of the ecosystem model (see suppl. Methods) and thus, gets indirectly stimulated via any increase in primary production. However, more intensive $CaCO_3$ export from the surface ocean would reduce the surface ocean CO_2-buffer capacity and reduce CO_2-uptake via the solubility pump. Due to the non-linearity of the CO_2 system it is not straightforward to quantify how the apparent storage (i.e. increase in DIC^{ca}, Fig. S 2.9) associated with this increase of the $CaCO_3$ counter pump translates into a CO_2-flux between ocean and atmosphere.

Concerning the reduction of the transfer efficiency under AU, we propose that this might be a result of an increase in water temperature below the cooled surface layer (Fig. S 2.10). Organic matter degradation speeds up under higher water temperatures, which results in shallower degradation depth. AU and the compensating downward flow result in a net downward heat flux to greater depth. This side effect of AU was discovered and discussed in previous papers and causes, after AU termination, a strong increase in surface air temperature and pCO_2^{atm} levels beyond the reference simulations (Oschlies et al., 2010; Keller et al.,

2014). Here we report that the AU-induced heat transport to greater depth also has a negative impact on the organic matter transfer efficiency during AU deployment.

Discussing the limits of our study, the used noLand model configuration does not allow for feedbacks of ocean-atmosphere interactions on the land component and vice versa. In our idealized model study, surface ocean and atmospheric cooling via AU hence does not increase the carbon uptake on land as reported in previous studies (Oschlies et al., 2010; Keller et al., 2014), nor does this land CO_2-uptake potentially affect the marine CO_2-uptake. Therefore, the earth's net carbon uptake via AU presented in our study might be higher, if the land biosphere component is included. Changes in our experimental protocol in how AU is simulated (e.g. pipe covered area, pipe length, upwelled volume, duration period, iron limitation) might change the ocean's net carbon uptake and the individual contributions via the solubility pump and the BCP as well (Yool et al., 2009; Oschlies et al., 2010; Koweek, 2022).

2.5. Conclusion and outlook

Our results indicate that only addressing processes associated with the BCP does not accurately reflect the CDR potential of AU. The additional carbon uptake of the ocean is strongly dependent on the CO_2 emission scenario. The BCP is able to take up additional carbon in the assumed global AU deployment under every emission scenario, but shows a low efficiency in exporting DIC^{rem} below the maximum pipe source depth of 1200m except for the central-east Pacific region. This suggests that most of the CO_2-uptake stimulated by AU and attributable to an increase of the BCP will potentially be rather short lived. The main driver for the AU-enhanced BCP is the decreased stratification and the increased access of primary producers to preformed nutrients, while the decrease in the transfer efficiency might be a side effect of faster organic matter degradation due to higher water temperatures below the sea surface.

The solubility pump shows a strong CO_2 emission scenario dependency and can lead to CO_2 outgassing under low emission scenarios, which can almost completely mitigate the additional CO_2-uptake via the BCP. Under high emission scenarios, the solubility pump can also take up equal amounts of additional CO_2 compared to the BCP. The solubility pump shows a high efficiency in exporting DIC^{pre} below the maximum pipes source depth and the large-scale

ocean circulation in the North Atlantic including deep-water formation seems to play a key role in this regard.

Additional studies including new model experiments might be able to quantify the single processes associated with the solubility pump and to further investigate the high efficiency CO_2 export regions identified in this study. Going beyond the Redfield world and assuming higher C-N ratios in organic matter produced via AU as proposed recently from experimental work (Baumann et al., 2021), as well as simulating the potentially limited supply of iron (Tagliabue et al., 2017) in pipe-covered areas could further impact projections of the quantitative potential of the biological carbon pump in this CDR technique.

Acknowledgement

We acknowledge discussions with colleagues from the Biogeochemical Modelling research unit at GEOMAR. M.J. acknowledges funding from German BMBF, Project Test-ArtUp (Grant Number: 03F0897A). This is a contribution to the CDRmare research mission funded by the German Alliance for Marine Research (DAM). The author(s) wish to acknowledge use of the PyFerret program for analysis and graphics in this paper. PyFerret is a product of NOAA's Pacific Marine Environmental Laboratory (Information is available at http:// ferret.pmel.noaa.gov/Ferret/). Open Access funding enabled and organized by Projekt DEAL.

Data statement

Model output and scripts for data processing are available from data.geomar.de (https://hdl.handle.net/20.500.12085/9e4c269c-8fa3-4bb9-994f-e8c7a5cdefbb)

2.6. Supporting Information

Introduction

Here we provide Supplementary Methods (Text S1), Supplementary Tables (S 2.1 to S 2.2) and Supplementary Figures (S 2.1 to S 2.10), which present details of our model experiments.

Text S1.

Supplementary Methods

UVic model

Model experiments are carried out with an ocean-sea-ice-atmosphere version of the UVic Earth System Model Version 2.9 (UVic-2.9.WK2021.noLand) as described in Koeve et al. (2020). UVic (Weaver et al., 2001) is an Earth system model of intermediate complexity (EMIC). Horizontal resolution is 3.6° in longitude and 1.8° in latitude direction. The ocean circulation model (MOM, Modular Ocean Model 2) includes physical parameterizations for diffusive mixing along and across isopycnals and eddy induced tracer advection (Gent & McWilliams, 1990). It has 19 vertical layers and layer thickness increases from 50 m at the surface to 500m in the deep ocean. Wind forcing is prescribed with monthly mean winds from NCAR/NCEP climatological data. The ocean biogeochemistry of this model is described in Keller et al. (2012). In short, the model simulates the nutrients phosphate and nitrate, two groups of phytoplankton (diazotrophs and ordinary phytoplankton), zooplankton, particulate detritus with explicit sinking, oxygen, total dissolved inorganic carbon (DIC) and alkalinity (ALK) as prognostic tracers. Production and degradation of organic matter affect nutrients, oxygen, DIC and ALK with a fixed elemental stoichiometry. Gas exchange of oxygen and DIC is simulated as in Orr et al. (1999). A diagnostic $CaCO_3$ cycle further shapes the distribution of DIC and ALK (Schmittner et al., 2008). The model includes a simple parameterization of iron limitation based on an iron concentration mask adopted from the BLING model (Galbraith et al., 2010). In order to avoid excessively long model spin-up times our idealized model experiments do not simulate sediment processes. Any organic detritus or $CaCO_3$ reaching the bottom of the model is dissolved in the deepest wet box instantaneously.

UVic-2.9.WK2021 includes a number of idealized model tracers, which allow us to measure the individual impact on the carbon cycle via the biological (soft tissue) carbon pump (DIC^{rem}) and the solubility pump (DIC^{pre}) (Bernardello et al., 2014; Koeve et al., 2020). This model version includes a suite of preformed tracers (preformed phosphate, PO_4^{pre}; preformed oxygen, O_2^{pre}; preformed DIC, DIC^{pre}; preformed alkalinity, ALK^{pre}). In the surface ocean (k=1) preformed tracers are set at every time step to the value of the respective bulk tracer (e.g.$PO_4^{pre} == PO_4$). In the interior ocean preformed tracers behave like a passive tracer, i.e. they do not have biogeochemical sinks or sources, while being transported and mixed by the ocean's circulation. DIC^{pre} is the preformed tracer of particular interest in this study as it allows us to quantify any changes in solubility pump carbon (see below). For the bulk tracers PO_4, O_2, DIC, ALK, we further simulate several tracers, which accumulate biogeochemical sinks and sources, but are set to zero in the surface ocean (k=1). DIC^{rem} is the respective tracer for the carbon uptake via the biological carbon pump. DIC^{rem} accumulates the sinks and source of organic matter degradation and production below the surface layer (k=1). The tracer behaves similar to the true oxygen utilization tracer (TOU-tracer) employed in Koeve et al. (2020). The idealized tracer Ideal-Age counts the time of a water mass below the surface layer (k=1), since it was last in contact with the atmosphere and therefore, provides additional information about the age of a water mass in the interior ocean (England, 1995; Koeve & Kähler, 2016). All previous mentioned tracers (except Ideal-Age) have the unit of mol m^{-3} in the model output.

Simulation of artificial upwelling

The simulation of artificial upwelling is adopted from previous studies conducted with an earlier version of the UVic model (Oschlies et al., 2010; Keller et al., 2014). Model tracers like nutrients, temperature, DIC and alike are transferred adiabatically from the lowest grid box at the end of the pipes to the surface grid box to simulate the effects of artificial upwelling on the ocean and atmosphere. The length of artificial upwelling pipes does not exceed 1000m and the velocity of upwelled water from the source depth to the surface layer is assumed to be 1cm/day averaged over the area of the grid box. A compensating down-welling flux through all intermediate levels ensures volume conservation. All prognostic tracers, which could have an impact on the stratification or the carbon cycle in the model are pumped up via artificial upwelling (e.g. temperature, DIC, ALK, PO_4, NO_3, O_2). Since our model does not include a dynamic iron cycle, we follow the approach of Keller et al. (2014) and assume

that artificial upwelling relaxes any iron limitation at the ocean surface (k=1) in regions where pipes are deployed (other primary production limiting factors such as light limitation are not affected by artificial upwelling and can limit nutrient uptake). This may be an overly optimistic assumption, since iron concentrations in the ocean interior are under control of scavenging by organic and inorganic particles causing elevated nutrient to dissolved iron ratios in the ocean interior (Tagliabue et al., 2017). Hence, our experiments considered a best-case scenario for the impact of artificial upwelling on a Redfield-like biological pump with constant element ratios (in particular $r_{C:P} = 106$).

The locations in which pipes are switched on and the source length of the pipes are decided at every time step by an algorithm, which is designed to maximize additional carbon uptake of the ocean and takes several initial conditions into account. First, pipes are not switched on in regions with a PO_4 surface water concentration greater than 0.4 mmol m^{-3} assuming that these regions are not limited by macronutrients and adding more nutrients from greater depth to the surface would not result in an enhancement of the biological carbon pump. Second, pipes are not switched on in regions and at depths, where a short term outgassing of CO_2 into the atmosphere is projected. This projection is based on the vertical distribution of tracers and the current pCO_2^{atm} (no horizontal water mass mixing or circulation taken into account by the runtime algorithm). For each of the potential source depth levels (k=2 to k=8), a potential seawater $pCO_2(k)$ is computed from T(k), S(k), ALK(k) and $DIC(k) – (PO_4(k) - PO_4(1))*r_{C:P}$ assuming surface pressure. This assumes complete utilization of upwelled nutrients (e.g. no iron or light limitation). The algorithm selects the k-level (hence pipe length) for which a maximum difference between the current surface pCO_2 and the potential $pCO_2(k)$ is found, i.e. which offers the maximum potential carbon drawdown into the ocean. If this difference is negative, pipes are turned off. Changes over time in the pipe covered area and the global average pipe length are shown in Fig. S 2.1 and S 2.2.

We note that the ‘projected’ pCO_2-difference is not necessarily identical with the surface pCO_2 difference between the artificial upwelling experiment and its respective reference run, in particular since the algorithm does not know about the surface pCO_2 in the independent reference experiment (see next section for details). Despite this limitation, regions with pipes turned on but negative (into the atmosphere) CO_2-flux anomaly (Pipe – Reference) are, however, rare and generally restricted to regions with strong horizontal currents (e.g. North Atlantic current, Kuroshio current), compare Fig. 2.3a and Fig. 2.3e.

Experiments carried out

Model experiments presented here are based on a spin-up procedure and model evaluation described in detail in Koeve et al. (2020) (see their Supplementary Methods). A reference simulation (without artificial upwelling, REF) is carried out starting in year 1765 and run with historical CO_2 emissions forcing until year 2005 and continued with four emission forcing pathways consistent with RCP 2.6 to RCP 8.5 pCO_2^{atm} concentration forcing (Fig. S 2.3) (Meinshausen et al., 2011). For runs with the UVic-2.9.WK2021.noLand model, emissions have been corrected for land-atmosphere interactions. The correction of the historical and future emission forcing is done by running REF for every historical and future emission scenario in a first step with the land component activated. Afterwards the individual net carbon fluxes between the land component and the atmosphere are diagnosed from the experiments. In a final step, the individual emission forcing pathways for the UVic-2.9.WK2021.noLand model version are offset by the respective and previously diagnosed net carbon fluxes between the land biosphere and the atmosphere (see Koeve et al., 2020 for details). This procedure ensures that the climate perturbation (ocean warming and circulation change) in the fully coupled and the noLand REF model agree. Carbon sources and sinks from the land component remain represented in the atmospheres carbon budget for the REF simulations, but land feedbacks associated with surface air temperature changes are intentionally excluded in the ArtUp simulations. In this idealized model study we do not consider the impact of non-CO_2 climate forcing (e.g. from N_2O, CH_4, aerosols) in particular since the UVic model lacks a prognostic atmospheric chemistry model and hence respective sinks of e.g. N_2O and CH_4 would not be well defined. The CO_2 emissions applied, represent CO_2 from fossil fuel burning and from land-use changes, in particular deforestation. A fifth simulation (no-emission) applying no CO_2-emissions is started from the year 1765 model state and run for 335 years. Simulations of artificial upwelling start in year 2020 and last until year 2100. We present results for this period only.

Separating the effects of artificial upwelling on marine carbon pumps

We use idealized tracers in order to evaluate how marine carbon storage is modified by artificial upwelling. In principle following concepts described in e.g. Bernardello et al. (2014) we separate carbon storage associated with three marine carbon pumps (Volk & Hoffert, 1985) as follows.

Biological carbon pump: While pumping nutrients to the surface has the potential to increase net primary production and export production of organic matter (Dutreuil et al., 2009; Yool et al., 2009; Oschlies, et al. 2010; Keller et al. 2014), this does not imply that the carbon storage associated with the biological carbon pump increase in lockstep (Koeve et al., 2020). Carbon storage from the biological carbon pump may be quantified from the apparent oxygen utilization or idealized tracers of it (Koeve & Kähler, 2016; Koeve et al., 2020) and the oxygen demand of organic matter degradation. Here we employ an explicit idealized DIC^{rem} tracer (Bernardello et al., 2014). This tracer is set to zero in the surface ocean (k=1) at every time step and accumulates the carbon from organic matter degradation and formation in all other model layers (the interior ocean). Note that this tracer is not affected by $CaCO_3$ production or dissolution.

Solubility pump: DIC^{pre} is used in this study in order to quantify the uptake of CO_2 of the ocean via physical-chemical processes (Bernardello et al., 2014; Koeve et al., 2020). Since we apply different CO_2-emission scenarios in this study and a higher pCO_2^{atm} may increase the ocean's CO_2 uptake via physical-chemical processes (Fig. S 2.7a), we can use DIC^{pre} to measure the impact of different emission scenarios in the context of artificial upwelling on the oceans carbon budget and distinguish it from e.g. biological related processes. DIC^{pre} adopts the value of DIC at the surface ocean (k=1) at every time step and preserves it while being transported to greater depth through ocean circulation. Thus, DIC^{pre} exclusively accumulates the CO_2 uptake at the ocean's surface and is influenced by e.g. pCO_2^{atm} (emission scenario), water temperature changes or other carbon-climate feedbacks.

$CaCO_3$ counter pump: The used UVic version contains a simple $CaCO_3$ counter pump approximation, but there is no explicit tracer of DIC stored in the interior ocean by means of the $CaCO_3$ counter pump. DIC^{ca}, however can be computed from $DIC^{ca} = DIC - DIC^{pre} - DIC^{rem}$. In UVic, the production of $CaCO_3$ (mol C m^{-3} s^{-1}) is connected to the detritus term of the NPZD (Nutrients - Primary Producers - Zooplankton - Detritus) ecosystem model and equivalent to 0.03 times the detritus production (same unit), while after production being immediately distributed and dissolved over depth following a declining exponential function (Schmittner et al., 2008). This process results in an export of DIC^{ca} and a respective twice as large ALK export from the surface to the interior ocean (see main text Discussion). Due to this well-known aspect of the $CaCO_3$ counter pump any increase (decrease) of it will constitute a loss (gain) of CO_2 of the ocean. Hence the explanatory power of a DICca tracer, which would indicate the opposite, is quite limited.

Table S 2.1: Changes in global DIC budget and below 1200m in Pg C between the experiments ArtUp_8.5 and REF_8.5 accumulated by the year 2100.

	DIC	DIC^{pre}	DIC^{rem}	DIC^{ca}
ΔDIC (Pg C)	80.61	35.53	40.05	5.03
$\Delta DIC^{\geq 1200m}$ (Pg C)	56.06	22.55	11.61	21.90

Table S 2.2: Remineralized detritus in Pg C / year integrated below 130m and below 1200m for the experiments ArtUp_8.5 and REF_8.5 for the year 2100, as well as the calculated transfer efficiency.

	rem._detr.$^{\geq 130m}$ (Pg C)	rem._detr.$^{\geq 1200m}$ (Pg C)	T_{eff}
REF_8.5	6.136	0.729	0.119
ArtUp_8.5	10.485	1.168	0.111
Δ	4.349	0.439	-0.008

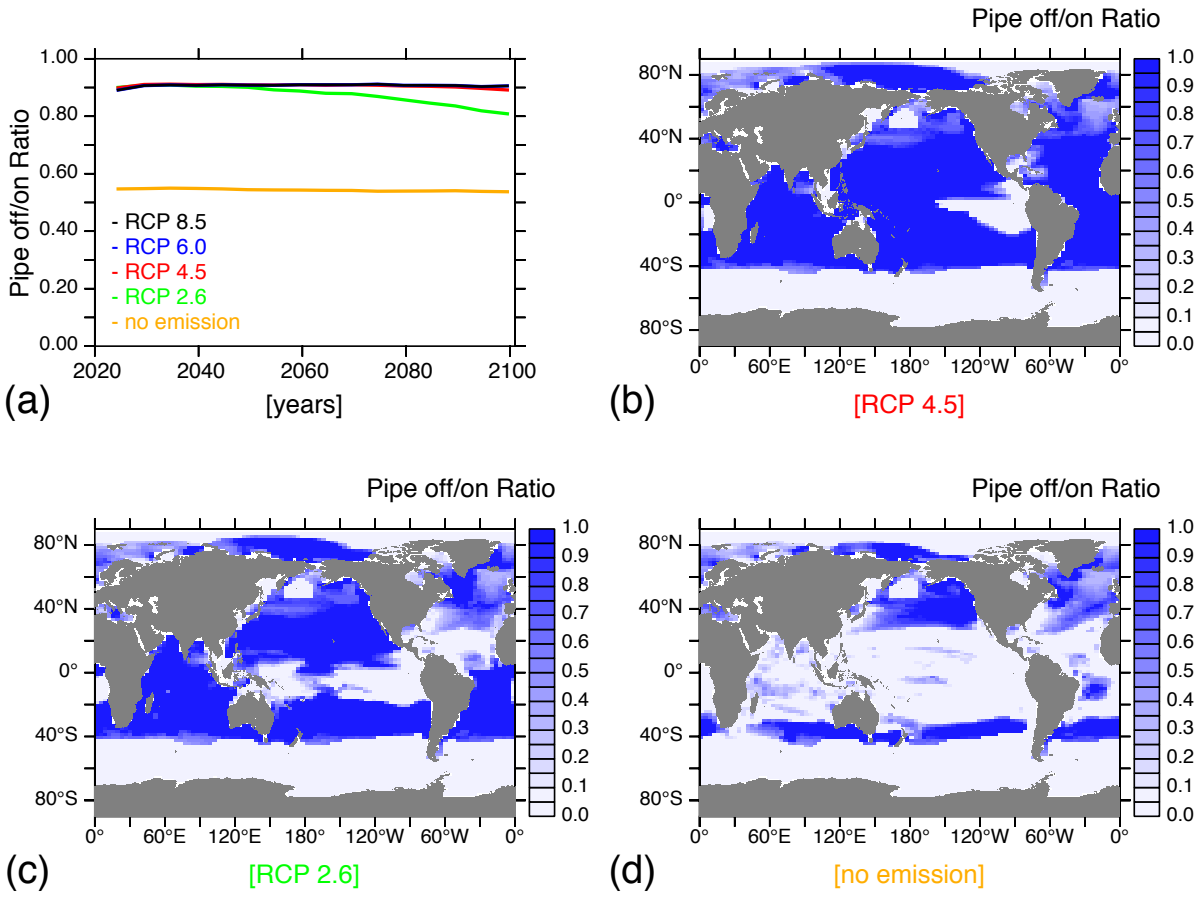

Figure S 2-1: Temporal and spatial resolved pipe covered area as a result of the applied pipe algorithm during model runtime. Pipe off/on ratio shows how long pipes were switched on with 1=365 days and 0=0 days. (a) Transient evolution of pipe off/on ration calculated over pipe covered area for all emission scenarios. Spatially resolved pipe off/on ratio for the year 2100 for RCP 4.5 (b), RCP 2.6 (c) and no-emission scenario (d).

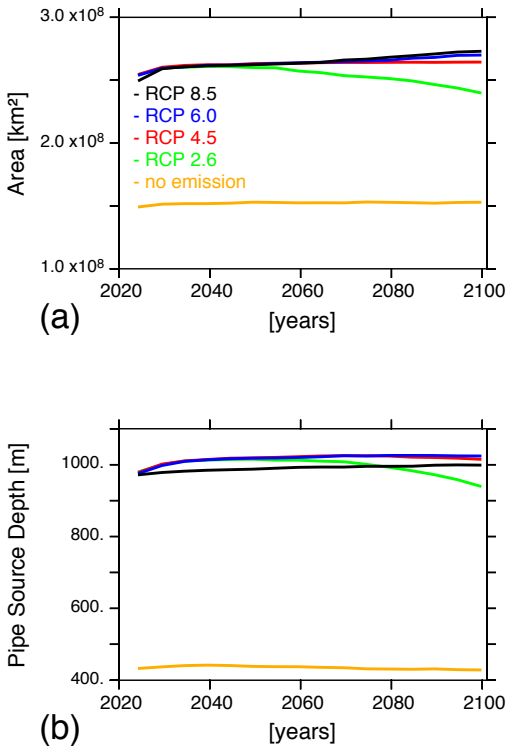

Figure S 2-2: Transient evolution of (a) pipe covered area (km²) and (b) average pipe source depth for all CO_2 emission scenarios in the ArtUp experiments.

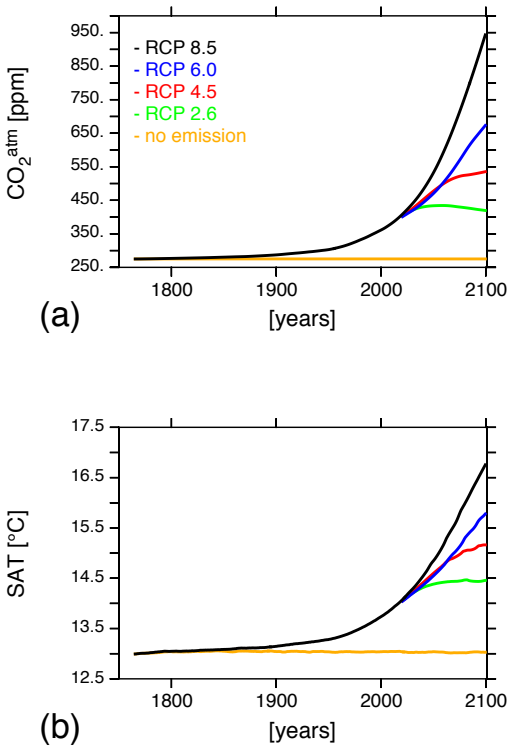

Figure S 2-3: Transient atmospheric properties between the year 1765 and 2100 of (a) pCO_2^{atm} (ppm) and (b) surface air temperature (°C) for all CO_2 emission scenarios in the REF experiments.

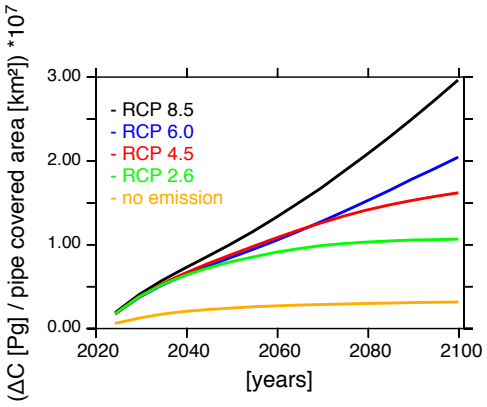

*Figure S 2-4: Cumulative changes of the carbon drawdown intensity in the pipe covered area ((ΔC [Pg] / pipe covered area [km²]) *10⁷) over time (2020 – 2100) for all CO_2 emission scenarios.*

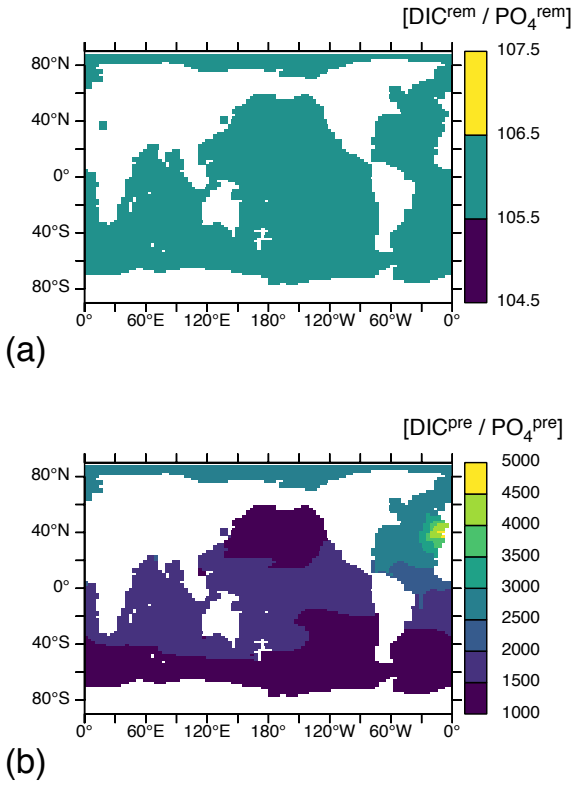

Figure S 2-5: DIC to PO_4 ratio (mol C / mol P) for (a) re-mineralized model tracers and (b) preformed model tracers at 1000 m depth for the REF_8.5 experiment in the year 2100.

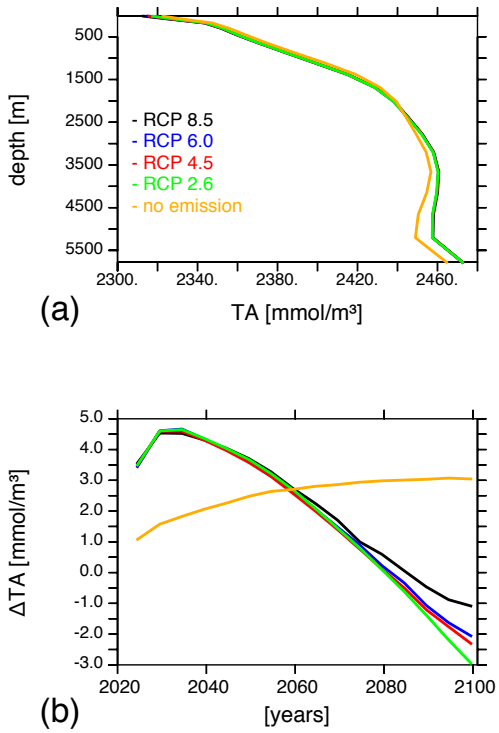

Figure S 2-6: Alkalinity concentrations and changes in the ocean. (a) Globally averaged alkalinity (mmol / m³) over depth for REF experiments in the year 2100 and (b) changes over time (2020 – 2100) of the alkalinity concentration at the ocean surface (k=1) via artificial upwelling (ArtUp – Ref; mmol / m³) for all CO_2 emission scenarios. The decrease of surface alkalinity over time under RCP 8.5 to RCP 2.6 is a consequence of the enhanced alkalinity export via the stimulated $CaCO_3$ counter pump (see main text for details).

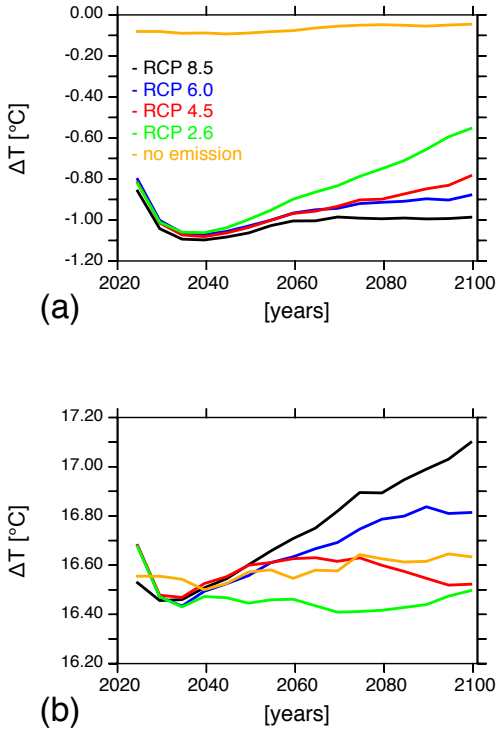

Figure S 2-7: Transient temperature changes in the ocean via artificial upwelling from 2020 to 2100. (a) Global average surface ocean (k=1) temperature change (°C) at pipe location (ArtUp – Ref) and (b) temperature change (°C) of upwelled water at pipe location ($ArtUp^{surface\ ocean} - ArtUp^{pipe\ source\ depth}$).

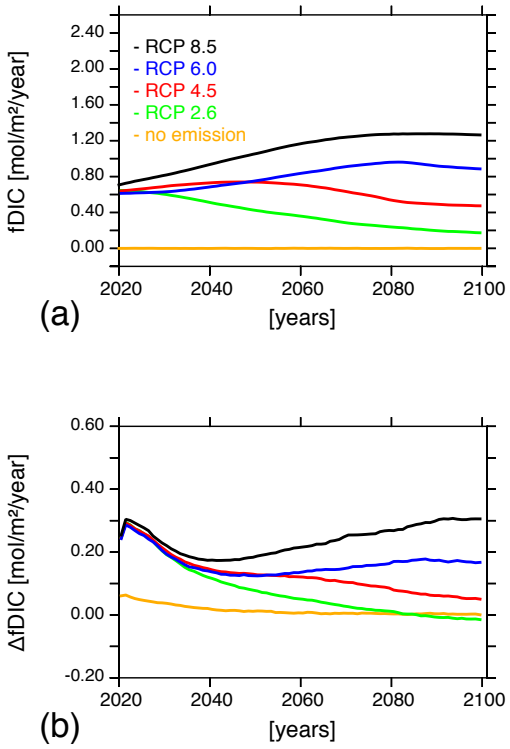

Figure S 2-8: Transient global average CO_2 flux (fDIC) from atmosphere to ocean (mol C / m^2 / $year^1$) from 2020 to 2100 for all CO_2 emission scenarios for (a) REF experiments and (b) changes via artificial upwelling (ArtUp – Ref).

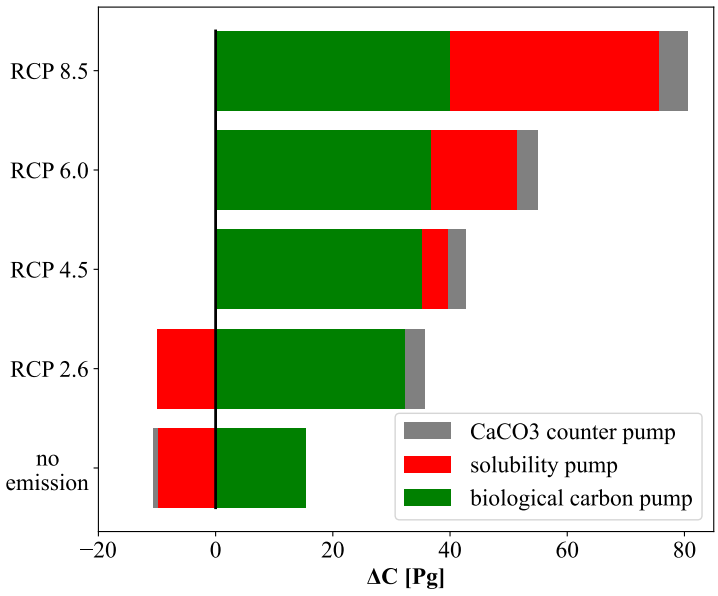

Figure S 2-9: Cumulative global net increase in the ocean's carbon budget in the year 2100 after 80 years of pipe deployment (Pg C) via artificial upwelling divided into the individual contributions of the biological carbon pump (green), the solubility pump (red) and the $CaCO_3$ counter pump (grey; see also main text Discussion).

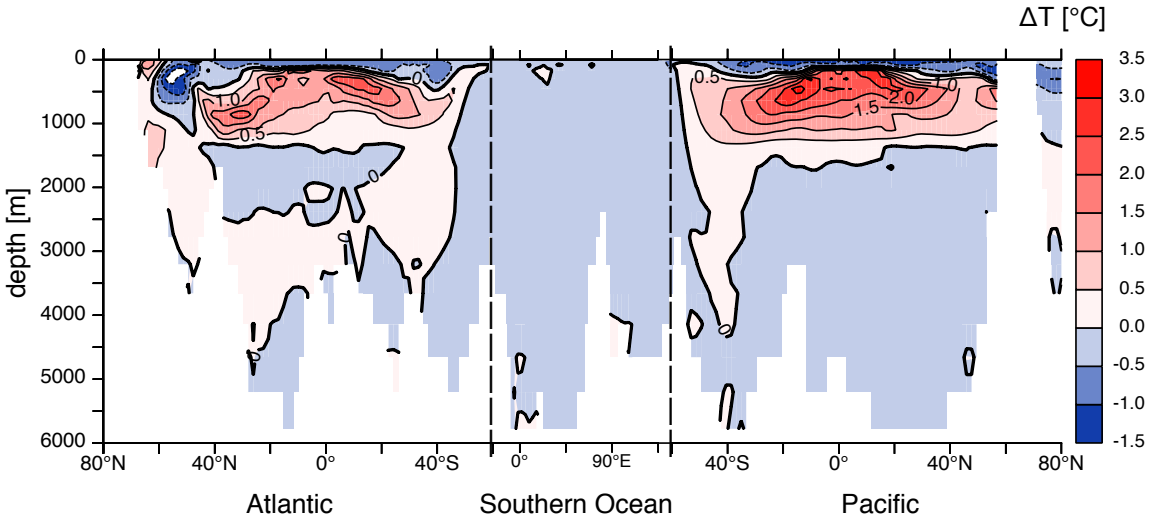

Figure S 2-10: Temperature change (°C) between the experiments ArtUp_8.5 and REF_8.5 (ArtUp – Ref) in the year 2100 after 80 years of pipe deployment along an Atlantic Ocean – Southern Ocean – Pacific Ocean transect.

3. The Response of the Ocean Carbon Cycle to Artificial Upwelling, Ocean Iron Fertilization and the Combination of both

This chapter is based on the paper 'The Response of the Ocean Carbon Cycle to Artificial Upwelling, Ocean Iron Fertilization and the Combination of both', which has been submitted to the Journal Environmental Research Letters by Jürchott, M., Koeve, W. & Oschlies., A. and is under review. Please refer to the published paper in due time.

Abstract

Artificial upwelling (AU) and ocean iron fertilization (OIF) both have been proposed as marine carbon dioxide removal (mCDR) methods to enhance ocean carbon uptake by stimulating the biological carbon pump. We simulate global and regional AU and OIF individually and the combination of both methods between the years 2025 and 2100 in ocean-atmosphere model experiments under the moderate RCP 4.5 CO_2-emission pathway and show that the combination of globally applied AU+OIF yields the greatest ocean carbon uptake potential of +103 Pg C until year 2100. Regional OIF simulated by itself poleward of 45° North and South is responsible for +87 Pg C additional ocean carbon uptake. AU-only experiments do not significantly enhance ocean carbon uptake due to the lack of iron in the upwelled waters. We find no consistent relationship between enhanced cumulative export production and changes in the ocean carbon inventory attributable to the biological carbon pump, which makes export production a poor indicator for additional ocean carbon uptake. We identified a strong decrease in the global ocean nitrate inventory (-567 Tmol N) until year 2100 as a consequence of globally applied AU+OIF due to an interrupted balance between N_2-fixation and denitrification.

3.1. Introduction

The CO_2 concentration in the Earth's atmosphere continuously rises since preindustrial times causing an increase in global surface air temperature (IPCC 2022). Over the last years, several marine carbon dioxide removal (mCDR) methods have been discussed in the context of compensating future hard-to-abate CO_2-emissions by increasing the ocean's ability to take up CO_2 from the atmosphere (NASEM 2022). One proposed mCDR idea is to use artificial upwelling (AU) to pump up nutrients from the interior ocean to the sea surface via vertical ocean pipes to stimulate the production and export of organic matter into the ocean interior i.e., the biological carbon pump (Lovelock & Rapley 2007). Focusing solely on the nutrient effect of AU, however, recently turned out to be insufficient to estimate the CDR potential of AU, since the CO_2 uptake via AU is strongly dependent on the future CO_2-emission pathway due to stimulated processes associated with the solubility pump (Jürchott et al., 2023). Furthermore, several modeling studies which tried to quantify the CDR potential of AU using Earth-system models followed a maximum potential approach for the biological carbon pump and / or did not consider iron in the pipe-covered area as a potentially limiting nutrient in the surface layer for net primary production and consequently export production (Yool et al., 2009, Oschlies et al., 2010, Keller et al., 2014, Jürchott et al., 2023). Not considering potential iron-limitation in the pipe-covered area can be translated, from a technical perspective, to the addition of sufficient amounts of bioavailable iron to the surface ocean, which is the purpose of the mCDR idea of ocean iron fertilization (OIF) (Aumont & Bopp 2006, Boyd et al., 2007, NASEM 2022).

In this model study we simulate global and regional AU, OIF and the combination of both methods between the years 2025 and 2100 to understand the role and the implications of potential iron-limitation for the mCDR-potential of AU. By using two configurations of an Earth System model of intermediate complexity with differences in their representation of the iron cycle combined with an idealized tracer approach under the RCP 4.5 CO_2-emission pathway we specifically investigate and quantify global ocean carbon uptake via AU and OIF individually and in combination, as well as the individual carbon uptake contributions via the biological carbon pump and solubility pump, regional differences, ecosystem impacts and side-effects.

3.2. Methods

3.2.1. Model configuration

In this study we use two individually calibrated configurations of the UVic 2.9 Earth System model of intermediate complexity (Keller et al., 2012, Weaver et al., 2001) with a dynamically coupled energy-balance atmosphere, sea-ice and ocean component (Gent & McWilliams 1990, Koeve et al., 2020, Orr et al., 1999), which differ in their representation of the marine iron cycle (Keller et al., 2012, Yao et al., 2019). In both model configurations all interactions with the land component are intentionally disabled (noLand) in order to isolate the effects of AU and OIF exclusively to the ocean, which allows us to better understand their impact on the marine carbon cycle. The three-dimensional ocean component has a spatial resolution of 3.6˚ longitude and 1.8˚ latitude and consists of 19 vertical levels with a 50 meter thick layer at the surface and up to 500 meter thick layers in the deep ocean. The model ocean contains a fully simulated carbon cycle with dissolved inorganic carbon (DIC) and alkalinity as prognostic model tracers. The nutrients phosphate and nitrate are calculated as prognostic tracers as well. A marine NPZD-ecosystem model represents the biological carbon pump, in which we assume a fixed C-N-P organic matter stoichiometry following Redfield ratio (Keller et al., 2012), in addition to a simple diagnostic $CaCO_3$ counter pump representation (Schmittner et al., 2008). Neither primary production nor the production or dissolution of $CaCO_3$ are sensitive to CO_2.

To easily distinguish between both individually calibrated UVic 2.9 model configurations and to ensure continuity with existing literature we refer to them by the names Fe_Mask (Keller et al., 2012) and Fe_Dyn (Nickelsen et al., 2015, Yao et al., 2019). In Fe_Mask iron-limitation is prescribed via an iron concentration mask at the oceans surface layer taken from the BLING model (Galbraith et al., 2010). Fe_Dyn contains a data-constrained and calibrated iron cycle with dissolved iron simulated as a prognostic tracer in the model ocean and includes iron-specific processes such as iron scavenging (Tagliabue et al., 2017) and hydrothermal sources (Yao et al., 2019). The N-Fe stoichiometry ratio for organic matter in the Fe_Dyn ecosystem model is 1 mol N per 10 µmol Fe and assumed to be constant (Yao et al., 2019). Since both model versions are individually calibrated, they start from slightly different initial conditions, but their performance for all relevant Earth-system variables during the simulated climate change transient is comparable (Fig. S 3.1, S 3.2, S 3.3, S 3.5). A detailed description of both model versions is given in the Supporting Information S1.

3.2.2. Separation of marine carbon pumps

We diagnose the individual impacts on the carbon cycle via the biological carbon pump and the solubility pump by introducing two idealized tracers, DIC^{remin} and DIC^{pre}, to the model (Koeve et al., 2020, Jürchott et al., 2023). The idealized tracer DIC^{remin} is set to zero upon contact with the atmosphere and increases in the interior ocean by the amount of DIC released into the water column via organic matter degradation, therefore exclusively counting the amount of DIC tracing back to the biological carbon pump. The idealized tracer DIC^{pre} adopts the total DIC value of the surface layer and preserves it while being transported to greater depth through ocean circulation. Thus, DIC^{pre} exclusively counts the amount of DIC added to the interior ocean via physical-chemical processes at the ocean's surface, which are associated with the solubility pump. Both idealized tracers are influenced by ocean circulation and water mixing, but do not interact with other model tracers.

3.2.3. Experimental design

Abc Following individual model spin-up under preindustrial pCO_2 conditions for both model configurations, we simulate the period from the year 1765 to 2005 with historical CO_2-emissions to the atmosphere, consistent with historical fossil fuel and land-use CO_2-emissions, and continue until the year 2100 with the moderate RCP 4.5 CO_2-emission pathway (Meinshausen et al., 2011). For the use of our two noLand model configurations, original CO_2-emission forcing data are corrected for the disabled land interactions to ensure that both simulations experience the same climate change as their fully coupled counterparts (Koeve et al., 2020). For details see Supporting Information S1.

The general design of the simulation of AU is adopted from a previous study conducted with an earlier version of the UVic model (Oschlies et al., 2010) and modified as described below. All model tracers and idealized tracers are transferred via AU adiabatically from the grid box at the pipe's source depth to the surface grid box, while a compensating down-welling flux through all intermediate levels ensures volume conservation. Pumping heat and salinity changes the density of the water and impacts water column physics and ocean circulation. The source depth of the AU-pipes is kept constant at 500 meters and the upwelling intensity is set to 0.5 cm day^{-1}, which translates into the upwelling of a 0.5 cm thick layer per day averaged over the entire grid box at the surface ocean by the pipes' activity. Both conditions are based

on an assessment of what the upper technically feasible limit of AU is at the current technological stage (Koweek 2022). The effects of OIF are simulated exclusively in Fe_Mask by relaxing any iron-limitation for phytoplankton and diazotrophs at the surface ocean (Keller et al., 2014). This OIF-implementation ensures, that iron is not limiting ecosystem productivity and is part of the default AU-approach in Keller et al., 2014 and Jürchott et al., 2023 in an effort to maximize a biological carbon pump response to AU. The AU approach in both studies can therefore be understood as our AU+OIF approach introduced in the next paragraph.

With the Fe_Mask model we carry out three sets of mCDR experiments, in which we simulate AU and OIF individually (Fe_Mask_AU-only, Fe_Mask_OIF-only), as well as both in combination (Fe_Mask_AU+OIF). For the Fe_Dyn model we simulate AU individually (Fe_Dyn_AU-only), since in Fe_Dyn iron is not just represented at the surface ocean but as a prognostic tracer at depth and is therefore subject to the upwelling via AU (see Tab. 1 as well). All four mCDR-simulations are carried out with either (i) a global application area approach, (ii) only in the region equatorward between 45˚N and 45˚S, or (iii) only in the region poleward of 45˚N and 45˚S covering high-latitude regions and only where the bathymetry allows for 500 m long vertical pipes (Fig. S 3.4). All three regions, in which we simulate both mCDR approaches individually and in combination, are kept constant over the duration of the experiments.

3.3. Results & Discussion

3.3.1. Carbon cycle & ecosystem response

Globally simulated AU+OIF yields the greatest ocean carbon uptake of +103 Pg C until year 2100, while global OIF-only is responsible for +95 Pg C (Fig 1a). We detect neither significant changes in the ocean carbon inventory in both globally simulated AU-only experiments, nor major shifts in the idealized DIC^{remin} and DIC^{pre} tracer contributions (Fig 1b, c). These results suggest, that AU-only is ineffective under the moderate RCP 4.5 CO_2 emission pathway to increase the oceans capacity of additional carbon uptake. Contributing factors, which lead to the ineffectiveness of AU-only to increase ocean carbon uptake, are (i) the low abundance of preformed nutrients at 500 meters depth (Fig. S 3.5, Jürchott et al., 2023), (ii) the constant mCDR application area, which does not allow for variations in the

pipe-covered area during model run time to maximize local ocean carbon uptake and avoid outgassing (Oschlies et al., 2010, Keller et al., 2014, Jürchott et al., 2023), (iii) a constant carbon-to-nutrient stoichiometry in organic matter (Keller et al., 2012) and (iv) the possibility for iron-limitation (see discussion below). Although recent mesocosm studies suggested, that AU might lead to increased C:N ratios compared to Redfield ratio (Baumann et al., 2021, Goldenberg et al., 2022, Baumann et al., 2023), they contradict with observed and lower C:N ratios in natural upwelling systems, since higher nutrient availability at the surface ocean is generally associated with lower carbon-to-nutrient ratios in biomass (Moreno and Martiny 2018).

The combination of globally applied AU+OIF yields a greater mCDR potential than solely anticipated via the individual ocean carbon uptake contributions detected in globally simulated AU-only and OIF-only experiments. The additional ocean carbon uptake in the AU+OIF and the OIF-only experiments is driven by an increase in DIC^{remin} (up to +122 Pg C), i.e., the ocean carbon inventory attributable to the biological carbon pump, which is to a minor extent compensated by a decrease in DIC^{pre} (up to -27 Pg C). Note that DIC^{remin} and DIC^{pre} don't entirely add up to the total ocean DIC inventory, since both idealized tracers intentionally don't capture interior ocean DIC changes attributable to the $CaCO_3$ counter pump. Since we apply a fixed carbon-to-nutrient stoichiometry, any increase in DIC^{remin} is a consequence of the utilization of preformed nutrients (Duteil et al., 2012) by primary producers (Jürchott et al., 2023). Furthermore, we detect a decrease in the global ocean phosphate inventory in the photic zone in AU+OIF and OIF-only experiments and respective phosphate accumulation in AU-only experiments (Fig. 3.1d). This accumulation suggests that upwelled phosphate via AU-only cannot be fully utilized by primary producers due to ecosystem limitation via other nutrients (see discussion below).

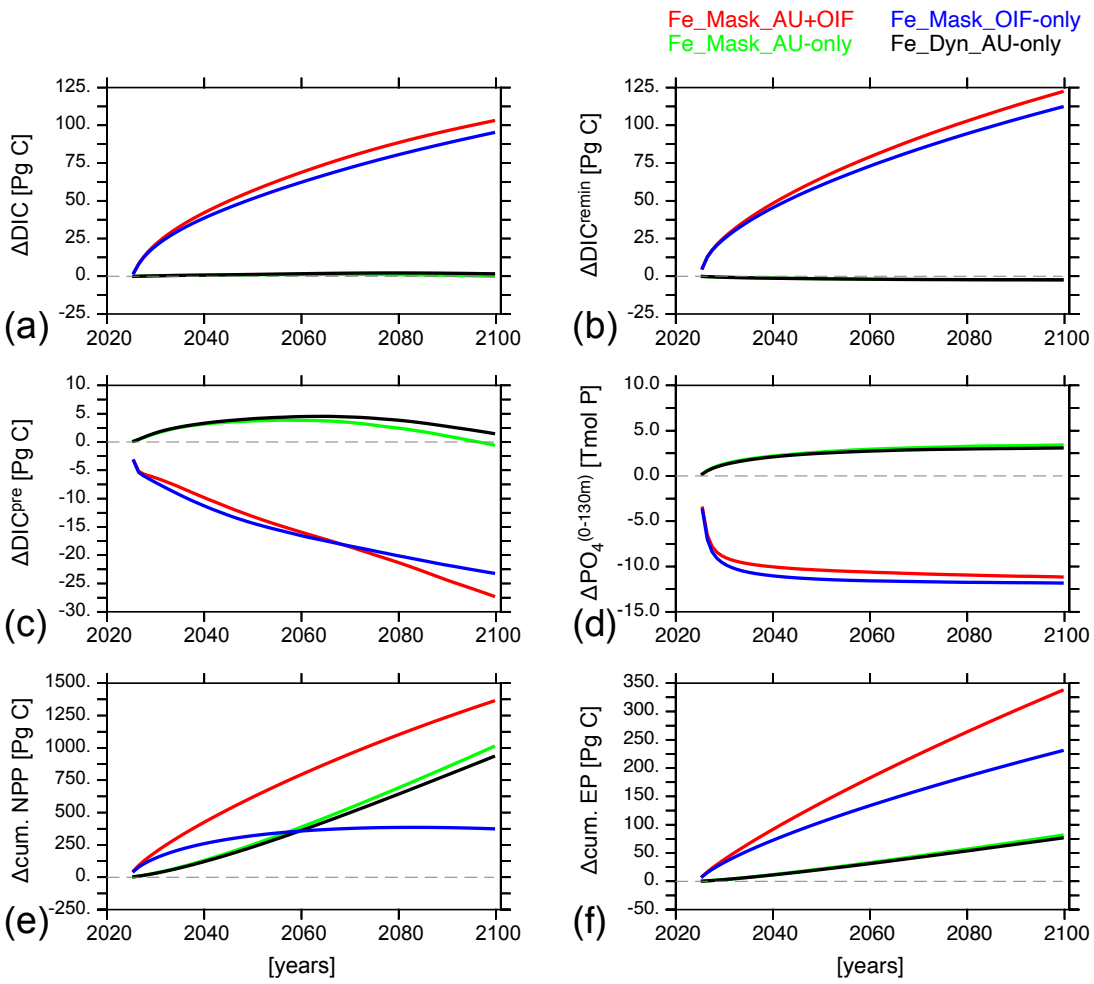

Figure 3-1: Global changes of marine carbon inventories (a-c) and fluxes (e, f), as well as of surface phosphate inventory (d) from experiments with globally applied artificial upwelling (AU) and ocean iron fertilization (OIF) experiments (see legend) carried out under a moderate CO_2 emission pathway. Changes are quantified from year 2025 to 2100 and expressed in comparison to the respective reference simulation without CDR. Carbon stocks, ΔDIC (a), ΔDIC^{remin} (b) and ΔDIC^{pre} (c) are in Pg C. ΔPO_4 (d) inventory in the upper 130 m is in Tmol P. Cumulative changes in net primary production (ΔNPP) (e) and export production (ΔEP) (f) are in Pg C. Color code: Fe_Mask_AU+OIF (red), Fe_Mask_OIF-only (blue), Fe_Mask_AU-only (green) and Fe_Dyn_AU-only (black). Green and black line are partly overlapping.

Our regional experiments reveal that the OIF-only simulation poleward of 45° North and South results in additional ocean carbon uptake of +87 Pg C, which can explain the bulk effect of the additional ocean carbon uptake detected in the globally simulated OIF-only experiment (Tab. 3.1). In contrast, AU-only experiments poleward of 45° North and South decrease the ocean carbon inventory by up to -20 Pg C in Fe_Dyn driven by a reduction in DIC^{pre} (-17 Pg C), i.e., changes in the solubility pump. Our mCDR-experiments poleward of 45° North and South cover high-nutrient-low-chlorophyl (HNLC) regions, in which primary producers are limited by iron (Morel & Price 2003). OIF in such regions does result in the utilization of preformed nutrients and can increase DIC^{remin} independent of a fixed carbon-to-

Table 3-1: Overview over conducted mCDR-model experiments and changes in Earth-system relevant parameters compared to the respective reference simulation as a consequence of simulated artificial upwelling (AU) + ocean iron fertilization (OIF), AU-only and OIF-only in the UVic 2.9 Fe_Mask model and AU-only simulated in the UVic 2.9 Fe_Dyn model. Each mCDR-approach combination has been applied globally, only equatorward between 45˚N and 45˚S and only poleward of 45˚N and 45˚S. Changes in stocks shown for year 2100, changes in cumulative net primary production (NPP) and export production (EP) from year 2025 until 2100 and changes for N_2-fixation and denitrification rates per year for year 2100.

mCDR area	UVic configuration & mCDR-approach	ΔDIC [Pg C]	ΔDIC^{pre} [Pg C]	ΔDIC^{remin} [Pg C]	Δcum. NPP [Pg C]	Δcum. EP [Pg C]	ΔO_2 [Pmol O_2]	ΔNO_3 [Tmol N]	ΔN_2-Fix. [Tmol N / yr]	ΔDenitr. [Tmol N / yr]	ΔSAT [˚C]
global (90˚) 345.500.000 [km^2]	Fe_Mask_AU+OIF	103	-27.2	122	1361	337	-15.5	-567	10.3	14.5	-0.45
	Fe_Mask_OIF-only	95.1	-23.2	112	375	231	-14.2	-333	3.23	4.21	-0.28
	Fe_Mask_AU-only	-0.03	-0.53	-2.68	1009	81.4	-0.08	-163	4.86	7.32	-0.15
	Fe_Dyn_AU-only	1.63	1.50	-2.30	932	76.5	-0.08	-206	2.86	6.30	-0.17
equatorward (45˚) 261.900.000 [km^2]	Fe_Mask_AU+OIF	22.0	-8.56	28.6	870	142	-2.76	-590	11.3	17.1	-0.23
	Fe_Mask_OIF-only	15.6	-4.43	20.0	-68.6	47.2	-1.77	-310	3.87	5.44	-0.03
	Fe_Mask_AU-only	0.08	-2.78	-0.55	993	78.9	-0.39	-162	4.85	7.29	-0.15
	Fe_Dyn_AU-only	1.26	-1.06	-0.32	910	73.5	-0.42	-205	2.83	6.23	-0.17
poleward (45˚) 90.530.000 [km^2]	Fe_Mask_AU+OIF	84.7	-23.9	101	577	222	-13.5	14.4	-0.35	-1.82	-0.23
	Fe_Mask_OIF-only	86.9	-22.0	102	524	211	-13.5	16.5	-0.37	-1.79	-0.24
	Fe_Mask_AU-only	-3.54	-0.99	-2.29	24.9	3.93	0.31	-7.01	0.04	0.12	0.02
	Fe_Dyn_AU-only	-19.9	-16.8	-2.66	28.8	3.47	0.42	-14.3	0.07	0.14	0.06

nutrient stoichiometry in the model ecosystem. AU-only experiments equatorward between 45˚ North and South yield no significant potential for mCDR and the combination of AU+OIF results in greater ocean carbon uptake (+22 Pg C) compared to OIF-only (+16 Pg C). We conclude that OIF is in our experiments the main driver for the increase in the oceans carbon inventory and AU-only experiments don't significantly change or even negatively impact ocean carbon uptake, especially if simulated poleward of 45˚ North and South.

Under all simulated mCDR approaches, cumulative net primary production and export production increases (Fig. 3.1e, f; Tab. 3.1). However, in the globally applied OIF-only simulation cumulative net primary production increase saturates after year 2060 due to the missing re-supply of interior ocean macro-nutrients to the surface as provided via AU. This plateau, however, does not limit continuous cumulative export production increase, which is in the OIF-only simulation even higher (+231 Pg C) compared to AU-only simulations (up to +81 Pg C), despite lower cumulative net primary production. We find no consistent relationship between cumulative export production to DIC^{remin}, which could be comprehensively applied to all simulated mCDR experiments and is consistent over time (Fig. 3.3a, S 3.6). Export production and organic matter respiration in the ocean interior, are key processes of ocean carbon uptake via the biological carbon pump (Frenger et al., 2024). While AU-only experiments stimulate export production, they fail to increase DIC^{remin}. The globally applied OIF-only simulation enhances cumulative export production and DIC^{remin} in a ratio of 2.1 to 1 until the end of the century. In combination with AU, we find a disproportionate additional increase in cumulative export production compared to only a minor increase in DIC^{remin} (2.8 to 1). Furthermore, our regional experiments reveal for AU+OIF and OIF-only experiments poleward of 45˚ North and South a cumulative export production to DIC^{remin} ratio again of about 2.1 to 1 until the end of the century, while the same ratio shifts to 5 to 1 for AU+OIF and to 2.4. to 1 for OIF only experiments equatorward between 45˚ North and South. We conclude that a change in export production remains under all simulated mCDR-experiments overall a poor indicator for changes in the ocean carbon inventory attributable to the biological carbon pump (Frenger et al., 2024). This is so despite the fact that our experimental design does not consider potential effects of AU, like changes in particle composition and sinking behavior, which has been observed in experimental work (Baumann et al., 2021, Baumann et al., 2023) and may add to the complexity of carbon export to storage ratio.

3.3.2. Iron-limitation under AU-only

As stated in the previous section, additional ocean carbon uptake driven via the biological carbon pump requires in our model the utilization of preformed nutrients due to the fixed carbon-to-nutrient stoichiometry in the model ecosystem. This means for the AU-only experiment performed with the Fe_Dyn UVic configuration, that the amount of phosphate, nitrate and iron prevalent at the surface ocean in addition to the upwelled nutrients via AU must exceed the required amount of nutrients to re-uptake the amount of upwelled DIC^{remin} via primary producers to cause a net increase in DIC^{remin}. We find an increase in the global mean surface phosphate and nitrate concentrations and a decrease in the dissolved surface iron concentration in the Fe_Dyn AU-only experiment (Fig. 3.2a, d, g) with high spatial variation (Fig. 3.2b, e, h). This lack of dissolved iron at the surface ocean, as also observed in natural HNLC-regions, prevents primary producers to fully utilize the upwelled phosphate and nitrate. As a consequence, the dissolved surface iron concentration limits additional ocean carbon uptake via the biological carbon pump.

To investigate the reason behind the lack of dissolved iron at the surface ocean, we convert all three nutrients at the pipes source depth via their individual carbon-to-nutrient stoichiometry into their DIC-equivalent concentration and divide by DIC^{remin} from the same depth (Fig. 3.2c, f, i). A ratio above one indicates an excess of the nutrient in relation to DIC^{remin} and would theoretically promote additional ocean carbon uptake at the surface ocean via the biological carbon pump. As shown in figure 3.2i, wide regions around the equator and North Pacific are iron-depleted in 500 meters depth in relation to DIC^{remin}, which can explain the average lack of dissolved iron at the surface ocean. Since this pattern is specific to the ratio derived from iron and DIC^{remin} (see Fig. 3.2c, f as well), we argue that it is a consequence of the iron-specific process iron-scavenging (Tagliabue et al., 2017), which exports iron via sticking itself to the surface of other sinking particles to greater depth compared to DIC, phosphate and nitrate. In contrast to the previously described pattern, in the Fe_Dyn AU-only experiment poleward of 45˚ North and South, we find a global inventory decrease in DIC^{remin} (-2.7 Pg C; Tab. 3.1), despite the upwelling of sufficient dissolved iron in relation to DIC^{remin} around the Southern Ocean. This decrease around the Southern Ocean (see Fig. S 3.7 as well) cannot be explained by the lack of iron in the upwelled waters, but is probably a consequence of the complex regional circulation patterns around the Southern Ocean (Marinov et al., 2006), which complicates the regional relationship between upwelled nutrients, export production and DIC^{remin} under AU-only even further.

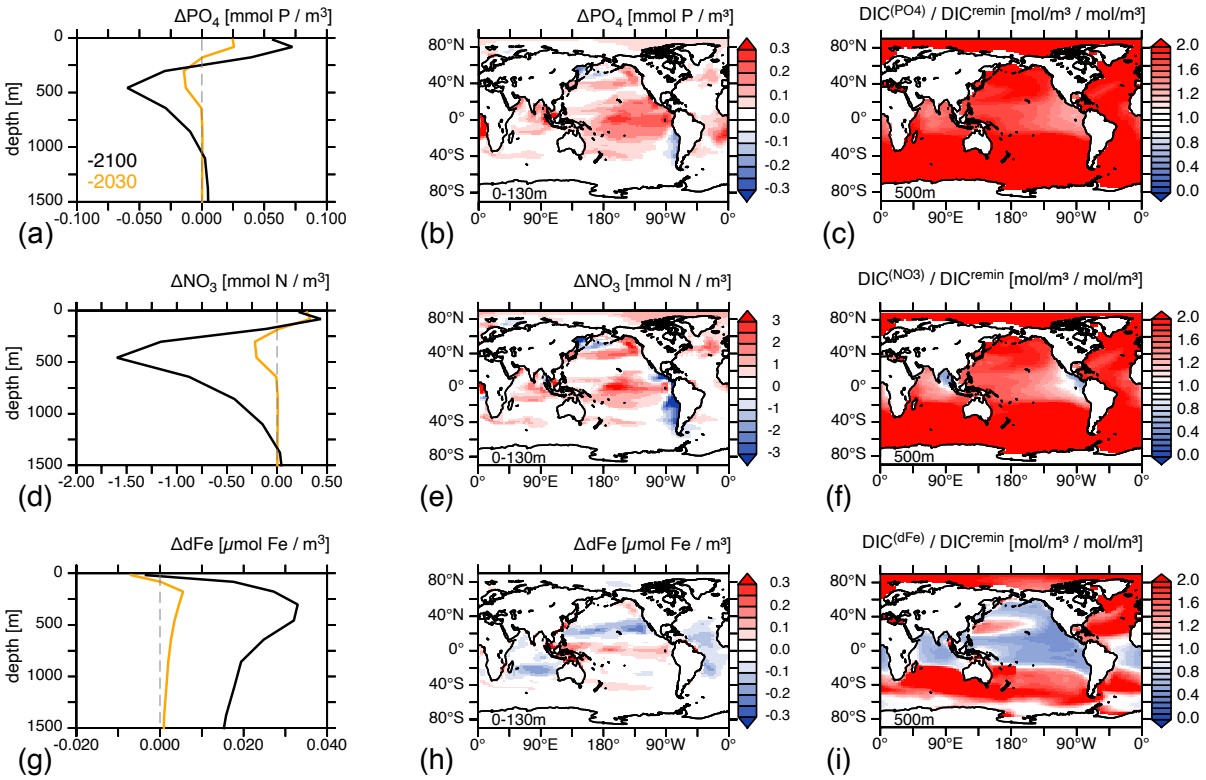

Figure 3-2: Average nutrient concentration changes due to globally simulated artificial upwelling (AU) in the UVic 2.9 Fe_Dyn model (Fe_Dyn_AU-only). Changes are expressed in comparison to the respective reference simulation without CDR. Left column: change in global average nutrient concentration over depth for ΔPO_4 (a), ΔNO_3 (d) and ΔdFe (g) for year 2030 (orange) and 2100 (black). Middle column: change in spatially resolved average surface nutrient concentration for upper 130 meter of water column for ΔPO_4 (b), ΔNO_3 (e) and ΔdFe (h) for year 2100. Right column: ratio between $DIC^{nutrient}$ to DIC^{remin} at 500 m depth and year 2100 for the AU experiment. Nutrient concentration is converted into its DIC-equivalent via fixed C-nutrient stoichiometry in mol m^{-3} and divided by DIC^{remin} in mol m^{-3} for PO_4 (c), NO_3 (f) and dFe (i). Ratio above (below) one indicates excess (lack) of nutrient in relation to DIC^{remin}.

The increase in the global mean surface phosphate concentration in the AU-only experiment performed with the Fe_Dyn UVic configuration is only possible due to an equal concentration decrease around the pipes source depth, i.e., a redistribution effect (Fig. 3.2a). As for dissolved iron, we find, except directly at the ocean surface, an increase in the dissolved iron concentration through the entire water column (Fig. 3.2g). Since atmospheric and hydrothermal iron sources are exactly the same between the reference and the AU-only experiments performed in Fe_Dyn, we argue that the continuous increase in cumulative net primary production, which can be thought of as a living short-term reservoir for iron, and the upwelling activity itself of AU extents the residence time for dissolved iron in the water column, despite enhanced export production and consequently enhanced iron-scavenging. The decrease in the global average nitrate concentration at the pipes source depth, however, is much greater compared to its increase at the ocean surface (Fig. 3.2d), which will be discussed in the next section.

3.3.3. Out-of-balance nitrogen cycle

We find in all experiments with globally simulated mCDR a decrease in the global ocean nitrate inventory of up to -567 Tmol N until year 2100 for the AU+OIF experiment. In both used UVic calibrations ocean nitrate concentrations can increase via N_2-fixation and decrease via denitrification in the absence of oxygen (Keller et al., 2012). In our reference simulations, both processes are in balance and keep the ocean nitrate inventory stable (Fig. S 3.3), despite that the global ocean oxygen inventory slowly declines as a response to increased stratification and an overall weakened overturning circulation (Helm et al., 2011). We detect in all globally simulated mCDR experiments a disproportionately stronger increase in denitrification compared to N_2-fixation (Fig. 3.3b), which leads to an overall decline in the ocean nitrate inventory (Tab. 3.1). The decline in the global ocean nitrate inventory may have potentially negative long-term consequences for the ocean ecosystem (Oschlies et al., 2019, Wu et al., 2023). The increase in denitrification happens in our model simulations via the expansion of naturally existing oxygen minimum zones in front of the Peruvian and Indian coastlines, which are included in our global and equatorward mCDR application areas (Fig. 3.3c, d). In our model simulations we neither simulate the production of the potent greenhouse gas N_2O, nor its impact on atmospheric temperatures. However, enhanced denitrification as detected in our mCDR experiments could cause the production of additional N_2O and, especially if upwelled via AU directly in contact with the atmosphere, might offset any atmospheric carbon reduction effect on atmospheric temperatures (Jin and Gruber 2003, Dutreuil et al., 2009). We conclude that AU, OIF and the combination of both disrupt the balance between N_2-fixation and denitrification towards a reduced global ocean nitrate inventory via the expansion of oxygen minimum zones and thus, potentially promote conditions for enhanced N_2O production.

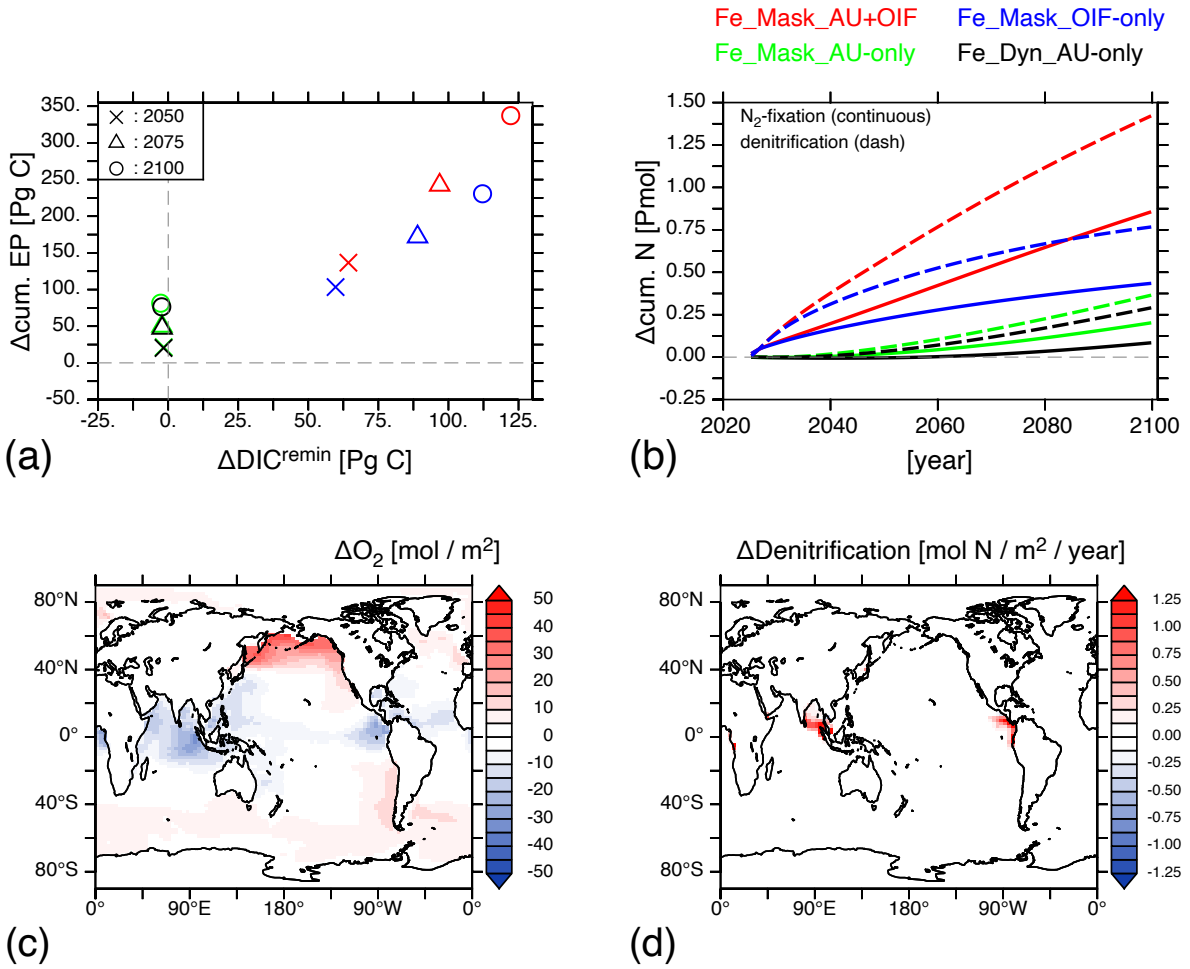

Figure 3-3: Global changes in variables associated with the biological carbon pump and their impact on the nitrogen cycle. Changes are expressed in comparison to the respective reference simulation without CDR. Relationship between changes in (a) cumulative export production (ΔEP) to ΔDIC^{remin} in Pg C for three timesteps and (b) cumulative changes in global ΔN_2-fixation (continuous lines) and Δdenitrification (dashed lines) in Pmol N. The same color code applies as in figure 1. Spatially resolved and vertically integrated changes for the Fe_Dyn global artificial upwelling (Fe_Dyn _AU-only) experiment for (c) ΔO_2 in mol m^{-2} and (d) Δdenitrification in mol N m^{-2} $year^{-1}$ for year 2100.

3.4. Conclusions

Our model experiments performed under the moderate RCP 4.5 emission pathway suggest that the combination of globally applied OIF+AU yields the greatest potential for additional ocean carbon uptake driven via the biological carbon pump, while AU-only experiments don't significantly increase the ocean carbon inventory. Further we show that the combination of globally applied AU+OIF yields a greater mCDR potential than solely anticipated via the individual ocean carbon uptake contributions detected in globally simulated AU-only and OIF-only experiments. For AU-only experiments, we identified iron as the limiting nutrient at the surface ocean, which limits the utilization of upwelled preformed phosphate and nitrate via primary producers and prevents additional ocean carbon uptake via the biological carbon

pump. For OIF-only experiments, the additional ocean carbon uptake is driven via the biological carbon pump poleward of 45˚ North and South covering HNLC-regions.

Net primary production increases under AU and OIF individually and in combination, which has the potential to increase fish-stocks and promote food production (Kirke 2003). The increase in net primary production translates into an increase in export production, but we find no consistent relationship between cumulative export production to DIC^{remin}, which could be comprehensively applied to all simulated mCDR approaches and ocean regions. Thus, a change in export production remains in our model experiments overall a poor indicator for changes in DIC^{remin}, which is a preferred metric for the contribution of biology to the marine carbon sink (Frenger et al., 2024). However, experimentally simulated changes in mesocosm studies due to AU in the C:N stoichiometry in phytoplankton , as well as the consideration of other nutrients such as silicate and the representation of diatoms and related possible changes in organic particle sinking speed, enhance the complexity of the potential biological carbon pump-response to AU (Baumann et al., 2021, Goldenberg et al., 2022, Baumann et al., 2023, Goldenberg et al., 2024), which is not represented in such great detail in our model experiments.

In our model experiments we detect an out-of-balance nitrogen cycle as a consequence of a disproportionately stronger increase in denitrification compared to N_2-fixation, which leads to an overall decline in the ocean nitrate inventory. A decline in the ocean nitrate inventory may have negative long-term consequences for the ecosystem (Oschlies et al., 2019, Wu et al., 2023). The increase in denitrification is a consequence of expanded oxygen minimum zones particularly in front of the Peruvian and Indian coastlines. Although we don't simulate N_2O in our model experiments, enhanced denitrification may lead to an increased production of N_2O and, especially if upwelled via AU directly in contact with the atmosphere, might offset any atmospheric carbon reduction effect on atmospheric temperatures (Jin and Gruber 2003, Dutreuil et al., 2009).

Acknowledgement

We acknowledge discussions with colleagues from the Biogeochemical Modelling research unit at GEOMAR. M.J. acknowledges funding from German BMBF, Project Test-ArtUp (Grant Number: 03F0897A). This is a contribution to the CDRmare research mission funded by the German Alliance for Marine Research (DAM) and to the Subtopic 6.3 “The future biological carbon pump” of the Helmholtz Earth and Environment research program “Changing Earth – Sustaining our Future” (POF IV). The author(s) wish to acknowledge discussions with members of the BM-carbon-theme group and the use of the PyFerret program for analysis and graphics in this paper.

Data statement

Model output and scripts for data processing are available from data.geomar.de (https://hdl.handle.net/20.500.12085/56ba983b-169d-4573-96ec-46bd3d925d7e)

3.5. Supporting Information

Introduction

Here we provide Supplementary Methods (Text S1) and Supplementary Figures (S 3.1 to S 3.7), which present details of our model experiments.

Text S1.

Supplementary Methods

UVic model

Model experiments are carried out with two individual ocean-sea-ice-atmosphere version of the UVic Earth System Model Version 2.9 of intermediate complexity (UVic-2.9.WK2021.noLand and UVic-2.9.FeDyn.WK2022.noLand), which only differ in their representation of the marine iron cycle (Keller et al., 2012, Yao et al., 2019). To easily distinguish between both UVic 2.9 model configurations and to ensure continuity with existing literature we refer to them by the names Fe_Mask (Keller et al., 2012) and Fe_Dyn (Nickelsen et al., 2015, Yao et al., 2019).

UVic (Weaver et al., 2001) is an Earth system model of intermediate complexity (EMIC). Horizontal resolution is 3.6° in longitude and 1.8° in latitude direction. The ocean circulation model (MOM, Modular Ocean Model 2) includes physical parameterizations for diffusive mixing along and across isopycnals and eddy induced tracer advection (Gent & McWilliams 1990). It has 19 vertical layers and layer thickness increases from 50 meter at the surface to 500 meter in the deep ocean. Wind forcing is prescribed with monthly mean winds from NCAR/NCEP climatological data. The model ocean contains a fully simulated carbon cycle with dissolved inorganic carbon (DIC) and alkalinity as well as nitrate and phosphate as prognostic model tracers. Gas exchange of oxygen and carbon dioxide is simulated as in Orr et al. (1999). Both Fe_Mask and Fe_Dyn model versions contain a marine NPZD (Nutrients - Primary Producers - Zooplankton - Detritus) ecosystem model to represent the biological carbon pump, in which we assume a fixed C-N-P organic matter stoichiometry following Redfield ratio (Keller et al., 2012), in addition to a simple $CaCO_3$ counter pump approximation (Schmittner et al., 2008). Neither primary production nor the production or

dissolution of $CaCO_3$ are sensitive to the CO_2 concentration. In order to avoid excessively long model spin-up times our idealized model experiments do not simulate sediment processes. Any organic detritus or $CaCO_3$ reaching the bottom of the model is dissolved in the deepest wet box instantaneously. The difference in the representation of the marine iron cycle between Fe_Mask and Fe_Dyn is described in the following paragraph.

In Fe_Mask iron-limitation is prescribed via an iron concentration mask at the oceans surface layer taken from simulations done with the BLING model (Galbraith et al., 2010). In contrast, Fe_Dyn contains a data-constrained and calibrated iron cycle (Nickelsen et al., 2015, Yao et al., 2019) with dissolved iron simulated as a prognostic tracer in the model ocean and iron-specific processes such as iron scavenging (Tagliabue et al., 2017) and hydrothermal sources are included (Yao et al., 2019). The N-Fe stoichiometry ratio for the ecosystem model in Fe_Dyn is 1 mol N per 10 μmol Fe and assumed to be constant (Yao et al., 2019).

Experimental design

Fe_Mask and Fe_Dyn have both been individually calibrated based on a spin-up procedure and model evaluation described in detail in Koeve et al. (2020) (see their Supplementary Methods). Since both model versions are individually calibrated, they start from slightly different initial conditions, but their performance for all relevant Earth-system variables during the simulated transient is comparable (Fig. S 3.1, S 3.2, S 3.3, S 3.5). Any differences between both model versions in their ocean carbon cycle response to artificial upwelling (AU) and ocean iron fertilization (OIF) should therefore not be a result of different initial conditions.

Two separate reference simulations (one each for Fe_Mask and Fe_Dyn and without AU or OIF) start in year 1765 and run with historical CO_2 emissions forcing until year 2005 and are continued until the year 2100 with the moderate RCP 4.5 CO_2-emission pathway (Meinshausen et al., 2011). CO_2 emissions have been corrected individually for Fe_Mask and Fe_Dyn to account for land-atmosphere carbon cycle interactions. The correction of the historical and future emission forcing is done by running both reference simulations under emission pathway RCP 4.5 in a first step with the land component activated. Afterwards the individual net carbon fluxes between the land component and the atmosphere are diagnosed from the experiment. In a final step, the RCP4.5 emission forcing pathway is offset by the

previously diagnosed net carbon flux between the land biosphere and the atmosphere (see Koeve et al., 2020 for details). This procedure ensures that the climate perturbation (ocean warming and circulation change) in the fully coupled and the noLand models do agree. Due to this procedure, carbon sources (e.g., land-use changes as a consequence of deforestation) and sinks from the land component remain represented in the atmospheres' carbon budget for both reference simulations, but any additional land feedbacks associated with AU's impact on surface air temperature are intentionally excluded. In this idealized model study, we do not consider the impact of non-CO_2 climate forcing (e.g., from N_2O, CH_4, aerosols) in particular, since the UVic model lacks a prognostic atmospheric chemistry model and a representation of respective marine processes. Hence sinks or sources of e.g., N_2O and CH_4 and their eventual changes associated with AU would not be well defined.

mCDR implementation

We simulate the effects of both OIF and AU individually and in combination from the year 2025 until 2100 (see next paragraphs and Tab. 3.1). The effects of OIF are simulated exclusively in Fe_Mask by relaxing any iron-limitation for phytoplankton and diazotrophs at the surface ocean (Keller et al., 2014). This change translates, from a technical perspective, into the addition of sufficient amounts of bioavailable iron for primary producers at the surface ocean. This OIF implementation is part of the default AU-approach in Keller et al. (2014) and Jürchott et al. (2023) in an effort to simulate a maximum potential biological carbon pump approach for AU. The general AU approach used in these studies can therefore be understood as our AU+OIF in combination experiments. The general design of the simulation of AU is adopted from a previous study conducted with an earlier version of the UVic model (Oschlies et al., 2010) and modified as described below. All ocean model tracers (e.g., temperature, salinity, DIC, alkalinity, PO_4, NO_3, O_2 and Fe in Fe_Dyn) and idealized tracers are transferred via AU adiabatically from the lowest grid box at the pipe's source depth to the surface grid box, while a compensating down-welling flux through all intermediate levels ensures volume conservation. The pumping of heat and salinity does change the density of the water and, as a consequence, impacts water column physics and ocean circulation. The source depth of the AU-pipes is 500 meters and the upwelling intensity is set to 0.5 cm day^{-1}, which translates into the upwelling of a 0.5 cm thick layer per day averaged over the entire grid box at the surface ocean by the pipe's activity. Both conditions are based on an assessment of what the upper technically feasible limit of AU is at the current

technological stage (Koweek 2022). In contrast to the AU experiments done in Oschlies et al. (2010), Keller et al. (2014) and Jürchott et al. (2023), we do not use an algorithm during model runtime to dynamically optimize pipe-length and pipe-deployment-area for maximum ocean carbon uptake. In all of our mCDR experiments application-areas (see Fig. S 3.4 and next paragraphs) and specific for AU pipe-length and upwelling intensity are kept constant for the entire duration of the experiments and independently of the resulting atmosphere to ocean CO_2 flux.

In Fe_Mask we simulate AU and OIF individually (Fe_Mask_AU-only, Fe_Mask_OIF-only), as well as both in combination (Fe_Mask_AU+OIF. For the Fe_Dyn model variant we carry out one CDR experiment, in which we simulate the impact of AU (Fe_Dyn_AU-only) on upwelling of macronutrients and iron alike. In Fe_Dyn iron is not just represented at the surface ocean but it is a prognostic tracer at all depth levels. Hence, only in Fe_Dyn iron is subject to the upwelling via AU. In Total, we simulate four individual mCDR experiments per application area (see next paragraph).

We repeat all four mCDR experiments with either a global application area, only equatorward between 45˚N and 45˚S or only poleward of 45˚N and 45˚S covering high-latitude regions (Fig. S 3.4 & Tab. 3.1). The application-areas for AU and OIF do not include continental shelfs shallower than 500 meters, since this bathymetry would conflict with the assumed AU pipe-length of 500 meters.

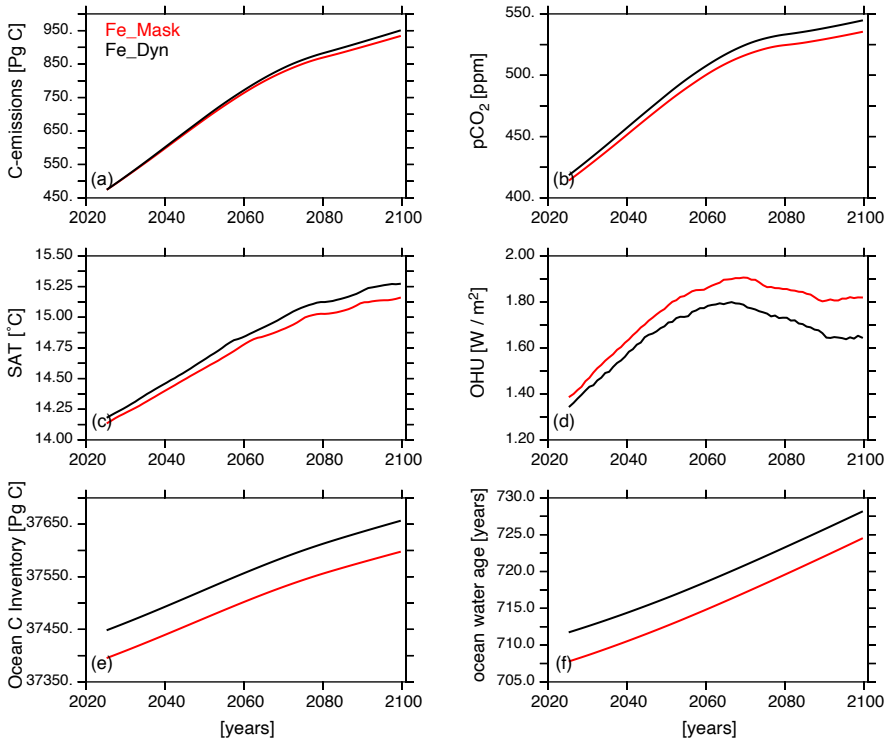

Figure S 3-1: Overview over major Earth-system variables during transient from year 2025 to 2100 for the reference simulation without mCDR for Fe_Mask (red) and Fe_Dyn (black). a) carbon emissions into the atmosphere in Pg C, b) atmospheric pCO_2 concentration in ppm, c) global mean surface air temperature (SAT) in ˚C, d) ocean heat uptake (OHU) in W m^{-2}, e) global total ocean carbon inventory in Pg C and f) global average ocean water age in years.

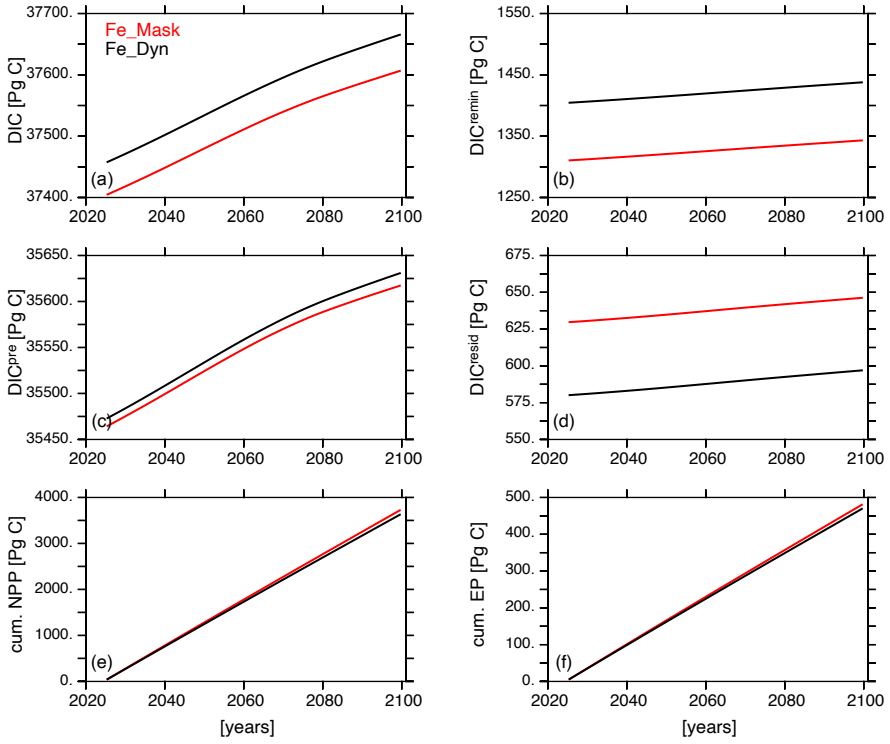

Figure S 3-2: Overview over major ocean variables during transient from year 2025 to 2100 for the reference simulation without mCDR for Fe_Mask (red) and Fe_Dyn (black). a) global ocean DIC inventory in Pg C split into individual contributions via b) the biological carbon pump (DIC^{remin}), solubility pump (DIC^{pre}) and residual DIC (DIC^{resid}). The residual DIC is the amount of DIC not captured via DIC^{remin} or DIC^{pre} and computed as DIC^{resid} = DIC - DIC^{remin} - DIC^{pre}. Cumulative change in e) net primary production (NPP) and export production (EP) in Pg C.

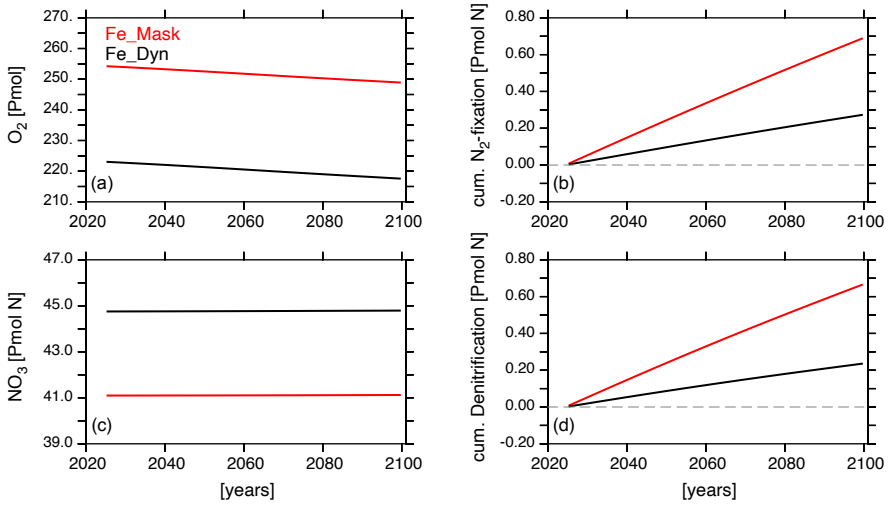

Figure S 3-3: Overview over ocean oxygen and nitrate inventory and nitrate related processes during transient from year 2025 to 2100 for the reference simulation without mCDR for Fe_Mask (red) and Fe_Dyn (black). Changes in global ocean a) oxygen inventory in Pmol and c) nitrate inventory in Pmol N. Cumulative changes in b) N_2-fixation and d) denitrification in Pmol N.

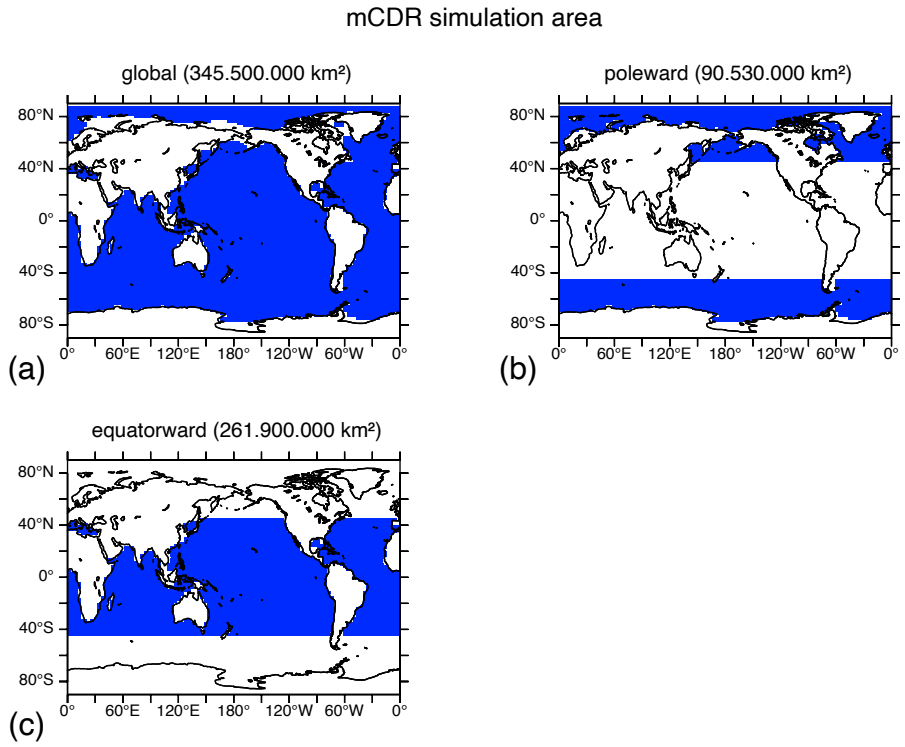

Figure S 3-4: Overview over simulated mCDR regions indicated in blue for a) global, b) poleward of 45˚ North and South and c) equatorward between 45˚ North and South simulations. All regions are kept constant over the duration of the mCDR simulations.

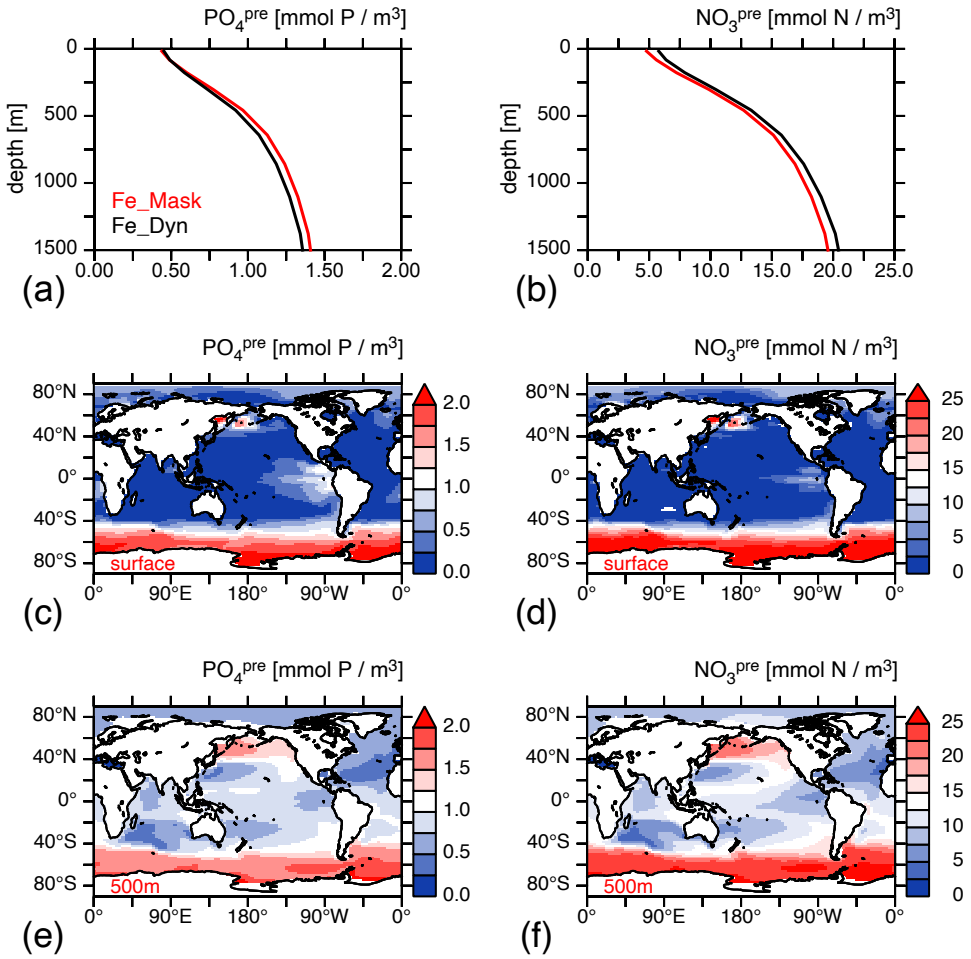

Figure S 3-5: Overview over preformed phosphate and preformed nitrate concentrations for the year 2025. Global mean (a) preformed phosphate and (b) preformed nitrate concentration over depth in mmol m^{-3} for the reference simulation without mCDR for Fe_Mask (red) and Fe_Dyn (black). Preformed phosphate and nitrate concentrations in Fe_Mask at the surface ocean (c, d) and at 500 meters depth (e, f) in mmol m^{-3}.

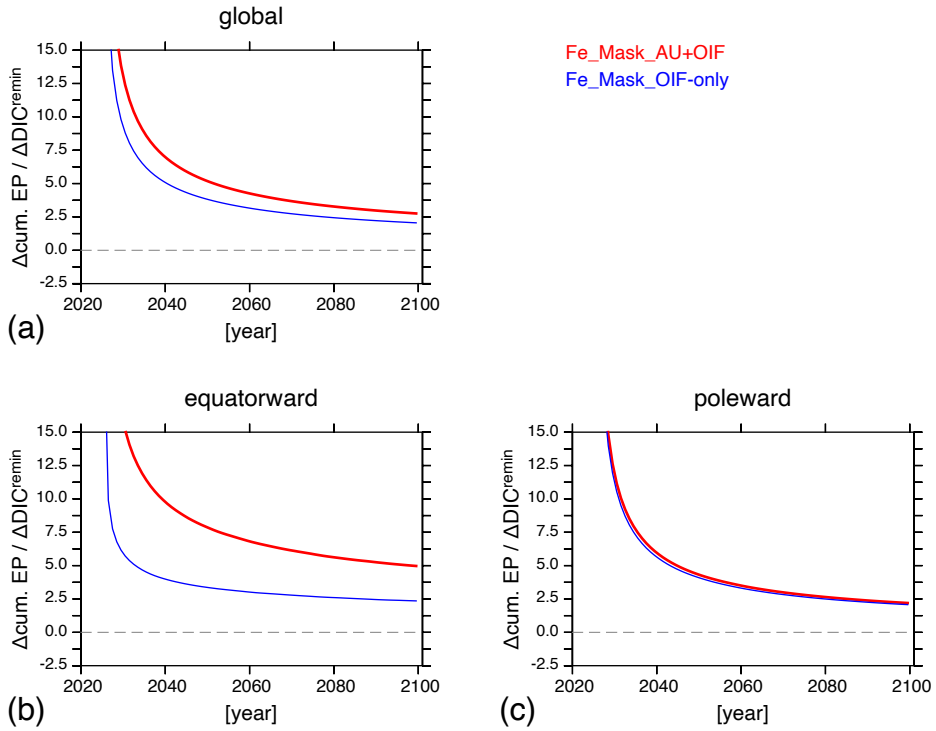

Figure S 3-6: Overview over ratio between Δ cumulative export production (EP) in Pg C and Δ DIC^{remin} in Pg C from year 2025 to 2100 compared to reference simulation without mCDR for (a) global, (b) equatorward and (c) poleward mCDR simulation area (see figure S 3.4) for the experiments AU+OIF (red) and OIF-only (blue) conducted with Fe_Mask.

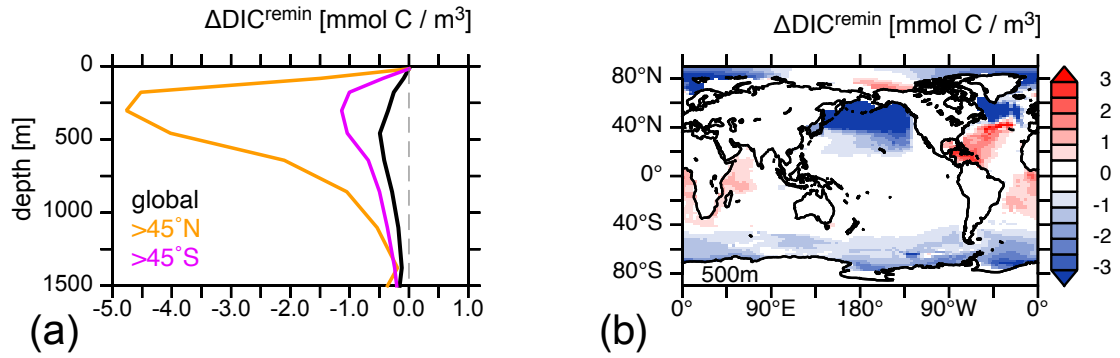

Figure S 3-7: Overview over changes in DIC^{remin} for poleward (see figure S 3.4) Fe_Dyn_AU-only simulation compared to reference simulation without mCDR for year 2100. (a) Change in global mean average DIC^{remin} concentration over depth (black) in mmol m^{-3} and individual shares northward of 45˚N (orange) and southward of 45˚S (purple). (b) Spatial pattern of change in DIC^{remin} in mmol m^{-3} at 500 meters depth.

4. Leaving the marine CDR narrative behind. A Re-Classification Attempt for Artificial Upwelling

This chapter contains the draft of the manuscript 'Leaving the marine CDR narrative behind. A Re-Classification Attempt for Artificial Upwelling' by Jürchott, M., Oschlies, A., Mengis, N., Frenger, I. & Koeve, W.

Abstract

Artificial upwelling (AU) is currently perceived and investigated as a marine carbon dioxide removal (mCDR) method in the scientific community. We challenge this perception and simulate large scale AU in an Earth system model of intermediate complexity between the years 2025 and 2100 under the CO_2 emission pathway RCP 4.5. We find a significant reduction in the atmospheric CO_2 concentration via AU (-12.1 Pg C) until the end of the century only, if the upwelled water maintains its temperature. The reduced atmospheric CO_2 concentration is, however, not a result of enhanced ocean carbon uptake, but a consequence of an enhanced terrestrial carbon sink, which is driven via a carbon climate feedback triggered by a reduction in surface air temperature (SAT; -0.2 ˚C) as a response to enhanced ocean heat uptake (OHU; +0.3 W m^{-2}). Following the linear TCRE relationship, we can only attribute 22 % of the decrease in global mean SAT to the effective global negative carbon emission effect (-23.5 Pg C) of AU, while the remaining 78 % are a direct consequence of enhanced OHU. If AU is assumed to leave the temperature profile unaffected (assuming efficient heat exchange within the upwelling device), neither the ocean or terrestrial carbon sink change significantly compared to the reference simulation, nor ocean heat uptake or global mean SAT. Our findings lead us to challenge the current classification of AU as a mCDR method and to propose the consideration of AU primarily as a global mean SAT management method.

4.1. Introduction

The increase in global mean surface air temperature (SAT) over the last centuries is a major threat to humanity and Earth's ecosystems and is caused by anthropogenic greenhouse gas emissions (IPCC 2021). The ocean and the land play a key role in regulating SAT by each naturally taking up ~25% of anthropogenic CO_2 emissions, while the ocean also took up more than 90% of the anthropogenic heat induced by greenhouse gas emissions over the last decades (IPCC 2013; IPCC 2021). At the same time, global mean SAT increase has been shown to correlate linearly with cumulative CO_2 emissions into the atmosphere since preindustrial times (Matthews et al., 2009, MacDougall 2016). This relationship implies that to halt future global mean SAT increase, we need to reach net zero CO_2 emissions. Now in practice, this would imply to reduce global CO_2 emissions as far as possible and to compensate any remaining CO_2 emissions with anthropogenic, negative CO_2 emissions, to reach a net-zero state (IPCC 2022). Such negative CO_2 emissions are to be achieved by the implementation of carbon dioxide removal (CDR) methods. The ultimate goal of any CDR method is therefore, to support the halt of future global mean SAT increase via the compensation of remaining CO_2 emissions.

One proposed CDR method is artificial upwelling (AU), which is based on the idea to upwell nutrient rich water from the ocean interior via long ocean pipes to stimulate the production and export of carbon-rich, organic particles from the surface into the deep ocean and cause a net CO_2 uptake of the ocean via the biological carbon pump (Lovelock & Rapley, 2007, NASEM 2022). Several Earth system model studies have already investigated the maximum global CDR potential of AU (Dutreuil et al., 2009; Yool et al., 2009, Oschlies et al., 2010, Keller et al., 2014, Jürchott et al., 2023). In contrast to the simplified idea of AU to only stimulate the biological carbon pump, only a few studies discussed changes of physical properties in the water column via AU and their missing consideration for additional ocean carbon uptake, as well as the direct SAT cooling effect of AU by upwelling cold water from the ocean interior to the surface ocean (Oschlies et al., 2010, Keller et al., 2014, Jürchott et al., 2023). Changes in global mean SAT via AU can be the result of two stimulated processes. First, AU can introduce negative CO_2 emissions to the Earth system, which reduces the atmospheric CO_2 concentration and leads to an overall colder climate. Second, the upwelling of cold water from the ocean interior to the surface ocean and the respective backflow of warm surface water to depth directly cools down the surface ocean and the atmosphere, which can be understood as an artificial enhancement in vertical heat exchange (Oschlies et al.,

2010, Kwiatkowski et al., 2015, Jürchott et al., 2023). Since AU has been initially proposed as a marine CDR method with potential ecosystem benefits, a detailed and quantitative assessment of AU's impact on Earth's carbon cycle in relation to its impact on Earth's heat distribution is missing. In this study we simulate large scale AU deployment in an Earth system model of intermediate complexity under the RCP 4.5 emission pathway to (a) investigate the importance of upwelling cold water for changes in the Earth's carbon cycle, (b) to quantitatively attribute changes in global mean SAT to AU's 1) effective global negative carbon emission potential and 2) its heat redistribution effect and (c) to discuss our new findings on AU in the context of a marine CDR method and challenge its current classification and perception in the scientific community.

4.2. Methods

4.2.1. Model description

In this study we use the UVic 2.9 Earth System Climate Model of intermediate complexity in a with-Land (Keller et al., 2012) and a no-Land (Koeve et al., 2020) model configuration. The complete with-Land model consists of three dynamically coupled model components: a three-dimensional ocean circulation model including a sea-ice model, a terrestrial model and a simple one-layer atmospheric energy-moisture balance model (Weaver et al., 2001). All model components share a spatial resolution of 3.6˚ longitude and 1.8˚ latitude and the ocean component consists of 19 vertical levels with a 50 m thick layer at the surface and up to 500 m thick layers in the deep ocean. The heat flux between all model components is interactively calculated and the ocean component includes physical parameterizations for diffusive mixing along and across isopycnals and eddy induced tracer advection (Gent & Mcwilliams, 1990). Terrestrial vegetation experiences a fertilization effect via atmospheric CO_2 concentrations and follows an optimality curve for vegetation growth dependent on SAT and soil organic matter respiration is sensitive to and accelerates by an increase in SAT (Meissner et al., 2003). The ocean component contains a fully simulated carbon cycle including DIC and alkalinity, as well as the nutrients phosphate, nitrate and iron, which are all calculated as prognostic tracers. A marine NPZD-ecosystem model to represent the biological carbon pump, in which we assume a fixed C-N-P-Fe organic matter stoichiometry (Keller et al., 2012; Nickelsen et al., 2015; Yao et al., 2019), and a simple $CaCO_3$ counter pump approximation are included (Schmittner et al., 2008). Primary production and the production or dissolution of $CaCO_3$ are

not sensitive to CO_2 and the process of iron scavenging via organic and inorganic particles is represented in the iron cycle of the calibrated Fe_Dyn model (Yao et al., 2019). The no-Land model configuration only differs from the with-Land configuration with respect to interactions between the atmospheric and terrestrial model components, which are disabled in the no-Land model configuration. The comparison between AU-experiments, which are introduced in the next section, performed with the no-Land and with-Land configuration, therefore, allows us to diagnose carbon concentration and carbon climate feedbacks (Arora et al., 2020) from the terrestrial model component. Experiment names introduced in the next section include the abbreviations "WL" for with-Land and "NL" for no-Land and refer to the used model configuration. A detailed description of both model versions is given in the Supporting Information S1.

4.2.2. Simulation of AU

The general design of the simulation of AU is adopted from a previous study conducted with an earlier version of the UVic model (Oschlies et al., 2010). Model tracers like temperature (heat), DIC, all nutrients and alike are transferred via AU adiabatically from the grid box at the pipe's source depth to the surface grid box, while a compensating down-welling flux through all intermediate levels ensures volume conservation. Pumping the model tracers temperature and salinity changes the density of the water and impacts water column physics, stratification and ocean circulation. In our experiments the pipe-covered area as well as the pipe length are kept constant over the entire duration of the experiment (see next paragraph). In addition to the standard simulation named AU-WL and AU-NL, where AU affects all model tracers, experiments named AU-WL-NO-TEMP and AU-NL-NO-TEMP are achieved by keeping temperature unaffected by AU, while all other model tracers remain directly redistributed via AU. Pipes simulated in NO-TEMP experiments could be achieved from an engineering perspective via cleverly designed heat exchangers in the pipes tube.

We simulate continuous AU in ocean grid cells between 60° North and 60° South to ensure all year light availability for primary producers and where the bathymetry allows for a constant pipe length of 500 meters. Additionally, we exclude regions where the oxygen concentration in 500 meter depth is lower than 50 mmol m^{-3} to avoid enhanced denitrification via an increase in export production (~282.700.000 km^2 global pipe cover) (Fig. S 4.1). The upwelling intensity is set to 0.5 cm day^{-1}, which translates into an upwelling of a 0.5 cm thick

layer per day averaged over the entire grid box at the surface ocean by the pipes' activity (~16.4 Sv globally). Pipe length and upwelling intensity are based on the assessment of Koweek 2022 of what the upper technically feasible limit of AU is at the current technological stage. Since we keep the pipe-covered area constant as part of our experimental protocol, we do not switch of local pipe activity, if local CO_2 outgassing occurs at an ocean surface grid cell.

4.2.3. Experimental design

Following model spin-up under preindustrial pCO_2 conditions we simulate the historical period from the year 1765 to 2006 with CO_2 emissions to the atmosphere, which are consistent with historical fossil fuel and land-use CO_2 emissions and continue until the year 2100 along the moderate RCP 4.5 CO_2 emission pathway (REF-WL, REF-NL) (Meinshausen et al., 2011). For the no-Land model configuration CO_2 emissions are reduced to account for the missing terrestrial carbon sink and to ensure, that both model configurations experience the same climate change in their reference simulations (Koeve et al., 2020.). AU is simulated from the year 2025 to 2100 in both model configurations and in both AU implementations (Tab. 4.1). The comparison between AU and AU-NO-TEMP experiments generally allows us to investigate the importance of upwelling cold water for changes in the Earth's carbon cycle and in combination with the no-Land and with-Land model configurations to quantify carbon concentration and carbon climate feedbacks.

One additional idealized experiment "REF-WL-ADJ-PCO2" is performed, which allows us to diagnose the effective global negative carbon emission potential of AU in comparison to the standard RCP 4.5 CO_2 emission pathway. It is set up the same way as the with-Land reference simulation (REF-WL), but we adjusted CO_2 emissions into the atmosphere via manipulating the model's CO_2 emission forcing file to match a similar atmospheric CO_2 concentration ± 1 Pg C as diagnosed from the AU-WL experiment (Fig. S 4.2). The adjustment has been done offline and by hand. Therefore, the REF-WL-ADJ-PCO2 experiment contains the information about how many Pg of CO_2 emissions we would need to avoid in order to reach the same atmospheric CO_2 concentration achieved via AU.

Table 4-1: Overview over conducted model experiments with additional information about model configuration, artificial upwelling implementation and applied CO_2 emission pathway. Abbreviations in the experiment names refer to with-Land (WL) and no-Land (NL) model configurations and standard (AU) and no-temperature (AU-NO-TEMP) artificial upwelling implementation.

experiment name:	UVic 2.9 configuration:	AU implementation:	CO_2 emission pathway
REF-WL	Atm. + Ocean + Land	no AU	RCP 4.5
REF-NL	Atm. + Ocean	no AU	RCP 4.5 – terrestrial carbon sink
AU-WL	Atm. + Ocean + Land	all ocean tracers	RCP 4.5
AU-NL	Atm. + Ocean	all ocean tracers	RCP 4.5 – terrestrial carbon sink
AU-WL-NO-TEMP	Atm. + Ocean + Land	no temperature	RCP 4.5
AU-NL-NO-TEMP	Atm. + Ocean	no temperature	RCP 4.5 – terrestrial carbon sink
REF-WL-ADJ-PCO2	Atm. + Ocean + Land	no AU	CO_2 emissions adjusted to match C_{atm} concentration (+/- 1 Pg C) of AU-WL experiment (Fig. S 4.2)

4.3. Results and Discussion

4.3.1. Carbon cycle & ocean ecosystem response

The direct temperature pumping effect of AU in our experiments is needed to cause a significant reduction in the atmospheric carbon reservoir (Fig. 4.1a). If AU pipes don't directly pump temperature, we cannot detect significant changes in the atmospheric, terrestrial or ocean carbon inventories independently whether land carbon concentration and climate feedbacks are included or excluded (Fig. 4.1c & e). Without the consideration of terrestrial carbon concentration and climate feedbacks, i.e., our AU-NL experiment, the ocean carbon inventory increases by 2.5 Pg C, if the upwelled water maintains its temperature. Since the ocean carbon inventory does not significantly change, if AU is assumed to leave the temperature profile unaffected, the 2.5 Pg C are a result of enhanced surface ocean CO_2 solubility, which increases via a reduction in water temperature (Jürchott et al., 2023). In contrast to the expectation of how a marine CDR method should impact the ocean carbon

inventory, if AU pipes do pump temperature and we consider terrestrial carbon concentration and climate feedbacks, i.e., our AU-WL experiment, the terrestrial carbon reservoir becomes the main sink for atmospheric carbon of +14 Pg C (see discussion around Fig. 4.2). At the same time the ocean carbon reservoir responds with minor outgassing of -2 Pg C until the end of the century via a carbon concentration feedback caused by the terrestrial carbon uptake (Keller et al., 2018). Conclusively, the overall impact of AU on the atmosphere's carbon reservoir in our model simulations is rather small and not driven by enhanced ocean carbon uptake, despite AU pipes being implemented in the ocean.

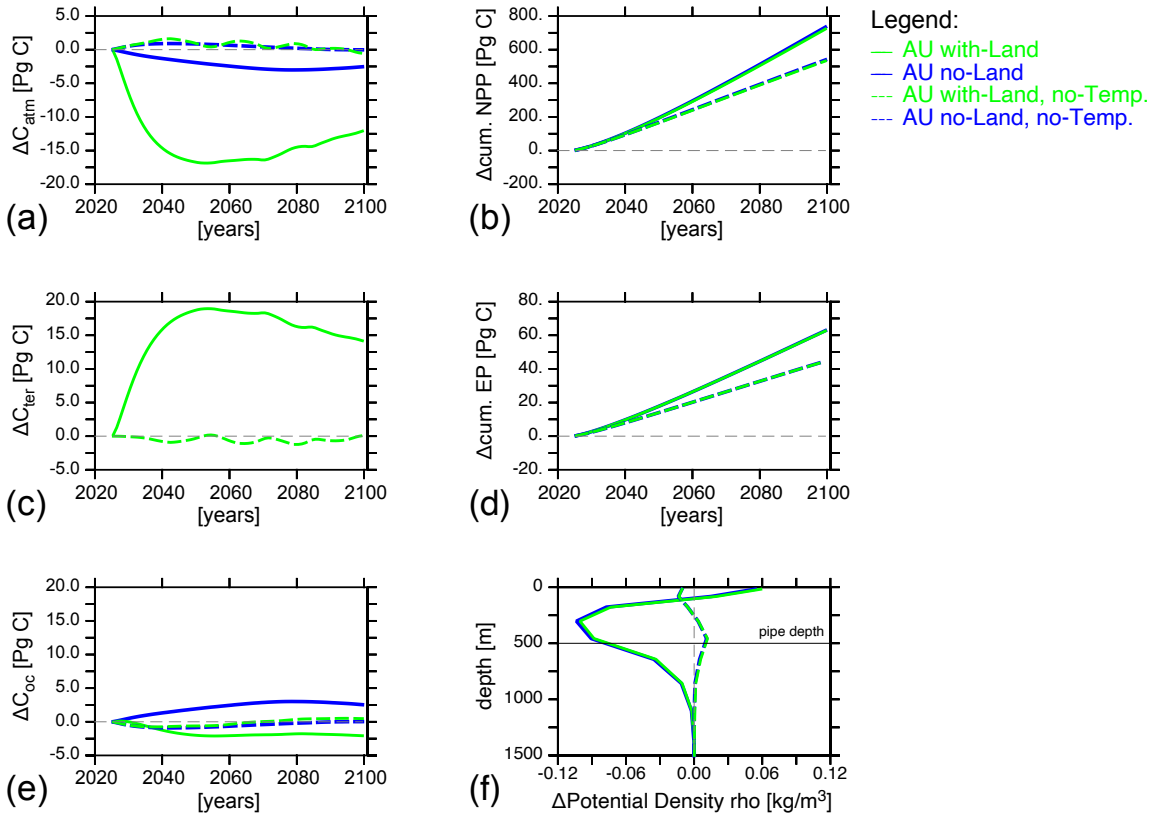

Figure 4-1: Global changes in Earth's main carbon reservoir inventories (left column) and ecosystem relevant variables (right column) due to artificial upwelling (AU) in comparison to the respective reference simulation (REF-WL, REF-NL). Changes in carbon reservoir inventories are shown for a) atmosphere, c) land and e) ocean in Pg C. Changes in the model ecosystem are shown via b) cumulative ocean net primary production (NPP) and d) export production (EP) in Pg C. f) vertical profiles of changes in laterally averaged potential density (rho) over depth in kg m^{-3} for year 2100. Green lines represent UVic with-Land (WL) and blue lines represent UVic no-Land (NL) model configuration experiments. In experiments with continuous lines AU pumps all ocean model tracers (AU) and in experiments with dashed lines AU pumps all ocean model tracers except temperature (AU-NO-TEMP). In panels b, d, f, green and blue lines are largely overlapping.

We find a strong and steady increase in cumulative ocean net primary production (NPP) of up to 734 Pg C until the end of the century in both AU-WL and AU-NL experiments in

comparison to the respective reference simulation, which is driven by the upwelling of nutrients and independently of terrestrial carbon feedbacks (Fig. 4.1b). The increase in ocean NPP translates into enhanced cumulative export production of up to 63 Pg C (Fig. 4.1d), but the ocean carbon reservoir remains almost unaffected. This is a consequence of the low abundance of preformed nutrients at 500 meters depth and potential iron limitation at the surface ocean (Duteil et al., 2012, Jürchott et al., 2023). Export production remains therefore a poor indicator for changes in the overall ocean carbon inventory in our experiments (Frenger et al., 2024). If AU pipes don't pump temperature (AU-WL-NO-TEMP, AU-NL-NO-TEMP), cumulative ocean NPP and export production decreases each by about 27 % in comparison to the standard AU_WL and AU-NL experiments. The likely major reason for this difference is the weakened ocean stratification, if AU pipes pump temperature (Fig. 4.1f), since the pumping of temperature reduces the density gradient between surface and interior ocean (Fig 4.3c), which impacts ocean mixing and thus, the resupply of nutrients from the interior ocean back to the surface ocean. We conclude that AU is highly effective in stimulating the model ecosystem, but we find no related increase in the ocean carbon inventory.

4.3.2. Terrestrial carbon climate feedback

The increase in the terrestrial carbon sink of +14 Pg C via AU until the end of the century is a result of a change in the balance between terrestrial carbon uptake and release processes (Fig. 4.2c). The main carbon sink on land in our experiments is terrestrial vegetation NPP, which is CO_2 and temperature sensitive, and the main source is soil organic matter respiration, which is temperature sensitive. Both processes compensate each other to a net terrestrial carbon sink in our REF-WL simulation (Fig. 4.2a). The CO_2 and temperature sensitivities included in the terrestrial model component imply a potential sensitivity of the terrestrial carbon cycle to the simulated future CO_2 emission pathway. Since AU decreases global mean SAT (Fig 4.3a), the terrestrial model component experiences a colder climate. Global terrestrial vegetation NPP initially increases as a consequence of reduced SAT (increased carbon sink), but with regional differences (Fig. 4.2b, c). Around the equator, too high SAT puts stress on terrestrial vegetation NPP, which gets relieved via the SAT cooling effect of AU and enhances terrestrial vegetation carbon uptake. In regions poleward of about 30˚, SAT is lower than optimal for terrestrial vegetation NPP already prior to AU deployment and declines even further due to AU, causing regionally reduced terrestrial vegetation carbon uptake. In contrast

to the regional response pattern in terrestrial vegetation NPP, soil organic matter respiration globally decreases as a consequence of reduced SAT (decreased carbon source) until mid-century (Fig. 4.2c, d). The net effect of both processes is an enhanced terrestrial carbon sink as shown in Fig. 1c, which can be understood as a carbon climate feedback driven by a reduced global mean SAT. However, the magnitude of terrestrial carbon climate feedbacks is highly variable in different Earth system models (Arora et al., 2020) and a different terrestrial model component could lead to a different response of the terrestrial carbon cycle to the SAT-induced changes via AU.

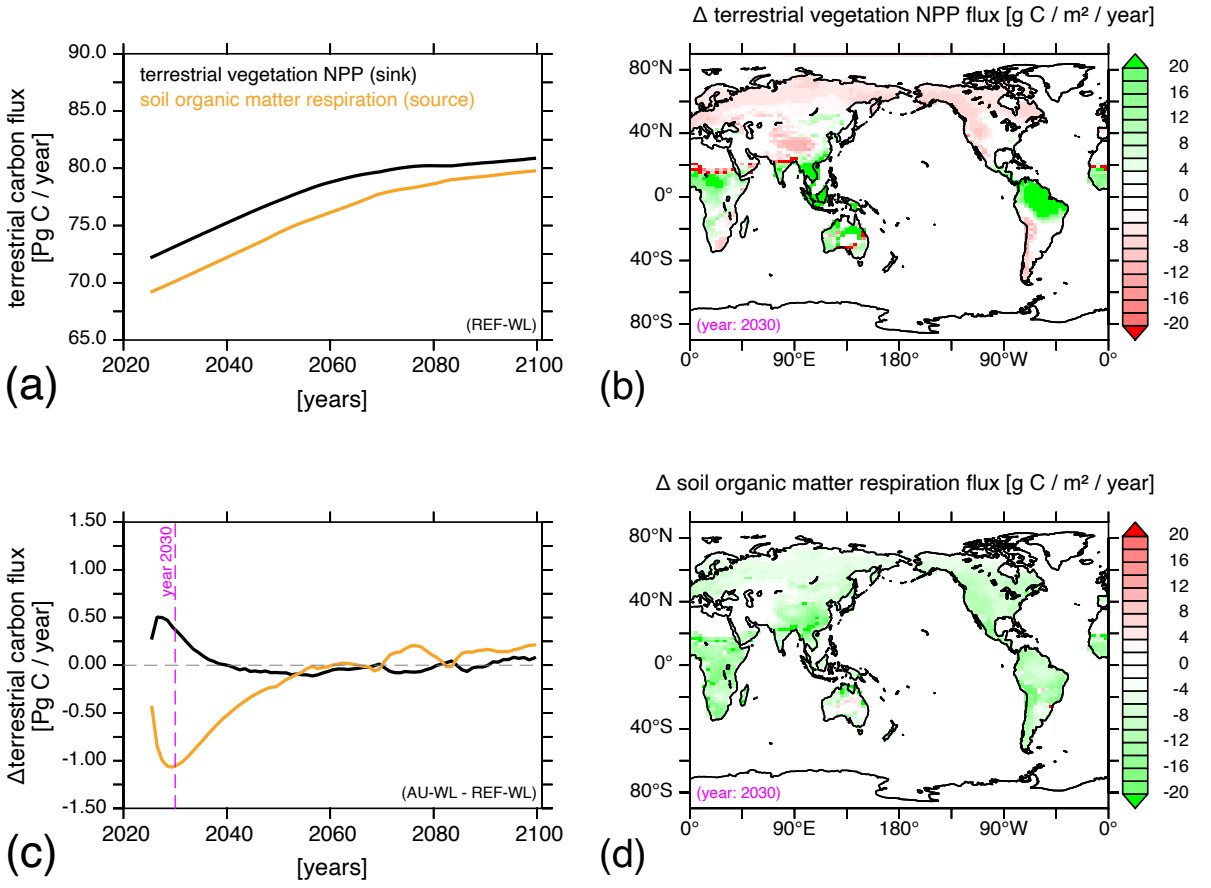

Figure 4-2: Overview over changes in terrestrial vegetation net primary production (NPP, black) and soil organic matter respiration (orange) carbon fluxes. a) transient change in the reference with-Land (REF_WL) experiment and c) induced changes due to standard artificial upwelling (AU-WL – REF-WL) in Pg C year^{-1} with spatial changes in b) terrestrial vegetation NPP and d) soil organic matter respiration in g C m^{-2} year^{-1} for the year 2030 with green (red) indicating an increase (decrease) in the local land carbon inventory.

4.3.3. Carbon cycle response vs. heat redistribution effect

AU strongly reduces global mean SAT by up to -0.37 ˚C after 10 years of pipe deployment and up to -0.2 ˚C until the end of the century in comparison to the respective reference simulation and largely independently of terrestrial carbon concentration and climate feedbacks (Fig 4.3a). At the same time OHU increases by up to 0.6 W m^{-2} until year 2035 and by up to 0.3 W m^{-2} until year 2100 in comparison to the respective reference simulation (Fig 4.3b) and the additional heat is stored in the ocean interior around the pipes source depth of 500 meters (Fig 4.3c). This interior ocean temperature increase might put stress on the mesopelagic ecosystem in the real-world ocean, which is not resolved in our Earth system model. These results suggest that AU is highly effective in reducing global mean SAT, which is the ultimate purpose of a CDR method. The detected decrease in global mean SAT via AU is, however, not only a consequence of the decrease in atmospheric CO_2 concentrations, i.e., its negative carbon emissions, but of the AU-induced increase in vertical heat exchange, which enhances OHU as well. We have generally a good theoretical understanding of how CDR technologies could impact the global carbon cycle and perturbate the Earth system and we don't expect severe negative global consequences, if we stop these CDR technologies (Keller et al., 2014). In contrast, changes in the Earth's heat budget, including a deliberate change as done with AU, has been previously suggested to pose a much greater risk with long-term uncertainties and probably cannot be stopped once introduced without severe consequences for the entire Earth system (Oschlies et al., 2010, Keller et al., 2014).

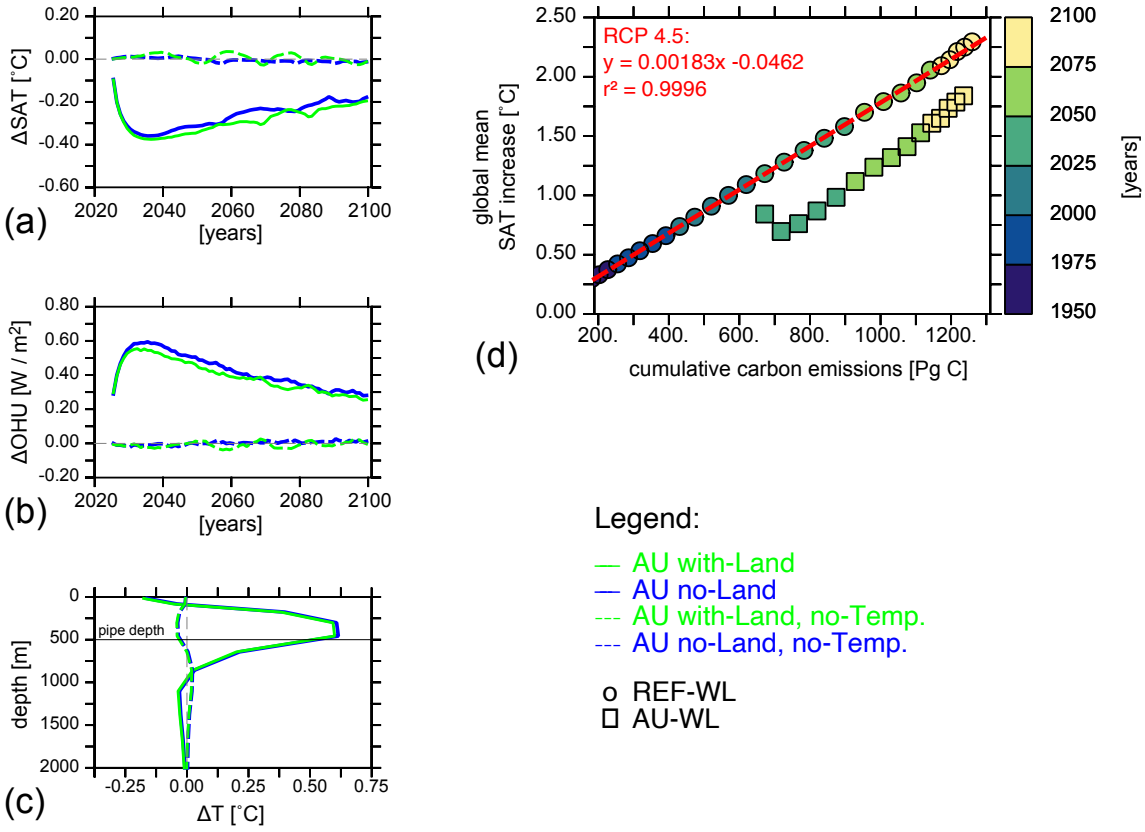

Figure 4-3: Global changes in Earth's heat distribution (left column) due to artificial upwelling (AU) in comparison to the respective reference simulation and changes in relationship between cumulative carbon emissions in Pg C and global mean surface air temperature (SAT) in ˚C (TCRE). Changes in heat distribution are shown in a) global mean SAT in ˚C and b) ocean heat uptake (OHU) in W m^{-2} over time and c) vertical profiles of changes in laterally averaged water temperature for year 2100 with the same color code as in figure 1. d) TCRE relationship since year 1765 and shown from year 1950 to 2100 with historical carbon emissions until year 2006 and continued with the moderate emission pathway RCP 4.5 for UVic 2.9 with-Land Earth system model (REF-WL, circle) and changes due to AU (SAT impact from AU-WL experiment and effective negative carbon emissions from REF-WL-ADJ-PCO2 experiment, square). Red dashed line represents linear regression function for reference simulation, which is in good agreement with MacDougall et al., 2016.

To quantitively attribute changes in global mean SAT to either AU's impact on the global carbon cycle or its impact on OHU, we use the linear relationship between global mean SAT to cumulative carbon emissions (TCRE relationship), which for our UVic with-Land reference experiment (REF-WL) under RCP 4.5 has a 1.78 ˚C increase in global mean SAT per 1000 Gt carbon emitted into the atmosphere (Fig 4.3d). To do so, we first need to translate the atmospheric pCO_2 reduction via AU into its effective negative carbon emission potential, which is the purpose of our idealized REF-WL-ADJ-PCO2 experiment. This step is necessary, because a decrease in the atmosphere's carbon inventory should not be confused and transferred one to one into effective negative carbon emissions, since over the last few decades only around 50 % of positive anthropogenic CO_2 emissions remained in the atmosphere, the so-called airborne fraction (IPCC 2013), and a similar less than 100%

airborne fraction can be expected for negative carbon emissions. The detected net decrease in the atmosphere's carbon inventory of -12 Pg C until year 2100 (Fig 4.1a) translates into -23.5 Pg C of effective negative carbon emissions as diagnosed via the REF-WL-ADJ-PCO2 experiment (Fig S 4.2d). Note that this estimation assumes no significant changes in ocean and land carbon sinks and OHU in comparison to the with-Land reference (REF-WL) simulation performed under the standard RCP 4.5 CO_2 emission pathway. As shown in Fig. 4.3d, the standard AU with-Land (AU-WL) experiment significantly deviates from the linear path of the TCRE relationship towards a lower global mean SAT that is lower than expected from cumulative carbon emissions alone, which indicates a disproportionately stronger impact of AU on global mean SAT compared to the Earth's carbon cycle. The detected decrease of -0.2 ˚C in global mean SAT via AU until the end of the century would theoretically require a total of -107 Pg C of effective negative carbon emissions according to the TCRE relationship. The diagnosed -23.5 Pg C of effective negative carbon emissions from the REF-WL-ADJ-PCO2 experiment can therefore only explain 22 % of the decrease in global mean SAT, while the remaining 78 % are a consequence of enhanced OHU. We conclude that the increase in OHU via AU is primarily responsible for the decrease in global mean SAT, while AU's effective negative carbon emission potential is of secondary importance for the realized SAT change.

4.4. Conclusions

The purpose of a marine CDR method is to achieve negative carbon emissions via enhanced ocean carbon uptake and thereby, reduces further global mean SAT increase. We find under the RCP 4.5 CO_2 emission pathway significant changes in global mean SAT and in the atmospheric CO_2 concentration compared to the reference simulation without AU only, if AU directly impact Earth's heat distribution by upwelling cold water from the ocean interior. If AU directly impacts Earth's heat distribution, the atmospheric carbon reservoir decreases by 12 Pg C, but the effect is driven by an enhanced terrestrial carbon sink and mainly via reduced soil organic matter respiration and not by ocean carbon uptake, which might have negative long-term implications for the durability of the sequestered carbon. Our model simulations further suggest that the redistribution of heat in the Earth system via AU is needed for a significant reduction in the atmospheric carbon reservoir. However, since the reduction in the atmospheric carbon reservoir is driven via a carbon climate feedback related to the terrestrial

carbon cycle, the magnitude of this effect might change in different Earth system models (Arora et al., 2020) and could be sensitive to the simulated future CO_2 emission pathway (Jürchott et al., 2023).

The reduced atmospheric CO_2 concentration via AU translates into an effective negative carbon emission effect of -23.5 Pg C, which, following the TCRE relationship, contributes to 22 % to the detected -0.2 ˚C decrease in global mean SAT, with the remaining 78 % being a consequence of enhanced OHU. The marine ecosystem in our model benefits from AU due to the supply of nutrients from the ocean interior, but the water temperature increase around 500 meters depth as a consequence of enhanced OHU might put stress on the mesopelagic ecosystem in the real-world ocean, which is not resolved in our Earth system model in such great detail. Our new and quantitative findings lead us to challenge the classification of AU as a marine CDR method and to propose the consideration of AU primarily as a global mean SAT management method with the potential for surface ocean ecosystem benefits.

Acknowledgement

We acknowledge discussions with colleagues from the Biogeochemical Modelling research unit at GEOMAR. M.J. acknowledges funding from German BMBF, Project Test-ArtUp (Grant Number: 03F0897A). This is a contribution to the CDRmare research mission funded by the German Alliance for Marine Research (DAM) and to the Subtopic 6.3 “The future biological carbon pump” of the Helmholtz Earth and Environment research program “Changing Earth – Sustaining our Future” (POF IV). The author(s) wish to acknowledge discussions with members of the BM-carbon-theme group and the use of the PyFerret program for analysis and graphics in this paper.

Data statement

Model output and scripts for data processing are available from data.geomar.de (https://hdl.handle.net/20.500.12085/15050575-e68d-4f7c-90c0-e9cde1525ea1)

4.5. Supporting Information

Introduction

Here we provide Supplementary Methods (Text S1) and Supplementary Figures (S 4.1 to S 4.2), which present details of our model experiments.

Text S1.

Supplementary Methods

UVic model

UVic (Weaver et al., 2001) is an Earth system model of intermediate complexity (EMIC) with a shared horizontal resolution of 3.6° in longitude and 1.8° in latitude direction for all individual model components. In this study we use the calibrated UVic 2.9 Fe_Dyn version in a with-Land (Yao et al., 2019) and a no-Land (Koeve et al., 2020) model configuration. The fully coupled with-Land model configuration consists of three dynamically coupled model components: a three-dimensional ocean circulation model including a sea-ice model, a terrestrial model and a simple one-layer atmospheric energy-moisture balance model.

In the atmospheric energy-moisture balance model the heat and water fluxes to the ocean, sea-ice and land model components are interactively calculated. Wind forcing is prescribed with monthly mean winds from NCAR/NCEP climatological data. The CO_2-concentration in the atmosphere dynamically reacts to changes in ocean and land carbon uptake / outgassing behavior, as well as introduced emissions via CO_2-emission forcing (Meinshausen et al., 2011, see next section), and thus, allows for carbon concentration and carbon climate Earth system feedbacks (Keller et al., 2018).

The ocean circulation model (MOM, Modular Ocean Model 2) includes physical parameterizations for diffusive mixing along and across isopycnals and eddy induced tracer advection (Gent & McWilliams, 1990). It has 19 vertical layers and layer thickness increases from 50 meter at the surface to 500 meter in the deep ocean. The model ocean contains a fully simulated carbon cycle with dissolved inorganic carbon (DIC) and alkalinity as well as the nutrients nitrate, phosphate and iron as prognostic model tracers. Gas exchange of oxygen and

DIC is simulated as in Orr et al. (1999). The model ocean contains a marine NPZD (Nutrients - Primary Producers - Zooplankton - Detritus) ecosystem model to represent the biological carbon pump, in which we assume a fixed C-N-P organic matter stoichiometry following Redfield ratio (Keller et al., 2012) and a fixed N-Fe organic matter stoichiometry of 1 mol N per 10 μmol Fe (Yao et al., 2019), in addition to a simple $CaCO_3$ counter pump approximation (Schmittner et al., 2008). Neither primary production nor the production or dissolution of $CaCO_3$ are sensitive to CO_2. In order to avoid excessively long model spin-up times our idealized model experiments do not simulate sediment processes. Any organic detritus or $CaCO_3$ reaching the bottom of the model is dissolved in the deepest wet box instantaneously.

The terrestrial model is based on the Hadley Center model TRIFFID and contains vegetation and an interactive carbon cycle with five soil depth levels (Meissner et al., 2003, Keller et al., 2012). Terrestrial vegetation growth is sensitive to surface air temperature changes and experiences a fertilization effect via atmospheric CO_2 concentrations. Soil organic matter respiration is sensitive to and accelerates by an increase in surface air temperature (Meissner et al., 2003).

In the no-Land model configuration, we intentionally disabled all interactions with the terrestrial model component. As a direct consequence all terrestrial carbon concentration and carbon climate feedbacks are disabled in this model configuration, which allows us (i) to better understand such feedbacks in comparison with experiments conducted with the with-Land model configuration and (ii) provides insights on the impact of AU solely on the marine carbon cycle.

Experimental design

We follow the model spin-up procedure under preindustrial pCO_2 conditions and model evaluation described in detail in Koeve et al. (2020) (see their Supplementary Methods). Afterwards, we simulate the period from the year 1765 to 2005 with historical CO_2-emissions to the atmosphere, consistent with historical fossil fuel and land-use CO_2-emissions, and continue until the year 2100 with the moderate RCP 4.5 CO_2-emission pathway as our reference experiment (Meinshausen et al., 2011). For the use of the no-Land model configuration, original CO_2-emission forcing data are corrected for the disabled land

interactions to ensure that the no-Land reference experiment experiences the same climate perturbation (ocean warming and circulation change) as its fully coupled with-Land counterpart (Koeve et al., 2020). The correction of the historical and future CO_2-emission forcing is done by first running the fully coupled with-Land reference experiment and diagnose the net carbon fluxes between the land component and the atmosphere. Afterwards, the RCP4.5 CO_2-emission forcing pathway for the no-Land model configuration is offset by the previously diagnosed net carbon flux between the land biosphere and the atmosphere (see Koeve et al., 2020 for details). Due to this procedure, we ensure that carbon sources (e.g., land-use changes as a consequence of deforestation) and sinks from the land component remain represented in the atmosphere's carbon budget for the no-Land model configuration, but any additional land carbon concentration and carbon climate feedbacks associated with the system perturbation via artificial upwelling are excluded. In this idealized model study, we do not consider the impact of non-CO_2 climate forcing (e.g., from N_2O, CH_4, aerosols) in particular, since the UVic model lacks a prognostic atmospheric chemistry model and hence respective sinks of e.g., N_2O and CH_4 would not be well defined.

Artificial upwelling implementation

The general design of the simulation of artificial upwelling is adopted from a previous study conducted with an earlier version of the UVic model (Oschlies et al., 2010) and modified into two different artificial upwelling implementations (standard artificial upwelling and no-Temperature). In the standard artificial upwelling experiments all ocean model tracers (e.g., temperature, salinity, DIC, alkalinity, PO_4, NO_3, Fe and O_2) and idealized tracers are transferred via artificial upwelling adiabatically from the lowest grid box at the pipe's source depth to the surface grid box, while a compensating down-welling flux through all intermediate levels ensures volume conservation. The pumping of heat and salinity does change the density of the water and, as a consequence, impacts water column physics and ocean circulation. The source depth of the artificial upwelling pipes is kept constant at 500 meters and the upwelling intensity is set to 0.5 cm day^{-1}, which translates into the upwelling of a 0.5 cm thick layer per day averaged over the entire grid box at the surface ocean by the pipe's activity. Both conditions are based on an assessment of what the upper technically feasible limit of artificial upwelling is at the current technological stage (Koweek 2022).

The pipe-covered area is kept constant over the entire duration of all artificial upwelling experiments. It includes only ocean grid cells between 60˚ North and 60˚ South to ensure all year light availability for primary producers and in which the bathymetry allows for a constant pipe length of 500 meters. Additionally, we exclude regions where the oxygen concentration in 500 meters depth in the reference with-Land experiment in year 2100 is lower than 50 mmol m^{-3} to avoid enhancing denitrification via the local stimulation of export production (~282.700.000 km^2 global pipe cover) (Fig. S 4.1).

In the no-Temperature experiments the artificial upwelling pipes pump all ocean model tracers except temperature, which has implications on changes in the ocean heat uptake, surface ocean carbon and oxygen solubility, surface air temperature and associated terrestrial carbon concentration and carbon climate feedbacks.

Reference-with-Land-adjusted-pCO2 experiment

We perform one additional "REF-WL-ADJ-PCO2" (Reference-with-Land-adjusted-pCO2) experiment, which allows us to diagnose the effective global negative carbon emission associated with the reduction in atmospheric CO_2 concentrations in the artificial upwelling, with-Land (AU-WL) experiment. This idealized experiment is set up the same way as the with-Land reference simulation (REF-WL), but we adjusted CO_2 emissions into the atmosphere to match a similar atmospheric CO_2 concentration ± 1 Pg C as diagnosed from the AU with-Land (AU-WL) experiment (Fig. S 4.2a-d). The manipulation of the model's initial RCP 4.5 CO_2 emission forcing file to match the atmospheric CO_2 concentration from the AU-WL experiment has been done offline via multiple repetitions of the REF-WL-ADJ-PCO2 experiment and followed each time by diagnosing the difference between the AU-WL and the REF-WL-ADJ-PCO2 pCO_2-concentration and adjustments of the CO_2 emission forcing file. This experimental setup is necessary to investigate the effective global negative carbon emission potential of artificial upwelling, since over the last few decades only around 50 % of positive anthropogenic CO_2 emissions remained in the atmosphere, the so-called airborne fraction, and a similar less than 100% airborne fraction can be expected for negative carbon emissions (Fig S 4.2e). The direct translation of a reduction in atmospheric CO_2 concentrations into an effective negative CO_2 emission potential would therefore be inaccurate.

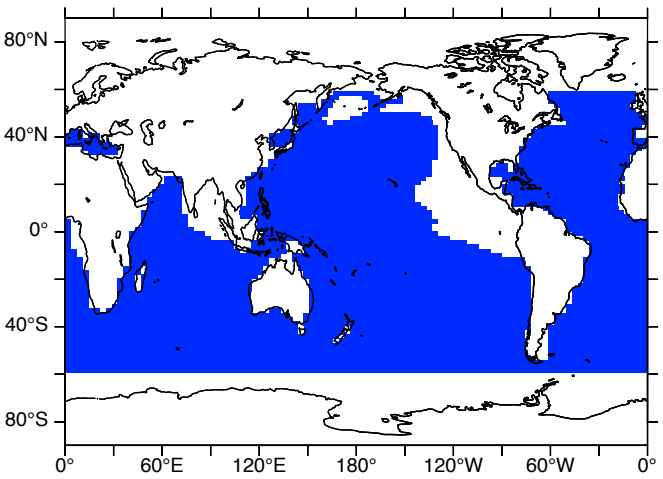

Figure S 4-1: Overview over pipe-covered area (blue) for all performed artificial upwelling experiments. The pipe-covered are is kept constant over the entire duration of the experiments.

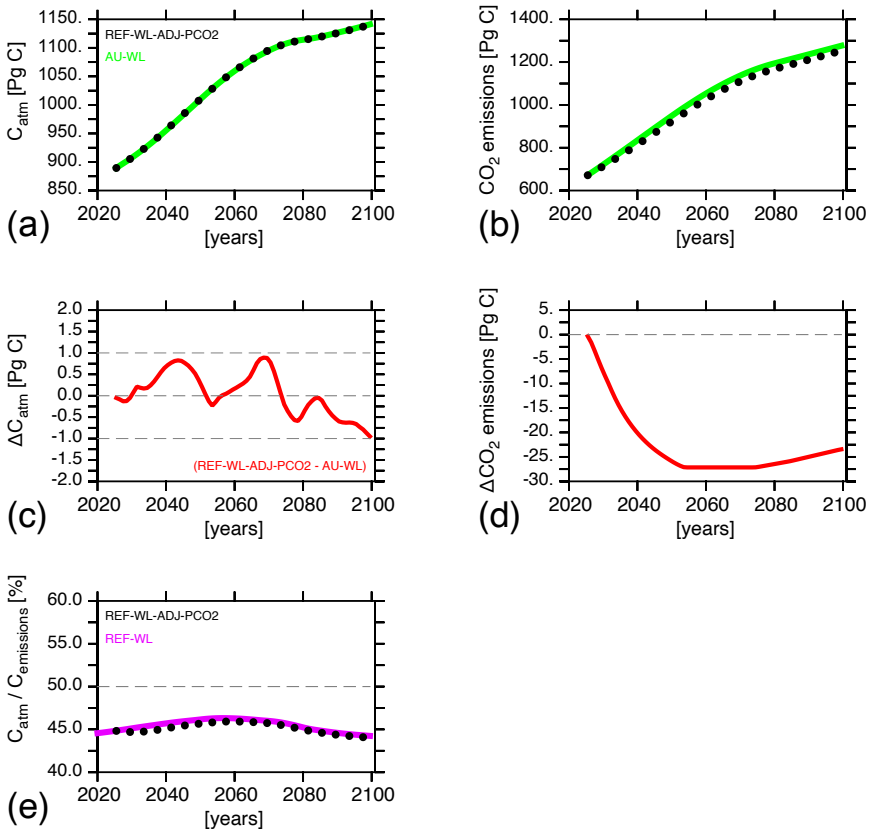

Figure S 4-2: Overview over CO_2-emissions emitted into the atmosphere (b) and atmospheric CO_2-concentrations (a) for artificial upwelling, with-Land (AU-WL, green) and REF-WL-ADJ-pCO2 (black doted) experiments in Pg C, as well as their difference (c, d) in red in Pg C. Panel (e) shows fraction of carbon in %, which was emitted and stayed in the atmosphere for REF-WL-ADJ-pCO2 (black doted) and reference, with-Land (REF-WL) experiments.

5. Conclusion and Outlook

5.1. Summary and Conclusion

Artificial upwelling has been initially proposed and gained attention as a CDR method with the aim to fertilize the surface ecosystem via artificially upwelling nutrient-rich deep water to cause a CO_2-flux from the atmosphere into the ocean interior. In this thesis my co-authors and I use the UVic 2.9 Earth system model of intermediate complexity to simulate future large-scale applications of artificial upwelling to further investigate its maximum CDR-potential and to develop a quantitative understanding of the underlying processes including co-dependencies, limitations and side-effects.

In chapter 2 **"Artificial Upwelling – A Refined Narrative"** we examine in a first step the impact of future CO_2-emission pathways on the maximum additional ocean carbon uptake potential of artificial upwelling between the years 2020 and 2100 and find an overall increase in the marine carbon inventory in all artificial upwelling experiments, but the magnitude of the increase depends strongly on the future CO_2-emission pathway and ranges from 1 Pg C $year^{-1}$ under RCP 8.5 to 0.3 Pg C $year^{-1}$ under RCP 2.6. In a second step, we make use of two idealized model tracers, which allow us to quantitively attribute changes in the ocean carbon inventory to the biological carbon pump and to the solubility pump. While the marine carbon inventory attributable to the biological carbon pump increases in all artificial upwelling experiments and only shows a moderate CO_2-emission pathway dependency, the carbon inventory attributable to the solubility pump responds with CO_2-outgassing under RCP 2.6, but becomes equally effective in CO_2-uptake under RCP 8.5 in comparison to the biological carbon pump. We further discuss three processes, which influence the physical-chemical carbon uptake at the surface ocean and are impacted by artificial upwelling. First, artificial upwelling pumps up alkalinity to the surface ocean, which naturally increases with depth in most ocean regions due to the function of the $CaCO_3$-counter pump. An increase in alkalinity at the surface ocean will result in additional ocean carbon uptake and this process recently turned out to be CO_2-emission pathway dependent (Schwinger et al., 2024). Second, artificial upwelling pumps up preformed DIC in our experiments, which was last in contact with the atmosphere several centuries ago and therefore, equilibrated under preindustrial pCO_2

conditions. If upwelled to the surface ocean and in contact with a much higher future atmospheric pCO_2 concentration, the upwelled preformed DIC causes CO_2-uptake from the atmosphere, which is strongly dependent on the atmospheric pCO_2 concentration and thus, depends on the future CO_2-emission pathway. The third process relates to changes in ocean temperatures, which gets influenced via artificial upwelling by pumping up cold water to the surface and the backflow of warm water into the ocean interior. Since a higher future CO_2-emission pathway results in an overall warmer surface ocean, the difference between interior ocean and surface ocean temperatures increases with a higher future CO_2-emission pathway as well. Thus, the relative cooling effect of artificial upwelling increases with a higher future CO_2-emission pathway, which in lockstep further increases CO_2-solubility. Furthermore, we find an increase in interior ocean temperatures as a consequence of the backflow of warm surface water. Higher interior ocean temperatures speed up organic matter respiration and reduce in our RCP 8.5 artificial upwelling experiment transfer efficiency by -7.2%. As a consequence, only 29% of the increase in ocean carbon uptake attributable to the biological carbon pump ends up in the deep ocean below the simulated maximum pipe source depth. We conclude that the initial narrative of additional ocean carbon uptake via artificial upwelling being driven via the biological carbon pump is too simplified and misses quantitatively important ocean carbon response processes associated with the solubility pump.

In the third chapter **"The Response of the Ocean Carbon Cycle to Artificial Upwelling, Ocean Iron Fertilization and the Combination of both"** we further investigate the ocean carbon uptake potential of artificial upwelling with a specific focus on iron-limitation for the marine ecosystem. For this purpose, we first simulate global and regional artificial upwelling between the years 2025 and 2100 under the RCP 4.5 CO_2-emission pathway in a UVic version, which contains iron as a prognostic tracer at depth. Additionally, we simulate artificial upwelling and ocean iron fertilization individually and in combination in a UVic version, which contains iron only via a prescribed concentration mask at the surface ocean and which has been used in chapter 2 as well. We find that globally simulated artificial upwelling by itself does neither significantly increase the total ocean carbon inventory, nor the carbon inventory attributable to the biological carbon pump. We investigated iron as the limiting nutrient for the ecosystem, which limits the uptake of upwelled preformed nutrients next to remineralized nutrients and thus, additional ocean carbon uptake attributable to the biological carbon pump. Ocean iron fertilization simulated by itself, especially poleward of 45˚ North and South, is responsible for +86.85 Pg C additional ocean carbon uptake, since the Southern Ocean is classified as a high-nutrient-low-chlorophyl (HNLC) region and limited by

iron. However, the combination of globally applied artificial upwelling and ocean iron fertilization yields an ocean carbon uptake response (+103 Pg C), which exceeds the ocean carbon uptake potential of both methods individually and is driven via the biological carbon pump. We find in all marine CDR experiments discussed in chapter 3 an increase in export production of organic matter, but cannot find a consistent relationship between the increase in export production and the response of the ocean carbon inventory attributable to the biological carbon pump, which makes export production overall a poor indicator for additional ocean carbon uptake. The increase in export production and associated respiration at depth also promotes the expansion of already existing oxygen minimum zones and causes a disproportionately larger increase in denitrification than N_2-fixation, which reduces the overall ocean nitrate inventory with possible negative long-tern consequences for the ocean ecosystem (Oschlies et al., 2019, Wu et al., 2023). Overall, artificial upwelling simulated by itself is in our model experiments ineffective as a marine CDR method and requires simultaneously applied ocean iron fertilization to enhance ocean carbon uptake.

The direct impact of artificial upwelling on ocean temperatures discussed in chapter 2 and its ineffectiveness as a marine CDR method discovered in chapter 3 inspired the investigation in chapter 4 **"Leaving the marine CDR narrative behind. A Re-Classification Attempt for Artificial Upwelling"**, which explores the impact of artificial upwelling on Earth's main carbon reservoirs in relation to its impact on global mean surface air temperature and underlying co-dependencies. In this chapter we use the UVic 2.9 model, which contains iron as a prognostic tracer at depth, under the moderate RCP 4.5 CO_2-emission pathway between the years 2025 and 2100 in a no-Land and a with-Land configuration and simulate two close-to-global AU implementations, which either do or do not directly redistribute ocean heat. We find that Earth's carbon and heat budgets both only significantly change, if artificial upwelling directly redistributes ocean heat, which highlights the importance of pumping temperature for additional ocean carbon uptake via the solubility pump discussed in chapter 2. The detected decrease in global mean surface air temperature is much greater and out of relation in comparison to the negative CO_2-emissions effect of artificial upwelling as suggested by the TCRE (Transient Climate Response to cumulative Emissions) relationship. Additionally, in the with-Land model configuration the terrestrial carbon inventory increases by +14 Pg C as a consequence of decreased global mean surface air temperature, mainly due to a reduction in soil organic matter respiration (carbon climate feedback). Simultaneously, the ocean carbon inventory looses -2 Pg C via a carbon concentration feedback as a response to the additional terrestrial carbon uptake and reduced atmospheric pCO_2 concentrations

(figure 1.2c). The results presented in chapter 4 challenge and do not agree with the classification of artificial upwelling as a marine CDR method, since its impact on the carbon cycle is minor compared to its impact on global mean surface air temperature and the minor atmospheric pCO_2 reduction is not driven by additional ocean, but terrestrial carbon uptake.

The results discussed in this thesis lead to the overall conclusion that artificial upwelling implemented by itself does not significantly introduce negative CO_2 emissions to the Earth system, but is effective in (i) supporting additional ocean carbon uptake primarily achieved via ocean iron fertilization and (ii) in reducing global mean surface air temperature via its direct impact on the redistribution of heat in the Earth system. However, the large-scale simulation of artificial upwelling comes at the cost of elevated interior ocean temperatures, which leads to further issues, if artificial upwelling would be abruptly stopped (Oschlies et al., 2010), regional expansion of oxygen minimum zones and enhanced denitrification. The current classification of artificial upwelling as a marine CDR method does therefore, not represent its function and potential impact on the Earth system.

1.1. Outlook

The UVic 2.9 Earth system model of intermediate complexity is a suitable tool to simulate large-scale artificial upwelling, to quantitatively assess its maximum CDR potential and to develop a quantitative understanding of the underlying processes including co-dependencies, limitations and side-effects. However, simplifications such as a fixed carbon-to-nutrient stoichiometry, a fixed organic particle sinking speed and the overall simplified structure of the model ecosystem cannot fully represent the complexity of Earth's ecosystems. Other processes such as a prognostic silicate cycle and the representation of diatoms, which are the most abundant primary producers in natural upwelling systems (Chavez and Messié 2009, Kämpf and Chapman 2016), are currently missing in the used UVic 2.9 model versions. Including those processes and considering the impact of artificial upwelling on e.g., organic matter stoichiometry and sinking speeds as observed in mesocosm studies (Baumann et al., 2021, Goldenberg et al., 2022, Goldenberg et al., 2024) might further improve our understanding on the impact of artificial upwelling on the ocean carbon cycle and the biological carbon pump, but could as well pose the risk of model overfitting, if only the observed effects would be implemented, but not the underlying mechanisms, which lead to the observed effects. Furthermore, a fully coupled and prognostic N_2O-cycle connected to the

process of denitrification in the ocean could be useful to further assess possible side-effects concerning artificial upwelling and provide a new perspective on the net effect of artificial upwelling on global mean surface air temperature via including N_2O as a non-CO_2 greenhouse gas (Jin and Gruber, 2003, Dutreuil et al., 2009). Future studies with the UVic 2.9 model could further investigate the response of individual ocean regions to artificial upwelling, although a higher spatial resolution could be advantageous depending on the simulated scale of artificial upwelling. Finally, the simulation of artificial upwelling, implemented the same way as presented in this thesis, in other Earth system models as part of a model intercomparison project (MIP) or in differently parameterized versions of the same Earth system model could provide further insights into the sensitivity of the carbon cycle, heat budget, co-dependencies, carbon concentration and carbon climate feedbacks to artificial upwelling.

Bibliography

Abrahams, A., Schlegel, R. W., & Smit, A. J. (2021). Variation and change of upwelling dynamics detected in the world's eastern boundary upwelling systems. *Frontiers in Marine Science*, *8*, 626411. DOI:10.3389/fmars.2021.626411

Amann, T., Baatz, C., Böttcher, M., Geden, O., Keller, D.P., Kopf, A., Merk, C., Milinski, S., Mintenbeck, K., Oschlies, A., Pongratz, J., Proelß, A., Rehder, G., Rickels, W., Riebesell, U., Sswat, M., Tank, L., Wallmann, K., Westmark, L., Wölfelschneider, M. and Zimmer, M. (2024) *World Ocean Review: The Ocean – A Climate Champion? How to Boost Marine Carbon Dioxide Uptake.* World Ocean Review, 8. Maribus, Hamburg, Germany, 243 pp. ISBN:978-3-86648-733-8

Arora, V. K., Katavouta, A., Williams, R. G., Jones, C. D., Brovkin, V., Friedlingstein, P., ... & Ziehn, T. (2020). Carbon–concentration and carbon–climate feedbacks in CMIP6 models and their comparison to CMIP5 models. *Biogeosciences*, *17*(16), 4173-4222. DOI:10.5194/bg-17-4173-2020

Aumont, O., & Bopp, L. (2006). Globalizing results from ocean in situ iron fertilization studies. *Global Biogeochemical Cycles*, *20*(2). DOI:10.1029/2005GB002591

Babiker, M., G. Berndes, K. Blok, B. Cohen, A. Cowie, O. Geden, V. Ginzburg, A. Leip, P. Smith, M. Sugiyama, F. Yamba, 2022: Cross-sectoral perspectives. In IPCC, 2022: *Climate Change 2022: Mitigation of Climate Change. Contribution of Working Group III to the Sixth Assessment Report of the Intergovernmental Panel on Climate Change* [P.R. Shukla, J. Skea, R. Slade, A. Al Khourdajie, R. van Diemen, D. McCollum, M. Pathak, S. Some, P. Vyas, R. Fradera, M. Belkacemi, A. Hasija, G. Lisboa, S. Luz, J. Malley, (eds.)]. Cambridge University Press, Cambridge, UK and New York, NY, USA. DOI:10.1017/9781009157926.005

Bakun, A. (1997). Patterns in the ocean: ocean processes and marine population dynamics. *Oceanographic Literature Review*, *5*(44), 530.

Baumann, M., Taucher, J., Paul, A. J., Heinemann, M., Vanharanta, M., Bach, L. T., Spilling, K., Ortiz, J., Aristegui, J., Hernández, N., Baños, I., & Riebesell, U. (2021). Effect of intensity

and mode of artificial upwelling on particle flux and carbon export. *Frontiers in Marine Science*, 1579. DOI:10.3389/fmars.2021.742142

Baumann, M., Goldenberg, S. U., Taucher, J., Fernandez-Mendez, M., Ortiz, J., Haussmann, J., & Riebesell, U. (2023). Counteracting effects of nutrient composition (Si: N) on export flux under artificial upwelling. *Frontiers in Marine Science*. DOI:10.3389/fmars.2023.1181351

Bernardello, R., Marinov, I., Palter, J. B., Galbraith, E. D., & Sarmiento, J. L. (2014). Impact of Weddell Sea deep convection on natural and anthropogenic carbon in a climate model. *Geophysical Research Letters*, *41*(20), 7262-7269. DOI:10.1002/2014GL061313

Boot-Handford, M. E., Abanades, J. C., Anthony, E. J., Blunt, M. J., Brandani, S., Mac Dowell, N., ... & Fennell, P. S. (2014). Carbon capture and storage update. *Energy & Environmental Science*, *7*(1), 130-189. DOI:10.1039/C3EE42350F

Boyd, P. W., Jickells, T., Law, C. S., Blain, S., Boyle, E. A., Buesseler, K. O., ... & Watson, A. J. (2007). Mesoscale iron enrichment experiments 1993-2005: synthesis and future directions. *science*, *315*(5812), 612-617. DOI:10.1126/science.1131669

Boysen, L. R., Lucht, W., Gerten, D., Heck, V., Lenton, T. M., & Schellnhuber, H. J. (2017). The limits to global-warming mitigation by terrestrial carbon removal. *Earth's Future*, *5*(5), 463-474. DOI:10.1002/2016EF000469

Brack, D., & King, R. (2021). Managing land-based CDR: BECCS, forests and carbon sequestration. *Global Policy*, *12*, 45-56. DOI:10.1111/1758-5899.12827

Bui, M., Adjiman, C. S., Bardow, A., Anthony, E. J., Boston, A., Brown, S., ... & Mac Dowell, N. (2018). Carbon capture and storage (CCS): the way forward. *Energy & Environmental Science*, *11*(5), 1062-1176. DOI:10.1039/C7EE02342A

Cessi, P. (2019). The global overturning circulation. *Annual review of marine science*, *11*(1), 249-270. DOI:10.1146/annurev-marine-010318-095241

Chase, Z., Strutton, P. G., & Hales, B. (2007). Iron links river runoff and shelf width to phytoplankton biomass along the US West Coast. *Geophysical Research Letters*, *34*(4). DOI:10.1029/2006GL028069

Chavez, F. P., & Messié, M. (2009). A comparison of eastern boundary upwelling ecosystems. *Progress in Oceanography*, *83*(1-4), 80-96. DOI:10.1016/j.pocean.2009.07.032

Copernicus Climate Change Service (C3S) (2019): Sea surface temperature daily data from 1981 to present derived from satellite observations. Copernicus Climate Change Service (C3S) Climate Data Store (CDS). DOI:10.24381/cds.cf608234 (Accessed on 14-05-2024)

Dale, A. W., Sommer, S., Lomnitz, U., Montes, I., Treude, T., Liebetrau, V., ... & Wallmann, K. (2015). Organic carbon production, mineralisation and preservation on the Peruvian margin. *Biogeosciences*, *12*(5), 1537-1559. DOI:10.5194/bg-12-1537-2015

De Baar, H. J., Boyd, P. W., Coale, K. H., Landry, M. R., Tsuda, A., Assmy, P., ... & Wong, C. S. (2005). Synthesis of iron fertilization experiments: from the iron age in the age of enlightenment. *Journal of Geophysical Research: Oceans*, *110*(C9). DOI:10.1029/2004JC002601

Dixon, T., & Romanak, K. D. (2015). Improving monitoring protocols for CO2 geological storage with technical advances in CO2 attribution monitoring. *International Journal of Greenhouse Gas Control*, *41*, 29-40. DOI:10.1016/j.ijggc.2015.05.029

Duteil, O., Koeve, W., Oschlies, A., Aumont, O., Bianchi, D., Bopp, L., Galbraith, E., Matear, R., Moore, J. K., Sarmiento, J. L., & Segschneider, J. (2012). Preformed and regenerated phosphate in ocean general circulation models: can right total concentrations be wrong?. *biogeosciences*, *9*(5), 1797-1807. DOI:10.5194/bg-9-1797-2012

Dutreuil, S., Bopp, L., & Tagliabue, A. (2009). Impact of enhanced vertical mixing on marine biogeochemistry: Lessons for geo-engineering and natural variability. *Biogeosciences*, *6*(5), 901–912. DOI:10.5194/bg-6-901-2009

England, M. H. (1995). The age of water and ventilation timescales in a global ocean model. *Journal of Physical Oceanography*, *25*(11), 2756-2777. DOI:10.1175/1520-0485(1995)025<2756:TAOWAV>2.0.CO;2

Fay, A. R., Munro, D. R., McKinley, G. A., Pierrot, D., Sutherland, S. C., Sweeney, C., & Wanninkhof, R. (2024). Updated climatological mean Δ f CO 2 and net sea–air CO 2 flux over the global open ocean regions. *Earth System Science Data*, *16*(4), 2123-2139. DOI:10.5194/essd-16-2123-2024

Frenger, I., Landolfi, A., Kvale, K., Somes, C. J., Oschlies, A., Yao, W., & Koeve, W. (2024). Misconceptions of the marine biological carbon pump in a changing climate: Thinking outside the “export” box. *Global Change Biology*, *30*, e17124. DOI:10.1111/ gcb.17124

Fuhrmann, A., Knopf, S., Thöle, H., Kästner, F., Ahlrichs, N., Stück, H. L., ... & Kuhlmann, G. (2024). CO2 storage potential of the Middle Buntsandstein Subgroup-German sector of the North Sea. *International Journal of Greenhouse Gas Control*, *136*, 104175. DOI:10.1016/j.ijggc.2024.104175

Fuss, S., Canadell, J. G., Peters, G. P., Tavoni, M., Andrew, R. M., Ciais, P., ... & Yamagata, Y. (2014). Betting on negative emissions. *Nature climate change*, *4*(10), 850-853. DOI:10.1038/nclimate2392

Galbraith, E. D., Gnanadesikan, A., Dunne, J. P., & His-cock, M. R. (2010). Regional impacts of iron-light colimitation in a global biogeochem- ical model. *Biogeosciences*, *7*(3), 1043–1064. DOI:10.5194/bg-7-1043-2010

Gent, P. R., & Mcwilliams, J. C. (1990). Isopycnal mixing in ocean circulation models. *Journal of Physical Oceanography*, *20*(1), 150–155. DOI:10.1175/1520-0485(1990)020<0150:IMIOCM>2.0.CO;2

GESAMP (2019) High level review of a wide range of proposed marine geoengineering techniques. (Boyd, P.W. and Vivian, C.M.G., eds.). London, UK, GESAMP Joint Group of Experts on the Scientific Aspects of Marine Environmental Protection, 143pp. (GESAMP Reports and Studies 98). DOI:10.25607/OBP-1944

Goldenberg, S. U., Taucher, J., Fernandez-Mendez, M., Ludwig, A., Aristegui, J., Baumann, M., ... & Riebesell, U. (2022). Nutrient composition (Si: N) as driver of plankton communities during artificial upwelling. *Frontiers in Marine Science*, *9*, 1015188. DOI:10.3389/fmars.2022.1015188

Goldenberg, S. U., Spisla, C., Sánchez, N., Taucher, J., Spilling, K., Sswat, M., ... & Riebesell, U. (2024). Diatom-mediated food web functioning under ocean artificial upwelling. *Scientific Reports*, *14*(1), 3955. DOI:10.1038/s41598-024-54345-w

Hartmann, J., West, A. J., Renforth, P., Köhler, P., De La Rocha, C. L., Wolf-Gladrow, D., Dürr, J., & Scheffran, J. (2013). Enhanced chemical weathering as a geoengineering strategy

to reduce atmospheric carbon dioxide, supply nutrients, and mitigate ocean acidification. *Reviews of Geophysics*, *51*(2), 113-149. DOI:10.1002/rog.20004

Helm, K. P., Bindoff, N. L., & Church, J. A. (2011). Observed decreases in oxygen content of the global ocean. *Geophysical Research Letters*, *38*(23). DOI:10.1029/2011GL049513

Hutchins, D. A., DiTullio, G. R., Zhang, Y., & Bruland, K. W. (1998). An iron limitation mosaic in the California upwelling regime. *Limnology and Oceanography*, *43*(6), 1037-1054. DOI:10.4319/lo.1998.43.6.1037

Hutchins, D. A., Hare, C. E., Weaver, R. S., Zhang, Y., Firme, G. F., DiTullio, G. R., ... & Bruland, K. W. (2002). Phytoplankton iron limitation in the Humboldt Current and Peru Upwelling. *Limnology and Oceanography*, *47*(4), 997-1011. DOI:10.4319/lo.2002.47.4.0997

IPCC, 1990: *First Assessment Report*, Cambridge University Press, Cambridge, United Kingdom and New York, NY, USA.

IPCC, 1995: *Contribution of Working Group I to the Second Assessment Report of the Intergovernmental Panel on Climate Change*, Cambridge University Press, Cambridge, United Kingdom and New York, NY, USA.

IPCC, 2013: *Climate Change 2013: The Physical Science Basis. Contribution of Working Group I to the Fifth Assessment Report of the Intergovernmental Panel on Climate Change* [Stocker, T.F., D. Qin, G.-K. Plattner, M. Tignor, S.K. Allen, J. Boschung, A. Nauels, Y. Xia, V. Bex and P.M. Midgley (eds.)]. Cambridge University Press, Cambridge, United Kingdom and New York, NY, USA, 1535 pp. DOI:10.1017/CBO9781107415324

IPCC, 2018: *Global Warming of 1.5°C. An IPCC Special Report on the impacts of global warming of 1.5°C above pre-industrial levels and related global greenhouse gas emission pathways, in the context of strengthening the global response to the threat of climate change, sustainabledevelopment,andeffortstoeradicatepoverty*[Masson-Delmotte,V.,P.Zhai,H.-O.Pörtner,D.Roberts,J.Skea,P.R.Shukla,A.Pirani, W. Moufouma-Okia, C. Péan, R. Pidcock, S. Connors, J.B.R. Matthews, Y. Chen, X. Zhou, M.I. Gomis, E. Lonnoy, T. Maycock, M. Tignor, and T. Waterfield (eds.)]. Cambridge University Press, Cambridge, UK and New York, NY, USA, 616 pp. DOI:10.1017/9781009157940

IPCC, 2021: *Climate Change 2021: The Physical Science Basis. Contribution of Working Group I to the Sixth Assessment Report of the Intergovernmental Panel on Climate Change*[Masson-Delmotte, V., P. Zhai, A. Pirani, S.L. Connors, C. Péan, S. Berger, N. Caud, Y. Chen, L. Goldfarb, M.I. Gomis, M. Huang, K. Leitzell, E. Lonnoy, J.B.R. Matthews, T.K. Maycock, T. Waterfield, O. Yelekçi, R. Yu, and B. Zhou (eds.)]. Cambridge University Press, Cambridge, United Kingdom and New York, NY, USA, In press. DOI:10.1017/9781009157896

IPCC, 2022: Summary for Policymakers [P.R. Shukla, J. Skea, A. Reisinger, R. Slade, R. Fradera, M. Pathak, A. Al Khourdajie, M. Belkacemi, R. van Diemen, A. Hasija, G. Lisboa, S. Luz, J. Malley, D. McCollum, S. Some, P. Vyas, (eds.)]. In: *Climate Change 2022: Mitigation of Climate Change. Contribution of Working Group III to the Sixth Assessment Report of the Intergovernmental Panel on Climate Change* [P.R. Shukla, J. Skea, R. Slade, A. Al Khourdajie, R. van Diemen, D. McCollum, M. Pathak, S. Some, P. Vyas, R. Fradera, M. Belkacemi, A. Hasija, G. Lisboa, S. Luz, J. Malley, (eds.)]. Cambridge University Press, Cambridge, UK and New York, NY, USA. DOI:10.1017/9781009157926.001

IPCC, 2023: Summary for Policymakers. In: Climate Change 2023: Synthesis Report. Contribution of Working Groups I, II and III to the Sixth Assessment Report of the Intergovernmental Panel on Climate Change [Core Writing Team, H. Lee and J. Romero (eds.)]. IPCC, Geneva, Switzerland, pp. 1-34. DOI:10.59327/IPCC/AR6-9789291691647.001

Jiao, N., Zhang, Y., Zhou, K., Li, Q., Dai, M., Liu, J., ... & Huang, B. (2014). Revisiting the CO 2" source" problem in upwelling areas–a comparative study on eddy upwellings in the South China Sea. *Biogeosciences*, *11*(9), 2465-2475. DOI:10.5194/bg-11-2465-2014

Jin, X., & Gruber, N. (2003). Offsetting the radiative benefit of ocean iron fertilization by enhancing N2O emissions. *Geophysical research letters*, *30*(24). DOI:10.1029/2003GL018458

Jürchott, M., Oschlies, A., & Koeve, W. (2023). Artificial upwelling—A refined narrative. *Geophysical Research Letters*, *50*(4), e2022GL101870. DOI:10.1029/2022GL101870

Kämpf, J., & Chapman, P. (2016). *Upwelling systems of the world* (pp. 31-42). Springer International Publishing Switzerland. DOI:10.1007/978-3-319-42524-5

Keller, D. P., Oschlies, A., & Eby, M. (2012). A new marine ecosystem model for the University of Victoria Earth System Climate Model. *Geoscientific Model Development*, *5*(5), 1195-1220. DOI:10.5194/gmd-5-1195-2012

Keller, D. P., Feng, E. Y., & Oschlies, A. (2014). Potential climate engineering effectiveness and side effects during a high carbon dioxide-emission scenario. *Nature Communications*, *5*(1), 1–11. DOI:10.1038/ncomms4304

Keller, D. P., Lenton, A., Littleton, E. W., Oschlies, A., Scott, V., & Vaughan, N. E. (2018). The effects of carbon dioxide removal on the carbon cycle. *Current climate change reports*, *4*(3), 250-265. DOI:10.1007/s40641-018-0104-3

Kemper, J., Riebesell, U., & Graf, K. (2022). Numerical flow modeling of artificial ocean upwelling. *Frontiers in Marine Science*, *8*, 804875. DOI:10.3389/fmars.2021.804875

Kemper, J., Mense, J., Graf, K., Kröger, J., & Riebesell, U. (2023). Towards Reliable Performance Predictions for Stommel's Perpetual Salt Fountain.

Kirke, B. (2003). Enhancing fish stocks with wave-powered artificial upwelling. *Ocean Coastal Manag*. 46, 901–915. DOI:10.1016/S0964-5691(03)00067-X

Kithil, P. W. (2006, April). A device to control sea surface temperature and effects on hurricane intensity. In *27th Conference on Hurricanes and Tropical Meteorology* (p. 3B).

Koeve, W., Wagner, H., Kähler, P., & Oschlies, A. (2015). 14 C-age tracers in global ocean circulation models. *Geoscientific Model Development*, *8*(7), 2079-2094. DOI:10.5194/gmd-8-2079-2015

Koeve, W., & Kähler, P. (2016). Oxygen utilization rate (OUR) underestimates ocean respiration: A model study. *Global Biogeochemical Cycles*, *30*(8), 1166-1182. DOI:10.1002/2015GB005354

Koeve, W., Kähler, P., & Oschlies, A. (2020). Does Export Production Measure Transient Changes of the Biological Carbon Pump's Feedback to the Atmosphere Under Global Warming?. *Geophysical Research Letters*, *47*(22). DOI:10.1029/2020GL089928

Köhler, P., Hartmann, J., & Wolf-Gladrow, D. A. (2010). Geoengineering potential of artificially enhanced silicate weathering of olivine. *Proceedings of the National Academy of Sciences*, *107*(47), 20228-20233. DOI:10.1073/pnas.1000545107

Koweek, D. A. (2022). Expected limits on the potential for carbon dioxide removal from artificial upwelling. *Frontiers in Marine Science*, *9*, 841894. DOI:10.3389/fmars.2022.841894

Kwiatkowski, L., Ricke, K. L., & Caldeira, K. (2015). Atmospheric consequences of disruption of the ocean thermocline. *Environmental Research Letters*, *10*(3), 034016. DOI:10.1088/1748-9326/10/3/034016

Lampitt, R. S., Achterberg, E. P., Anderson, T. R., Hughes, J. A., Iglesias-Rodriguez, M. D., Kelly-Gerreyn, B. A., Lucas, M., Popova, E. E., Sanders, R., Shepherd, J. G., Smythe-Wright, D., & Yool, A. (2008). Ocean fertilization: a potential means of geoengineering?. *Philosophical Transactions of the Royal Society A: Mathematical, Physical and Engineering Sciences*, *366*(1882), 3919-3945. DOI:10.1098/rsta.2008.0139

Lovelock, J. E., & Rapley, C. G. (2007). Ocean pipes could help the Earth to cure itself. *Nature*, *449*(7161), 403-403. DOI:10.1038/449403a

MacDougall, A.H. The Transient Response to Cumulative CO2 Emissions: a Review. *Curr Clim Change Rep* **2**, 39–47 (2016). DOI:10.1007/s40641-015-0030-6

Macreadie, P. I., Costa, M. D., Atwood, T. B., Friess, D. A., Kelleway, J. J., Kennedy, H., ... & Duarte, C. M. (2021). Blue carbon as a natural climate solution. *Nature Reviews Earth & Environment*, *2*(12), 826-839. DOI:10.1038/s43017-021-00224-1

Marinov, I., Gnanadesikan, A., Toggweiler, J. R., & Sarmiento, J. L. (2006). The southern ocean biogeochemical divide. *Nature*, *441*(7096), 964-967. DOI:10.1038/nature04883

Martin, J. H., Gordon, R. M., & Fitzwater, S. E. (1990). Iron in Antarctic waters. *Nature*, *345*(6271), 156-158. DOI:10.1038/345156a0

Matthews, H. D., Gillett, N. P., Stott, P. A., & Zickfeld, K. (2009). The proportionality of global warming to cumulative carbon emissions. *Nature*, *459*(7248), 829-832. DOI:10.1038/nature08047

Meinshausen, M., Smith, S. J., Calvin, K. V., Daniel, J. S., Kainuma, M. L. T., Lamarque, J.-F., et al. (2011). The RCP greenhouse gas concentrations and their extension from 1765 to 2300. *Climatic Change*, *109*(1–2), 213–241. DOI:10.1007/s10584-011-0156-z

Meissner, K. J., Weaver, A. J., Matthews, H. D., & Cox, P. M. (2003). The role of land surface dynamics in glacial inception: a study with the UVic Earth System Model. *Climate Dynamics*, *21*, 515-537. DOI:10.1007/s00382-003-0352-2

Morel, F. M., & Price, N. M. (2003). The biogeochemical cycles of trace metals in the oceans. *Science*, *300*(5621), 944-947. DOI:10.1126/science.1083545

Moreno, A. R., & Martiny, A. C. (2018). Ecological stoichiometry of ocean plankton. *Annual review of marine science*, *10*, 43-69. DOI:10.1146/annurev-marine-121916-063126

National Academies of Sciences, Engineering, and Medicine. 2022. *A Research Strategy for Ocean-based Carbon Dioxide Removal and Sequestration*. Washington, DC: The National Academies Press. DOI:10.17226/26278

Nickelsen, L., Keller, D. P., & Oschlies, A. (2015). A dynamic marine iron cycle module coupled to the University of Victoria Earth System Model: the Kiel Marine Biogeochemical Model 2 for UVic 2.9. *Geoscientific Model Development*, *8*(5), 1357-1381. DOI:10.5194/gmd-8-1357-2015

O'Neill, B. C., Tebaldi, C., Van Vuuren, D. P., Eyring, V., Friedlingstein, P., Hurtt, G., ... & Sanderson, B. M. (2016). The scenario model intercomparison project (ScenarioMIP) for CMIP6. *Geoscientific Model Development*, *9*(9), 3461-3482. DOI:10.5194/gmd-9-3461-2016

Orr, J. C., Najjar, R., Sabine, C. L., & Joos, F. (1999). Abiotic-HOWTO, internal OCMIP report, LSCE/CEA Saclay, Gif-sur-Yvette, France (p. 25).

Ortiz, J., Arístegui, J., Taucher, J., & Riebesell, U. (2022). Artificial upwelling in singular and recurring mode: Consequences for net community production and metabolic balance. *Frontiers in Marine Science*, *8*. DOI:10.3389/fmars.2021.743105

Oschlies, A., Pahlow, M., Yool, A., & Matear, R. J. (2010). Climate engineering by artificial ocean upwelling: Channelling the sorcerer's apprentice. *Geophysical Research Letters*, *37*(4). DOI:10.1029/2009GL041961

Oschlies, A., Koeve, W., Landolfi, A., & Kähler, P. (2019). Loss of fixed nitrogen causes net oxygen gain in a warmer future ocean. *Nature Communications*, *10*(1), 2805. DOI:10.1038/s41467-019-10813-w

Paulmier, A., Ruiz-Pino, D., & Garçon, V. (2008). The oxygen minimum zone (OMZ) off Chile as intense source of CO2 and N2O. *Continental Shelf Research*, *28*(20), 2746-2756. DOI:10.1016/j.csr.2008.09.012

Paulmier, A., & Ruiz-Pino, D. (2009). Oxygen minimum zones (OMZs) in the modern ocean. *Progress in Oceanography*, *80*(3-4), 113-128. DOI:10.1016/j.pocean.2008.08.001

Pires, J. C., Martins, F. G., Alvim-Ferraz, M. C., & Simões, M. (2011). Recent developments on carbon capture and storage: An overview. *Chemical engineering research and design*, *89*(9), 1446-1460. DOI:10.1016/j.cherd.2011.01.028

Pollard, R., Tréguer, P., & Read, J. (2006). Quantifying nutrient supply to the Southern Ocean. *Journal of Geophysical Research: Oceans*, *111*(C5). DOI:10.1029/2005JC003076

Proelss, A. (2022). Law of the sea and geoengineering. In *The Law of the Sea* (pp. 93-120). Routledge. DOI:10.4324/9781003091196

Renforth, P., & Henderson, G. (2017). Assessing ocean alkalinity for carbon sequestration. *Reviews of Geophysics*, *55*(3), 636-674. DOI:10.1002/2016RG000533

Riebesell, U., Körtzinger, A., & Oschlies, A. (2009). Sensitivities of marine carbon fluxes to ocean change. *Proceedings of the National Academy of Sciences*, *106*(49), 20602-20609. DOI:10.1073/pnas.0813291106

Riebesell, U., Czerny, J., von Bröckel, K., Boxhammer, T., Büdenbender, J., Deckelnick, M., ... & Schulz, K. G. (2013). A mobile sea-going mesocosm system–new opportunities for ocean change research. *Biogeosciences*, *10*(3), 1835-1847. DOI:10.5194/bg-10-1835-2013

Schmittner, A., Oschlies, A., Matthews, H. D., & Galbraith, E. D. (2008). Future changes in climate, ocean circulation, ecosystems, and biogeochemical cycling simulated for a business-as-usual CO2 emission scenario until year 4000 AD. *Global biogeochemical cycles*, *22*(1). DOI:10.1029/2007GB002953

Schwinger, J., Bourgeois, T., & Rickels, W. (2024). On the emission-path dependency of the efficiency of ocean alkalinity enhancement. *Environmental Research Letters*. DOI:10.1088/1748-9326/ad5a27

Siegel, D. A., DeVries, T., Doney, S. C., & Bell, T. (2021). Assessing the sequestration time scales of some ocean-based carbon dioxide reduction strategies. *Environmental Research Letters*, *16*(10), 104003. DOI:10.1088/1748-9326/ac0be0

Solomon, S., D. Qin, M. Manning, R.B. Alley, T. Berntsen, N.L. Bindoff, Z. Chen, A. Chidthaisong, J.M. Gregory, G.C. Hegerl, M. Heimann, B. Hewitson, B.J. Hoskins, F. Joos, J. Jouzel, V. Kattsov, U. Lohmann, T. Matsuno, M. Molina, N. Nicholls, J. Overpeck, G. Raga, V. Ramaswamy, J. Ren, M. Rusticucci, R. Somerville, T.F. Stocker, P. Whetton, R.A. Wood and D. Wratt, 2007: Technical Summary. In: *Climate Change 2007: The Physical Science Basis. Contribution of Working Group I to the Fourth Assessment Report of the Intergovernmental Panel on Climate Change* [Solomon, S., D. Qin, M. Manning, Z. Chen, M. Marquis, K.B. Averyt, M. Tignor and H.L. Miller (eds.)]. Cambridge University Press, Cambridge, United Kingdom and New York, NY, USA.

Tagliabue, A., Bowie, A. R., Boyd, P. W., Buck, K. N., Johnson, K. S., & Saito, M. A. (2017). The integral role of iron in ocean biogeochemistry. *Nature*, *543*(7643), 51-59. DOI:10.1038/nature21058

Thoni, T., Beck, S., Borchers, M., Förster, J., Görl, K., Hahn, A., Mengis, N., Stevenson, A., & Thrän, D. (2020). Deployment of negative emissions technologies at the national level: a need for holistic feasibility assessments. *Frontiers in Climate*, *2*, 590305. DOI:10.3389/fclim.2020.590305

UNFCC (2015). Adoption of the Paris Agreement. FCCC/CP/2015/L.9/Rev.1.

Volk, T., & Hoffert, M. I. (1985). Ocean carbon pumps: Analysis of relative strengths and efficiencies in ocean-driven atmospheric CO2 changes. *The carbon cycle and atmospheric CO2: natural variations Archean to present*, *32*, 99-110. DOI:10.1029/GM032p0099

Weaver, A. J., Eby, M., Wiebe, E. C., Bitz, C. M., Duffy, P. B., Ewen, T. L., Fanning, A. F., Holland, M. M., MacFadyen, A., Matthews, H. D., Meissner, K. J., Saenko, O., Schmittner, A., Wang, H., & Yoshimori, M. (2001). The UVic Earth System Climate Model: Model description, climatology, and applications to past, present and future climates. *Atmosphere-Ocean*, *39*(4), 361-428. DOI:10.1080/07055900.2001.9649686

Wu, J., Keller, D. P., & Oschlies, A. (2023). Carbon dioxide removal via macroalgae open-ocean mariculture and sinking: an Earth system modeling study. *Earth System Dynamics*, *14*(1), 185-221. DOI:10.5194/esd-14-185-2023

Yool, A., Shepherd, J. G., Bryden, H. L., & Oschlies, A. (2009). Low efficiency of nutrient translocation for enhancing oceanic uptake of carbon dioxide. *Journal of Geophysical Research: Oceans*, *114*(C8). DOI:10.1029/2008JC004792

Yao, W., Kvale, K. F., Achterberg, E., Koeve, W., & Oschlies, A. (2019). Hierarchy of calibrated global models reveals improved distributions and fluxes of biogeochemical tracers in models with explicit representation of iron. *Environmental Research Letters*, *14*(11), 114009. DOI:10.1088/1748-9326/ab4c52

List of Figures

List of Supplemental Figures

List of Tables

List of Supplemental Tables

Erklärung

Hiermit erkläre ich, dass die vorliegende Arbeit mit dem Titel: “Examine and quantifying the potential of artificial upwelling for its capacity for additional CO_2 uptake and long-term storage in the ocean.” von mir selbstständig angefertigt wurde. Bis auf zitierte Referenzen und Beratung meiner Betreuer wurden keine weiteren Quellen verwendet. Sie wurde weder im Rahmen eines Prüfungsverfahrens an anderer Stelle vorgelegt noch veröffentlicht. Diese Arbeit ist unter Einhaltung der Regeln guter wissenschaftlicher Praxis der Deutschen Forschungsgemeinschaft entstanden. Es wurde kein akademischer Grad entzogen.

Kiel, August 2024

Malte Jürchott